

NORTHWESTERN UNIVERSITY

HEXOKINASE 1 SUBCELLULAR LOCALIZATION REGULATES THE METABOLIC FATE
OF GLUCOSE

A DISSERTATION

SUBMITTED TO THE GRADUATE SCHOOL
IN PARTIAL FULFILLMENT OF THE REQUIREMENTS

for the degree

DOCTOR OF PHILOSOPHY

Field of the Driskill Graduate Program in Life Sciences

By

Adam De Jesus

EVANSTON, ILLINOIS

December 2020

© Copyright by Adam De Jesus 2020

All Rights Reserved

ABSTRACT

The product of hexokinase (HK) enzymes, glucose-6-phosphate, can be metabolized through glycolysis or directed to alternative pathways, such as the pentose phosphate pathway (PPP) to generate anabolic intermediates. HK1 contains an N-terminal domain that permits mitochondrial binding, but its physiologic significance remains unclear. We generated mice lacking the HK1 mitochondrial-binding domain. These mice have no overt phenotype, but display increased glucose flux through the PPP, decreased flux below the level of GAPDH, and a hyper-inflammatory response to lipopolysaccharide. The mechanism for the increased PPP flux is through glycolytic block at GAPDH, which is mediated by binding of cytosolic HK1 with S100A8/A9 and increased GAPDH nitrosylation through iNOS. Tissues from mice with conditions of low-grade inflammation, such as aging and diabetes, display increased cytosolic HK1 and cytokine production, along with reduced GAPDH activity. Our data indicate that HK1 mitochondrial-binding alters glucose fate and induces a pro-inflammatory response through regulation of GAPDH.

ACKNOWLEDGEMENTS

I would like to thank Meng Shang, Chunlei Chen, Yihan Chen, and Eric Xia for managing our mouse colony and genotyping the mice used for my thesis work. Thanks to Peng Gao PhD from the Metabolomics Core Facility at Robert H. Lurie Comprehensive Cancer Center of Northwestern University for performing metabolomics mass-spectrometry for our metabolomics experiments. I thank Young Ah Goo PhD from the Northwestern University Proteomics Center of Excellence for running the mass-spectrometry for our proteomics experiments. I thank Lynn Doglio PhD and Pei-Ken PhD from the Northwestern Transgenic and Targeted Mutagenesis for generating the $\Delta E1HK1$ mice, which were pivotal for my thesis. Thank you to Lisa Wilsbacher MD/PhD for mentorship and resources required for my experiments. A special thanks to my fellow lab mates Hidemichi Kouzu MD/PhD, Yuki Tatekoshi MD/PhD, Samuel Man-Lee PhD, Farnaz Keyhani Nejad PhD, and Paulina Stanczyk PhD for supporting my research and guiding my project. A special thank you to my thesis committee for all their support over the past 5 years. Funding for this work was provided through NRSA 5F31HL132552-04.

LIST OF ABBREVIATIONS

HFD	High Fat Diet
NCD	Normal Chow Diet
HK	Hexokinase
HK1	Hexokinase 1
HK2	Hexokinase 2
HK3	Hexokinase 3
HKDC1	Hexokinase Domain Containing 1
PKB	Protein Kinase B
PTPC	Permeability Transition Pore Complex
VDAC	Voltage Dependent Anion Channel
ANOVA	Analysis of Variance
ELISA	enzyme-linked immunosorbent assay
IL	interleukin
LPS	lipopolysaccharide
ROS	reactive oxygen species
RT-PCR	reverse transcriptase polymerase chain reaction
OMM	outer mitochondrial membrane
MBD	mitochondrial binding domain
TLR	toll like receptor
PPP	pentose phosphate pathway
GLUT	glucose transporter

DEDICATION

“If people knew how hard I had to work to gain my mastery, it would not seem so wonderful at all.”

- Michelangelo

“The fact of being an underdog changes people in ways that we often fail to appreciate. It opens doors and creates opportunities and enlightens and permits things that might otherwise have seemed unthinkable.”

-Malcolm Gladwell

Bill Nye the Science Guy was my first academic role model growing up. I would imagine myself wearing a lab coat and conducting experiments with beakers and brilliantly colored chemicals in pursuit of discovery. I didn't really know at the time what Science was or how research worked, but I knew it was something I wanted to do as an adult. I would tell my mother my lofty dreams and aspirations of becoming a scientist and she would always encourage me and fill me with confidence. She believed I could do anything I wanted to do and never once wavered in her belief in me. My mother, Rosalie De Jesus, is one of the most talented, creative and inspiring individuals I know, and I credit any ounce of creative brilliance I possess to her. She saw my potential as a scholar from the start and despite my failures growing up, she remained my biggest cheerleader. I owe more to her than I will ever be able to give. I dedicate this thesis to her, as a small token of appreciation for what I know is a debt I will never repay. Thank you, mom.

My father is a Mexican immigrant, who came to this country to give his children a better life. My

father sacrificed so much to assure my brothers and I had food, shelter, and an education. My father, Julian Garcia, was a stellar student growing up. However, after finishing high school, he was forced to discontinue his education to work as a rancher with my grandfather. My father wanted to pursue higher education, but was unable to attend college due to financial barriers. Growing up my dad would practice multiplication tables with me and play mental math problems and always prioritized my education. I am so lucky to have had a loving, kind, and brilliant father that always put me and my brothers first. Thank you, dad.

My brothers Jose, Cain, and Eden were my protectors, teachers, and best friends growing up. They didn't care how long I spent away at college or consumed with my graduate work, they were always there for me. Thank you all for being my friends and guides through this journey.

Lastly, I want to dedicate this thesis to my second author, best friend, lab-mate, and life-partner, Carolina Pusec. I doubt my thesis would have ever been completed without your assistance, guidance, and encouragement. Thank you for being the most wonderful part of my day throughout my PhD, I simply couldn't have done it without you.

TABLE OF CONTENTS

<u>ABSTRACT</u>	3
<u>ACKNOWLEDGEMENTS</u>	4
<u>LIST OF ABBREVIATIONS</u>	5
<u>DEDICATION</u>	6
<u>TABLE OF CONTENTS</u>	8
<u>LIST OF FIGURES AND TABLES</u>	11
<u>CHAPTER 1: REVIEW OF LITERATURE</u>	17
Mammalian Hexokinase (HK) Family Overview	18
Glucose Metabolism	18
Structure and Evolution	19
Regulation and Tissue Expression	21
Subcellular Distribution	22
HK Mitochondrial Binding	23
Consequence of HK Mitochondrial Binding	24
Immunity and Cancer Metabolism	27
Cancer Metabolism	27
HKs and Cancer	28
Immunometabolism	28
HKs and Immunity	30
<u>CHAPTER 2: ROLE OF HK1 MITOCHONDRIAL BINDING IN HEPG2 CELLS</u>	40
ABSTRACT	41

RESULTS	42
Over-expression of TrHK1 does not change enzymatic activity	42
TrHK1 expressing cells have altered glycolytic metabolism.....	42
TrHK1 Expressing Cells Have Reduced GAPDH Activity.....	43
TrHK1 expression increases cell proliferation.....	44
Mitochondrial Depolarization Induces Reversible HK1 Mitochondrial Dissociation.....	44
<u>CHAPTER 3: EFFECT OF HK1 MITOCHONDRIAL BINDING ON MACROPHAGE</u>	
<u>METABOLISM</u>	53
ABSTRACT.....	54
RESULTS	55
Generation of MBD deleted HK1 mouse model.....	55
Loss of HK1 Mitochondrial Binding Alters Glucose Flux	56
Constitutive HK1 Mitochondrial Dissociation Increases Inflammation.....	57
PPP Inhibition Reverses Hyper-Inflammation Induced by HK1 Mitochondrial Dissociation ..	59
GAPDH Activity is Attenuated in Macrophages with HK1 Mitochondrial Detachment	60
Cytosolic HK1 Mediates GAPDH Nitrosylation through S100A8/9 Binding	62
Obesity and Aging Mouse Models Display Increased Inflammation and Cytosolic HK1	63
<u>CHAPTER 4: CONCLUSION</u>	100
<u>METHODS.....</u>	105
Peritoneal Macrophages Isolation and Cell Culture	106
BMDM Isolation and Cell Culture.....	107
RNA Isolation, Reverse Transcription and Quantitative RT-PCR.....	108
Western Blots	108
Confocal Imaging.....	109
TMRE Colocalization	110

¹³C₆-glucose Tracing and Steady-State Metabolomics	110
Glucose Uptake Assay	111
Co-Immunoprecipitation- Western Blot.....	114
Co-Immunoprecipitation- Mass Spectrometry	114
Lactate Quantification Assay.....	115
<i>In vivo</i> Metabolic Studies.....	115
Mitochondrial and Cytosolic Subcellular Fractionation.....	116
HK Activity Assay.....	116
KEY RESOURCES TABLE	118
<u>REFERENCES</u>.....	130

LIST OF FIGURES AND TABLES

FIGURE 1. METABOLIC FATE OF G6P IN THE CELL.....	32
FIGURE 2. HK ENZYME STRUCTURE FOR DIFFERENT ISOFORMS AND EVOLUTIONARY TREE....	34
FIGURE 3. HK1 MITOCHONDRIAL BINDING DOMAIN.....	35
FIGURE 4. METABOLIC HALLMARKS OF CANCER CELLS.	36
FIGURE 5. AEROBIC GLYCOLYSIS SCHEMATIC.....	37
FIGURE 6. MACROPHAGE POLARIZATION	38
FIGURE 7. HK MITOCHONDRIAL BINDING AND METABOLIC EFFECTS.....	39
FIGURE 8. TRHK1 OVEREXPRESSION DOES NOT AFFECT INTRINSIC ENZYMATIC ACTIVITY.....	45
FIGURE 9. TRHK1 EXPRESSION REDUCES LACTATE PRODUCTION.	46
FIGURE 10. TRHK1 CELLS HAVE ALTERED GLUCOSE FLUX AND INCREASED PPP.....	47
FIGURE 11. TRHK1 EXPRESSING CELLS DISPLAY REDUCED GAPDH ENZYMATIC ACTIVITY. .	50
FIGURE 12. CELLS OVEREXPRESSING TRHK1 HAVE INCREASED PROLIFERATION.	51
FIGURE 13. REVERSIBLE HK1 MITOCHONDRIAL DISSOCIATION IS INDUCED BY MITOCHONDRIAL DEPOLARIZING STIMULI.....	52
FIGURE 14. SCHEMATIC OF $\Delta E1HK1$ MOUSE MODEL GENERATION.	65
FIGURE 15. $\Delta E1HK1$ INITIAL MOUSE MODEL CHARACTERIZATION.	66
FIGURE 16. $\Delta E1HK1$ BMDM AND PMS HAVE MITOCHONDRIAL DISSOCIATION OF HK1	67
FIGURE 17. BMDMS HAVE HIGH HK1 AND HK3 EXPRESSION AFTER LPS TREATMENT.	69
FIGURE 18. LOSS OF HK1 MITOCHONDRIAL BINDING ALTERS GLYCOLYTIC METABOLISM.	71
FIGURE 19. HK1 MITOCHONDRIAL DISSOCIATION DECREASES LOWER GLYCOLYTIC FLUX AND INCREASES PPP METABOLISM.....	72

FIGURE 20. BRAIN AND HEART TISSUE METABOLOMICS ANALYSIS SHOWS HIGHER PPP METABOLITES.	74
FIGURE 21. CONSTITUTIVE HK1 MITOCHONDRIAL DISSOCIATION INCREASES INFLAMMATION.	75
FIGURE 22. HK1 mRNA EXPRESSION IS NOT SIGNIFICANTLY ALTERED BETWEEN ΔE1HK1 AND WT BMDMs.	77
FIGURE 23. PPP INHIBITION REVERSES HYPER-INFLAMMATION INDUCED BY HK1 MITOCHONDRIAL DISSOCIATION.	79
FIGURE 24. mRNA EXPRESSION OF GLYCOLYTIC, PPP AND TCA CYCLE GENES IN BMDMs FROM WT AND ΔE1HK1 MICE.	82
FIGURE 25. GAPDH ACTIVITY IS ATTENUATED IN MACROPHAGES WITH HK1 MITOCHONDRIAL DETACHMENT.	83
FIGURE 26. INHIBITION OF GAPDH ACTIVITY IN RAW265.7 CELLS.	85
FIGURE 27. STEADY-STATE METABOLOMICS IN HEPG2 CELLS.	86
FIGURE 28. METABOLIC STUDIES AND GAPDH ACTIVITY MEASUREMENT IN HEPG2 CELLS. ..	87
FIGURE 29. PROTEOMIC ANALYSIS OF HEPG2 CELLS WITH FLHK1 AND TRHK1 OVEREXPRESSION.	88
FIGURE 30. Co-IP OF CYTOSOLIC HK1 WITH S100A8/9.	90
FIGURE 31. CYTOSOLIC HK1 MEDIATES GAPDH NITROSYLATION THROUGH S100A8/9 BINDING.	91
FIGURE 32. IN VIVO INHIBITION OF iNOS REVERSE ΔE1HK1 HYPER-INFLAMMATION.	93
FIGURE 33. BMDMs WITH iNOS INHIBITION ELIMINATES HYPER-INFLAMMATION IN ΔE1HK1 MICE.	94

FIGURE 34. WEIGHT AND BLOOD GLUCOSE IN MICE AFTER 27-WEEKS OF NC AND HFD.	95
FIGURE 35. DIABETES AND AGING ARE ASSOCIATED WITH HK1 MITOCHONDRIAL DISLOCATION AND INCREASED CYTOKINE PRODUCTION.	96
FIGURE 36. CYTOKINE PRODUCTION AND HK1 SUBCELLULAR LOCALIZATION IN MICE AFTER NC AND HFD.	98
FIGURE 37. CYTOKINE PRODUCTION AND HK1 SUBCELLULAR LOCALIZATION IN AGING MICE.	99
FIGURE 38. HK1 MITOCHONDRIAL DISSOCIATION INDUCED HYPER-INFLAMMATION MECHANISM	104
TABLE 1. OVERVIEW OF MAMMALIAN HKs.	33

INTRODUCTION

Hexokinases (HKs) represent the first committed step in glucose utilization by catalyzing the phosphorylation of glucose to glucose 6-phosphate (G6P), which traps glucose in the cell and commits it to downstream metabolic pathways (1–4). G6P can enter glycolysis for energy production, pentose-phosphate-pathway (PPP) for anabolic intermediates, hexosamine biosynthesis pathway (HBP) for protein glycosylation, or be converted to glucose-1-phosphate for glycogen synthesis (5,6). In mammals, five HK isozymes (HK1, HK2, HK3, glucokinase (GCK), and hexokinase domain-containing 1 (HKDC1)) have been identified, each with distinct tissue expression, subcellular localization, kinetics, and substrate specificities (7–9). The molecular weights of HK1, 2, 3, and HKDC1 are ~100 kDa, whereas GCK and yeast HKs have a molecular weight of 50 kDa. The protein and gene structure of the 100 kDa enzymes suggest that they evolved from a gene duplication and fusion of an ancestral yeast-like 50 kDa enzyme (10). Upon the duplication process, the N-terminal half of HK1 and HK3 became enzymatically inactive, whereas HK2 has maintained activity in both of its catalytic domains (11).

HK1 and HK2 also contain an N-terminal, 21-amino-acid hydrophobic sequence (12,13) that enables outer mitochondrial membrane (OMM) binding, possibly through its interaction with the family of mitochondrial bound voltage dependent anion channel (VDAC) proteins (14–17). This sequence, termed the mitochondrial binding domain (MBD), is encoded in exon 1, while exons 2-10 encode for the N-terminal domain and exon 10-18 encode for the C-terminal domain (18,19). Notably, HK1 and HK2 differ in their affinity for mitochondrial localization (20,21), with HK1 predominantly found on the OMM, while HK2 is in a dynamic balance between the mitochondria and cytosol that is regulated, in part, by insulin signaling (22,23). HK3 and GCK lack a corresponding N-terminal sequence and as a consequence are predominantly cytoplasmic

(24,10), although some reports suggest that HK3 may bind to the nuclear envelope (25).

Metabolic adaptations are inextricably linked to the immediate host defense against foreign pathogens (26–28). In the setting of innate inflammatory activation, there is a robust increase in glycolysis even in the setting of abundant oxygen, a metabolic program shared by rapidly proliferating cells called aerobic glycolysis (29–34). In addition to elevated glycolytic rate, there is increased glucose flux into the PPP and other ancillary metabolic pathways in immune cells following toll-like receptor (TLR) stimulation (6,35). In macrophages, HK1 mRNA is highly expressed after pro-inflammatory stimulation (36), and HK1-dependent glycolysis is important for proper inflammasome activation in M1 macrophages (37). In dendritic cells, fatty acid-induced inhibition of HK1 enhances TLR-mediated innate activation by reducing glycolytic reprogramming and facilitating mitochondrial reactive oxygen species (mtROS) production (38). These results indicated a major role for glucose metabolism through HK1 in the activation of inflammatory cells.

Despite extensive research on glucose metabolism, it remains unclear what factors determine the fate of glucose and regulate the entrance of G6P into a specific pathway. Elucidating this regulation is important for developing rational approaches to inflammatory diseases, cancer and its response to therapy and various diseases. In this dissertation, we demonstrate that the binding of HK1 to the mitochondria determines whether the product of the enzyme (G6P) is catabolized through glycolysis or shunted through anabolic PPP. We also show that constitutive dislocation of HK1 to the cytoplasm leads to a shift to the PPP and resulting in higher cytokine production and exaggerated inflammatory response to endotoxemia. The mechanism for the altered G6P metabolism by HK1 cellular distribution is through cytosolic HK1's interaction with S100A8/9, which induces S-nitrosylation of GAPDH and subsequent enzymatic inactivation.

Therefore, these data identify HK1 as an important metabolic switch between catabolic and anabolic metabolism through its subcellular localization.

CHAPTER 1: REVIEW OF LITERATURE

Mammalian Hexokinase (HK) Family Overview

Glucose Metabolism

Glycolysis is also referred to as the Embden-Meyerhof-Parnas pathway, named after the three pioneering scientists that elucidated the glycolytic process as a vital metabolic pathway present in essentially all living organisms from microbes to mammals (39). This pathway provides chemical substrates that produce energy in the form of ATP and biosynthetic intermediates necessary for cellular structure, function, and signaling (39,40). Hexokinase (HK) catalyzes the first committed step of glycolysis through ATP-dependent phosphorylation of glucose to generate glucose-6-phosphate (G6P) (41). The strong negative charge of the phosphate group on G6P prevents glucose from exiting the cell and helps maintain the concentration gradient that allows facilitated glucose flux into cells through glucose transporters (GLUT) (42,43). The intracellular trapping of G6P also commits glucose down one of several downstream metabolic pathways which serve the cells energetic, biosynthetic, glucose storage and inter- and intracellular signaling needs (**Figure 1**). Therefore, G6P is a branch point for several metabolic shunts that help meet the cells changing nutrient demands.

Canonically, G6P flows through glycolysis, which provides 2 net equivalents of ATP, 2 equivalents of NADH, and 2 equivalents of pyruvate that can be further metabolized by the TCA cycle to yield ~36 ATP (43). However, G6P is an important intermediate for the pentose phosphate pathway (PPP), which is a fundamental metabolic shunt off glycolysis that provides precursors for nucleotide synthesis and reducing molecules in the form of nicotinamide adenine dinucleotide phosphate (NADPH) for anabolic processes and anti-oxidant defense (44). The enzymatic reactions of the PPP are divided into the oxidative and non-oxidative branch. The oxidative branch is irreversible and metabolizes G6P to provide NADPH, ribulose 5-phosphate, and carbon dioxide

(44). The non-oxidative branch is a reversible pathway that metabolizes fructose 6-phosphate and glyceraldehyde 3-phosphate to produce ribose 5-phosphate for nucleotide synthesis(44). In addition, isomerization of G6P to glucose 1-phosphate and subsequent formation of uridine 5'-diphosphate (UDP)-glucose provides the precursor for glucose storage in the form of glycogen (45). UDP-glucose is added to the enzyme glycogenin via autocatalysis and provides the foci for further branching of glucose for energy storage in tissues (i.e., liver and muscle) (45). Moreover, HK provides two important entry points into the hexosamine biosynthetic pathway (HBP) via G6P and glucosamine 6-phosphate. HBP is a ubiquitous metabolic pathway that generates glycosylation intermediates for N and O-linked glycosylation of proteins for signaling for both intra and intercellular signaling (46).

In mammals, there are four well characterized HK isoforms referred to as HK1, HK2, HK3, HK4 (glucokinase-GCK), and a recently discovered 5th HK called hexokinase domain containing 1 (HKDC1) (9,10,47,48). Despite the high homology between the various HK isoforms, there are large differences in structure, enzymatic activity, regulation, tissue expression, and subcellular localization suggesting unique roles in the cell (24). Subsequent sections will discuss the various HK isoforms in detail, including structure, function, and localization. **Table 1** is a summary of the similarities and differences seen in the various HK family members.

Structure and Evolution

The five HK isoforms share a high degree of sequence homology, yet display differences in their enzymatic function, regulation, and subcellular localization (9). Human HKs are thought to have originated from an ancestral ~50 kDa HK that underwent Tandem gene duplication and fusion early in vertebrate evolution theoretically resulting in a HK gene with two active catalytic

domains (49). Subsequent gene duplications on different chromosomes then resulted in formation of HK1, HK2, HK3, and GCK. However, GCK lost the N-terminal domain (suggested by the fact that GCK C-terminal domain has high homology to the other HK isoforms) at some point during evolution and resulted in a ~50 kDa protein. A later tandem gene duplication then resulted producing HKDC1, and later mutations have altered both gene structure and function (61,62). Refer to **Figure 2** for a summary of HK structure and evolution.

The typical size of non-vertebrate HKs is ~50 kDa, while most vertebrate HKs (except GCK) are ~100 kDa (5,49). HK1-3 are all ~100 kDa and show strong product inhibition by G6P (**Table 1**), however, GCK is insensitive to this form of inhibition and is mainly regulated through hormones and subcellular localization (52–54). The glucose phosphorylating capacity of GCK is within physiologic range for vascular glucose concentration ($K_m \sim 6\text{mM}$ glucose) (55,56), while that of HK1-3 is found much lower ($K_m < 0.5\text{mM}$ glucose). This means that HK1-3 have very high affinity for glucose and will phosphorylate it upon contact, while GCK has a high capacity for glucose and therefore tissues expressing this HK have additional options for regulating metabolic flux beyond G6P production (57).

HK2 has retained catalytic activity of both N- and C-terminal halves, while HK1 and HK3 have been shown to lack N-terminal domain catalytic activity(58–60). However, HK1 has been shown to retain the ability to bind G6P to both the N and C-terminal domain, suggesting a regulatory role for the N-terminal half of HK1 (61–65). Similar to HK1, HK3 shows inactivity of the N-terminal domain, yet little is known about the regulatory or functional role of the N-terminal domain (60,66). The recently discovered HKDC1 enzyme has been shown to have higher K_m than even GCK, but many of this isoforms kinetic parameters remain poorly understood (47,67).

Regulation and Tissue Expression

The different HKs display selective tissue expression profiles, which is believed to be an important mode of regulating glucose metabolism in tissues, however, most tissue express multiple HK isoforms at varying levels (9,68). Historically, GCK is thought to have limited expression outside of the liver and pancreas (69–72), however recent studies have shown important roles for GCK in the pituitary gland and neuron subsets in the brain Neurons (73,74). GCK is highly expressed in the liver and functions as a regulator of whole body glucose metabolism (52,75). Aside from GCKs intrinsic kinetic properties, which are well suited for handling large glucose loads, it is exquisitely sensitive to hormonal regulation (75,76). Upon glucose withdrawal for 48hrs, GCK enzymatic activity drops by ~66% and its mRNA expression is almost undetectable (56,76).

HK1 is ubiquitously expressed in most tissues and is thought to serve a “housekeeping” role in most tissues to provide basal glucose phosphorylating activity. However, HK1 is known to have high expression in brain and kidney tissues with minimal expression in skeletal muscle and liver and is not known to be regulated by hormones such as insulin or glucagon (77,78). Conversely, HK2 is the predominant isoform found in insulin-sensitive tissues like skeletal muscle, heart tissue, and adipose tissue (not liver) (18). The gene encoding HK2 has multiple transcription factor binding sites in its promoter for canonical mediators of insulin, glucagon, p53, and hypoxia signaling (23,79,80). Expression of HK3 is highest in spleen, hematopoietic cells, and lung (81–84). The expression of *HKDC1* has been reported to be highest in colon, kidney, and brain, but displays upregulation in disease states such as non-alcoholic fatty liver disease (NAFLD) (47).

Subcellular Distribution

In addition to tissue distribution and hormonal regulation, HKs also show multiple subcellular localizations. Despite the wealth of research on the intracellular compartmentalization of HKs, this remains a poorly understood aspect of HK biology. Some of the earliest studies on HKs distinguished isoforms based on their presence in the particulate or soluble fraction of a cell lysate (85). As cell fractionation techniques improved it was found that the particulate enriched HKs were binding to mitochondria (i.e., HK1 and HK2) (86). With proteolytic digestion techniques it was later shown that only HK1 and HK2 isoforms bound to the outer mitochondrial membrane (OMM) (87,88). Subsequent studies used N-terminal domain GFP fusion constructs to demonstrate mitochondrial OMM localization (13). Analysis of HK1 and HK2 sequence revealed a conserved 20 amino acid domain at the N-terminus that confers OMM binding (89–91).

Importantly, this 20-amino acid N-terminal sequence is not shared by HK3 or GCK, which is in line with their mostly cytosolic localization. HK3 has been shown to localize to the nuclear envelope, however, these studies have not been rigorously validated and much remains to be discovered about its subcellular compartmentalization (25,92). Since *HKDC1* resulted from tandem gene duplication of *HK1*, it contains a highly homologous 20 amino acid N-terminal domain that confers OMM binding in hepatocytes and liver cancer cells (47). Since little else is known about the mitochondrial dynamics of this HKDC1 and is not the focus of this thesis, I will not elaborate further on HKDC1 or its mitochondrial effects in subsequent chapters.

Unlike the other HK isoforms, GCK has an inhibitory protein, glucokinase regulatory protein (GKRP), that is expressed in liver and regulates GCK at the protein level (93). Free GKRP is dynamically shuttled between the cytosol and nucleus and is able to bind GCK to localize it to the nucleus and essentially deprive it from cytosolic pools of glucose (94). GKRP senses rising

glucose levels in the cell and preferentially binds glucose instead of GCK, therefore during times of starvation GCK:GKRP are localized in the nucleus and refeeding results in release of GCK back into the cytosol and allows glucose processing by GCK (95).

HK Mitochondrial Binding

Early investigations revealed that HK1 and HK2 were predominantly bound to the OMM through a mitochondrial binding domain (MBD) located at the N-terminal domain (89,96,97). The MBD is a short 20 amino acid sequence that forms an alpha helix and is thought to insert on the OMM lipid bilayer (**Figure 3**) (89,98,99). In addition to direct insertion into the OMM, secondary interaction of HK1 and HK2 with voltage-dependent anion channel (VDAC) stabilizes the HK-OMM attachment (15,100). VDAC is a family of transmembrane, β -barrel proteins ubiquitously found on the mitochondrial surface that can bind to adenine nucleotide translocase (ANT) on the inner mitochondrial membrane (IMM) and regulates the flow of metabolites, namely ATP and ADP, between cytosol and mitochondria (101). VDAC and ANT are known to form a pore that links opens between the cytosol and mitochondrial inner matrix for exchange of ATP for ADP (100). This is needed to maintain production of ATP by ATP synthase enzyme in the electron transport chain (ETC) by replenishing mitochondrial ADP pools. The interaction of HK1 and HK2 with VDAC has been extensively studied and various *in silico* models have been proposed for this protein interaction (115,116).

The MBD-containing HKs display dynamic mitochondrial and cytosolic movement that is influenced by several documented factors (86,104). Early studies showed more HK1 in mitochondrial fractions with increased mitochondrial membrane mobility as assessed by low cholesterol to phospholipid ratio (105). G6P, in addition to inhibiting the enzymatic activity of

HK1 and HK2, also disrupts its mitochondrial binding and increases cytosolic localization of HKs (106). Interestingly, mildly increasing cellular alkalization was shown to increase mitochondrial HK activity as compared to the cytosolic compartment (107). Moreover, dicyclohexylcarbodiimide (DCCD) has been shown to covalently bind to VDAC and disrupt important HK binding contact sites necessary for mitochondrial binding, given further credibility to the HK-VDAC binding dynamic (108). Moreover, studies have shown that certain polyamines (109) and divalent cations (i.e., Mg^{2+} and Ca^{2+}) (110) can increase HK mitochondrial binding through stabilization of VDAC-HK binding, however follow-up studies have not confirmed these findings.

Important signaling pathways have also been shown to regulate HK mitochondrial binding. PKB (also called protein kinase B or RAC-alpha serine/threonine-protein kinase Akt) is the main intracellular mediator of the insulin signaling response and has been shown to phosphorylate HK2 at threonine-473 and increase mitochondria localization in the heart (23). Additionally, glycogen synthase kinase-3 β (GSK-3 β) has been reported to cause dissociation of HK1 (111) and HK2 (22,112) from the mitochondria in lymphocytes and cardiomyocytes, respectively, through phosphorylation of VDAC and disruption on VDAC-HK binding. Given that Akt phosphorylates and inhibits GSK-3 β (113–115), this may be a potential way cells regulate HK mitochondria to cytoplasm shuttling.

Consequence of HK Mitochondrial Binding

Since the discovery of HK-mitochondrial binding, it has been speculated that the purpose of this interaction is to allow HKs preferential access to mitochondrial ATP pools entering the cytoplasm through VDAC-ANT pore (89). Moreover, HK mitochondrial binding increase

enzymatic activity and glucose phosphorylating capacity as compared to cytosolic pools of HK (116). Together these findings formed the notion that HK mitochondrial binding increases cellular metabolic efficiency by coupling mitochondrial ATP production with cytosolic glucose consumption. However, considering that the K_m of HK1 and HK2 for ATP is well below the concentration present in the cytoplasm, ATP is usually not a limiting substrate for HK activity in the cell (**Table 1**). Therefore, more research is needed to validate this claim.

VDAC is an important mediator of the apoptotic cascade through mitochondrial release of cytochrome-C (100). HK binding to VDAC on the OMM has been shown to prevent opening of the permeability transition pore (PTP) and prevent release of cytochrome-C after treatment with apoptotic stimuli (117). Additionally, HK binding to VDAC also blocks recruitment of important apoptotic mediators, BCL2 associated X protein (Bax) and BCL2-antagonist/killer 1 (Bak) from binding to VDAC, which further blunts the cell death response (118).

As discussed above, the prevailing hypotheses for HK localization to the mitochondria is twofold, 1) to allow preferential access to mitochondrial ATP and 2) to prevent apoptosis by maintaining closure of VDAC. However, these two hypotheses seem to make contradictory claims. In the first case, HK is thought to localize to the mitochondria and associate with VDAC to gain preferential access to ATP that is passing to the cytosol from the mitochondria (9,15,89,103). In the second case, HK is suggested to maintain closure of VDAC-ANT pore and decrease the release of cytochrome C that would induce cellular apoptosis (119,120). It seems counterintuitive that HK mitochondrial binding would permit flow of ATP/ADP through VDAC pore, while preventing cytochrome-C release through VDAC pore closure. Together, these data indicate an incomplete understanding of HK1-VDAC binding.

Recently, there has been an emerging of interest in understanding the metabolic

consequences of HK mitochondrial interaction. Compartmentalization is an important factor in regulating enzymatic function and may direct the flow of nutrients to particular metabolic pathways (121). Since HK1 and HK2 have different binding affinities for the mitochondria, studies have shown that there are metabolic differences in how they shuttle G6P between catabolic and anabolic pathways (21). John et al, show that HK1, which is constitutively bound to the mitochondria at baseline, acts in a more catabolic capacity to produce ATP, however, HK2, which can shuttle dynamically between the cytosol and mitochondria, can direct the flow of glucose from ATP generation (mitochondrial bound) to glycogen production (cytosolic) (21). Adult and neonatal rat cardiomyocytes (ARCM and NRCM) display differences in their glucose utilization and express different HK isoforms with ARCM predominately expressing HK2, while NRCM express more HK1 (122).

Immunity and Cancer Metabolism

Cancer Metabolism

Metabolic reprogramming is a hallmark of cancer cells (123). Nearly a century ago, German physiologist, Otto Warburg, first observed the marked increase in glucose consumption by cancer cells (124,125); however, much of the work after this seminal discovery was focused on signaling, genetic mutations, and other non-metabolic aspects of tumor biology. Recently, there has been a resurgence of interest on how cellular metabolism influences and facilitates malignancy. Tumorigenesis changes cellular metabolism a multiple step including, 1) increased nutrient uptake, 2) changing metabolite flux to vital cell growth pathways, and 3) metabolic changes in epigenetic regulation (33) (**Figure 4**).

Glucose and amino acids are essential nutrients for sustained cancer growth and their uptake is increased in rapidly proliferating tumor cells (33). Glucose and glutamine are essential nutrients in mammalian cells that supply energy, in the form of ATP, and biosynthetic carbons for growth and proliferation (126–128). The massive upregulation of glucose utilization by anaerobic glycolysis to produce lactate despite abundant oxygen, is the definition of the Warburg effect or aerobic glycolysis as it is also known (129). Aerobic glycolysis is an inefficient way to generate ATP, however, has the advantage of supplying carbons needed for biosynthetic processes that are required for growth and proliferation (129) (**Figure 5**). Glutamine is a vital nutrient taken up by proliferating cells and supplies carbons and, importantly, nitrogen for many nitrogen dependent metabolites (130). Aspartate has recently been found to be another important amino acid required for tumor growth and proliferation and blocking its uptake is sufficient to halt tumor cell growth in various cancer cells (131–133).

As mentioned above, aerobic glycolysis allows for increased biosynthetic utilization of the glucose carbons rather than simply generating mitochondrial bound pyruvate for oxygen coupled

ATP production. Glycolysis has several shunts that allow for carbons to flow into biosynthetic pathways, including the PPP, serine to enter one-carbon metabolism (OCM) (134), and *de novo* fatty-acid synthesis (135), and glycogen synthesis (136). The PPP is important for producing the ribose sugar backbone of all nucleotides and generates NADPH which is an important anabolic reducing equivalent necessary for lipid synthesis and oxidative defense, which is vital for growth and proliferation of malignant cells (137–139).

HKs and Cancer

HK2 overexpression is observed in many types of cancers and is thought to help drive the large glycolytic flux seen in cancer cells (140–142). It has been shown that most tumors switch HK isoform to HK2 with hepatocellular carcinoma as a primer example in which GCK expression dramatically declines and HK2 expression increases (140). Some tumors were shown to have a hundred-fold higher HK2 expression than that of normal tissue (143). HK2 binding to the mitochondria is thought to be a major cell survival mechanism utilized by cancer cells, since higher mitochondrial bound HK2 is found in cancer cells (144). Although reports have shown that some HK1 dependent lung and brain cancers (145–147), HK1 is typically downregulated in favor of isotype switch to HK2.

Immunometabolism

Metabolite acquisition and proper utilization is essential for coordinated immunologic function. Different immune cell lineages require unique metabolic inputs and products to meet their environmental and intrinsic cell functions. By modulating their metabolic machinery, immune cells can meet the complex demands required for host immune defense and malignant cell

suppression. Importantly, there are two classes of immune subsets, myeloid and lymphoid derived cells (148). Myeloid cell lineage gives rise to red blood cells, platelets, granulocytes (neutrophils, eosinophils, and basophils) and macrophages. The lymphoid cell lineage gives rise to natural killer cells (NK cells), T-cells, and B-cells. Broadly speaking, the immune system is divided into two branches, the innate and adaptive system. The innate immune system is our first line of defense against invading pathogens and is composed epithelial cells, neutrophils, and macrophages, along with a host of other myeloid derived cells that function for specific pathogens (27). The adaptive immune system is composed to T-cells, which are further subdivided into CD4+ and CD8+ T-cells and have unique effector functions in host defense (149). B-cells are also part of the adaptive immune system and function mainly to produce antibodies which effectively create a memory of past infections for future defense against reinfection (150).

As discussed above, macrophages derive from the myeloid lineage and are a phagocytic cell of the innate immune system. They are one of the first cells recruited during an acute infection and help maintain tissue homeostasis. Since macrophages are responsible for inflammatory activation and subsequent resolution, they display exquisite plasticity that facilitates ability to rapidly respond to unique micro-environments (35). Macrophages initiate the early response to pathogen invasion through secretion of pro-inflammatory cytokines and subsequently change their phenotype to function in repair of damaged sites of inflammation (28). Macrophages are commonly subdivided into two groups, M1 (inflammatory) or M2 (anti-inflammatory) subsets. M1 are phenotypically categorized as “classically activated” and mediate the canonical inflammatory response through secretion of IL-1 β , IL-6, and TNF α and mediate phagocytosis and elimination of foreign material and organisms (30). M2 macrophages are known as “alternatively activated” and show a pro-fibrotic and anti-inflammatory phenotype in response to IL-4, among

other stimuli (151,152) (**Figure 6**).

In addition to changes in effector function, metabolic reprogramming has been shown to be a vital step in proper macrophage polarization (151). M2 polarized macrophages using IL-4 as a stimuli show higher rate of oxygen consumption (153). Additionally, M2 macrophages display upregulation of Peroxisome proliferator-activated receptor gamma (PPAR γ) and have been shown to upregulate fatty-acid oxidation (154). Together this suggests that M2 polarization leads to a more mitochondrial metabolic program that facilitates its anti-inflammatory and pro-fibrotic functions. In contrast, M1 macrophages that are activated by lipopolysaccharide (LPS) show upregulation of glycolysis similar to cancer cell metabolic switch to aerobic glycolysis (155). LPS binds to toll like receptor 4 (TLR4) on the cell surface (156). TLR4 activation leads to increased mRNA transcription of inflammatory cytokines in their un-cleaved pro-enzyme form, subsequent stimulation by a second signal (i.e., ATP, mitochondrial DNA, bacterial cell wall sugars or potassium influx) allows for inflammasome activation and cleavage and secretion of pro-inflammatory cytokines (156).

HKs and Immunity

Reports have shown that HK2 mitochondrial binding is an important mediator of inflammasome activation (157) and, more recently, observed to play a role in viral-mediated inflammation through binding of mitochondrial anti-viral signaling (MAVS) on the mitochondrial surface (158). In macrophages, HK1 mRNA is highly expressed after pro-inflammatory stimulation (36), and HK1-dependent glycolysis is important for proper inflammasome activation in M1 macrophages (37). In lymphocytes, HK1 mitochondrial binding was shown to enhance cellular respiration and promote effector memory CD8⁺ T-cell cytokine production (111). In

dendritic cells, fatty acid-induced inhibition of HK1 was shown enhance TLR-mediated innate activation by reducing glycolytic reprogramming and facilitating mitochondrial reactive oxygen species (mtROS) production (38).

In a genome-wide association study (GWAS) aimed at identifying novel genetic variants associated with sleep disordered breathing (SDB)-related hypoxemia, significant variants in HK1 and IL-18 genetic loci were found (159). Patients with SDB are known to have high levels of oxidative stress and pulmonary inflammation (160), which has been linked to subclinical alveolar macrophage-mediated inflammation (161). Recently, an epigenome-wide association study of asthma and wheeze identified an association between methylation at cg16658191 of HK1 gene (found within the body of exon-1) and adolescent asthma traits (162). They show that DNA methylation of cg16658191 is inversely associated with HK1 expression in mouse alveolar macrophages and that higher expression of HK1 was predictive of wheezing without a cold during infancy (162). Combined, these studies suggest an important role for HK1 in myeloid cells. In this thesis, I aim to understand what effect HK1 mitochondrial binding has on cellular metabolism (**Figure 7**).

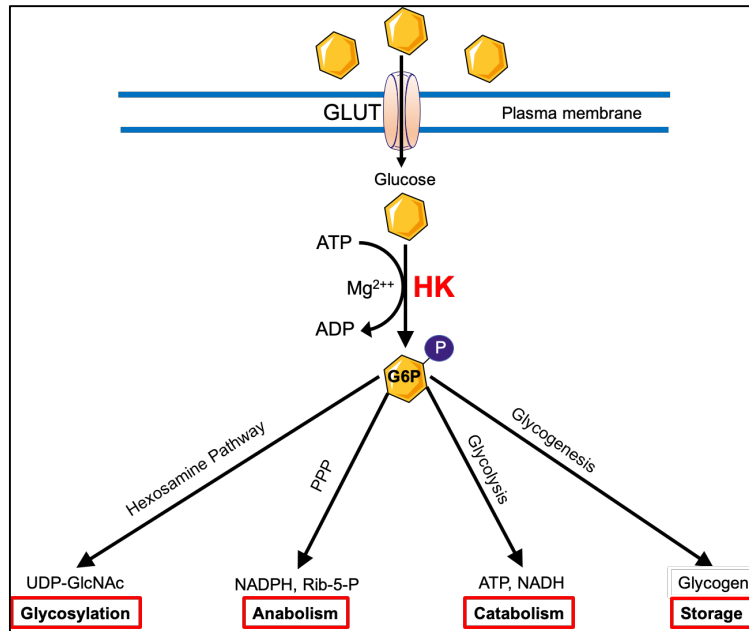


Figure 1. Metabolic fate of G6P in the cell.

HKs are central to cellular glucose metabolism and catalyze the first step of glucose metabolism via the ATP-dependent phosphorylation of glucose to yield G6P. G6P is the branch point for several important metabolic pathways including hexosamine pathway (UDP-GlcNAc), PPP (NADPH & Ribose 5-phosphate), glycolysis (ATP, NADH), and glycogenesis (UDP-glucose).

	HK1	HK2	HK3	HK4 (GCK)	HK5 (HKDC1)
MW (kDa)	~100	~100	~100	~50	~100
K _m for Glc (mM)	0.030	0.300	0.003	6	>50 ^a
K _m for ATP (mM)	0.5	0.7	1.0	0.6	?
Glc-6-P inhibition	+	+	+	-	?
Insulin regulation	-	+	?	+	?
Mitochondrial binding	+	+	-	-	+
Dominant tissue expression	Ubiquitous, brain, kidney	Muscle, adipose	Lung, spleen	Liver, pancreas	Colon, kidney, brain ^b

Table 1. Overview of mammalian HKs.

Key enzymatic parameters of all the known HK isoforms. Citations for recent papers summarizing enzymatic properties of HKDC1 are (a) (47) and (b) (67). Adapted from (50).

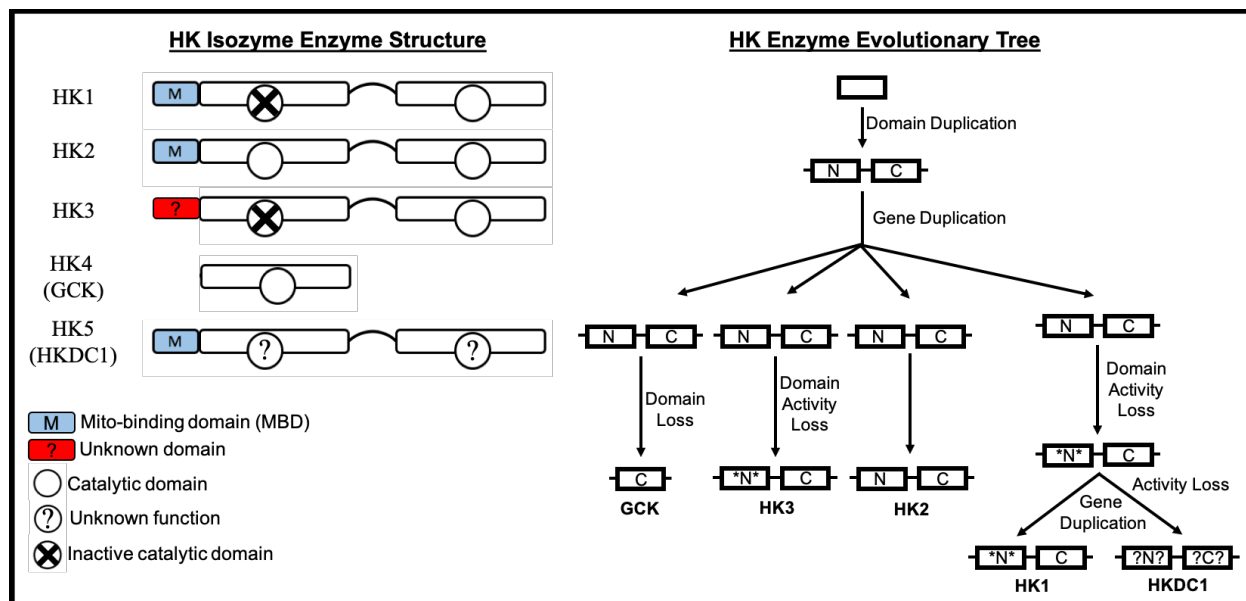


Figure 2. HK enzyme structure for different isoforms and evolutionary tree.

HK1, HK2, HKDC1 have a mitochondrial binding domain, while HK3 has an N-terminal domain with currently unknown function. HK1, HK2, HK3, HKDC1 are ~100kDa, while GCK is ~50kDa. Early in the evolution of HKs there was a gene duplication that resulted in an N and C terminal domain. Subsequent gene duplications likely from genome duplications on different chromosomes. Independent mutations resulted in loss of N-terminal domain to make GCK, Loss of N-terminal domain activity resulted in HK3, while HK2 retained both catalytic domain intact. Tandem gene duplication of HK1 resulted in HKDC1 located immediately upstream of HK1 gene. Adapted from (10).

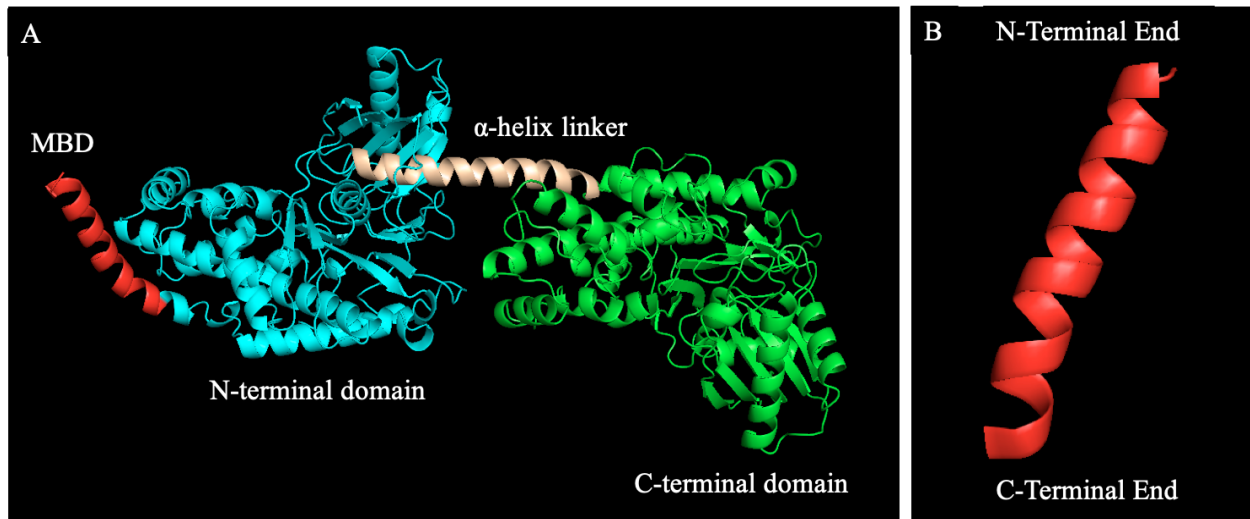


Figure 3. HK1 mitochondrial binding domain.

A) Cartoon diagram of HK1 generated using PyMOL of rat brain HK1 crystal structure PDB reference ID: 1bg3 (99). N-terminal MBD (red) of first 21 amino acids of rat brain HK1 crystal structure which confers mitochondrial binding, N-terminal domain (cyan), linker α -helical region (white), and C-terminal catalytic domain (green). B) magnified view of MBD α -helical secondary structure.

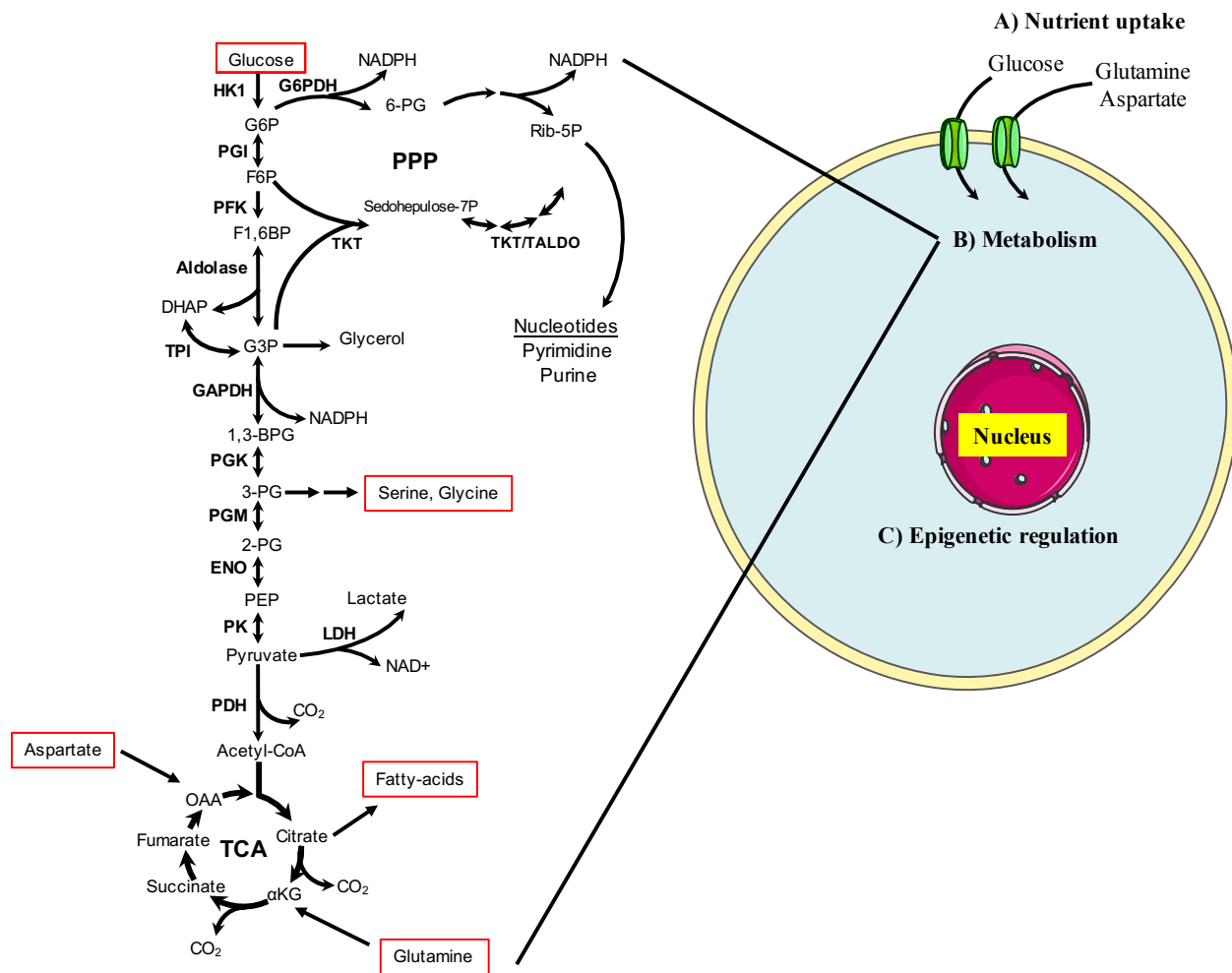


Figure 4. Metabolic hallmarks of cancer cells.

Cancer progression is characterized by distinct metabolic alterations including increased uptake of glucose, glutamine, and aspartate which sustain cellular growth and proliferation. These metabolic inputs feed several intracellular metabolic pathways that supply cancer cells with fuel and biomass to grow and divide. Changes in cellular metabolism ultimately funnel into epigenetic changes that tailor the cells metabolic function to meet the demands of tumor growth and replication. Adapted from (163).

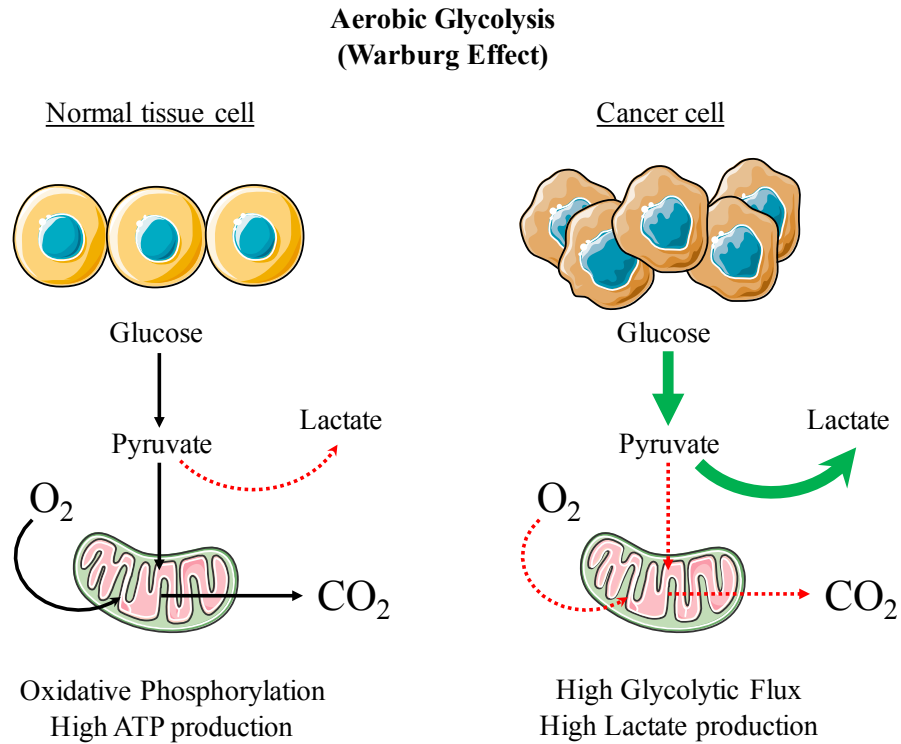


Figure 5. Aerobic glycolysis schematic.

Under normal conditions, cells typically utilize oxidative phosphorylation to meet their energetic demands. Cancer cells show a typified switch to glycolytic metabolism even in the face of abundant oxygen. This diversion of metabolites from entering the mitochondria results in high levels of lactate production (129).

Macrophage Polarization

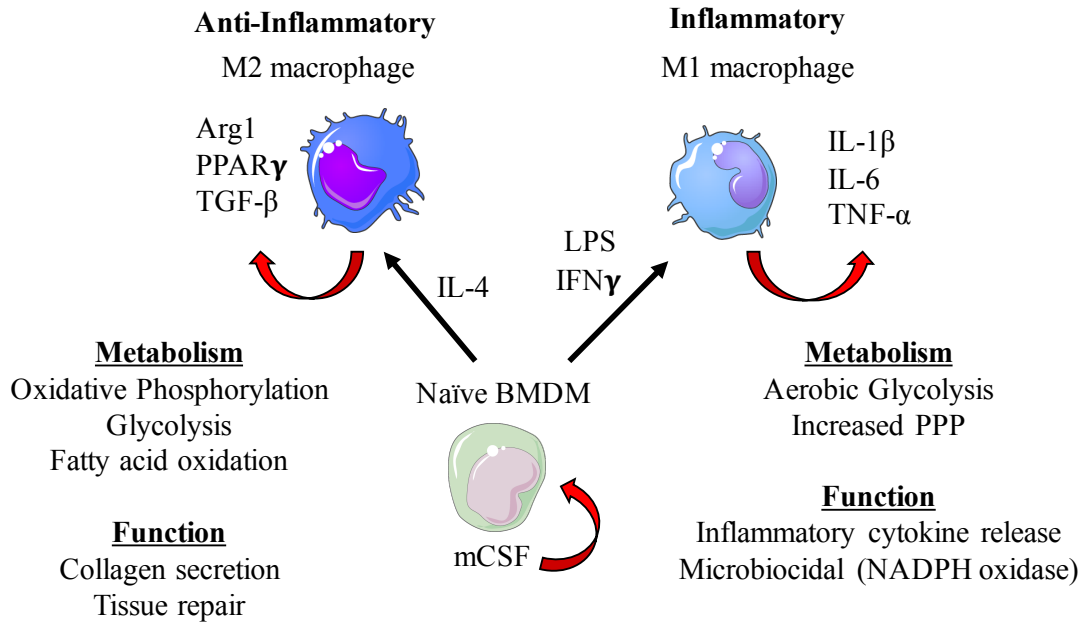


Figure 6. Macrophage polarization

Macrophages generally have two possible phenotypic fates. M2 macrophages are generated by stimulation with IL-4 and M1 macrophages are generated by stimulation with LPS and IFN γ . M1 macrophages elaborate an inflammatory program, while M2 macrophages function in an anti-inflammatory program.

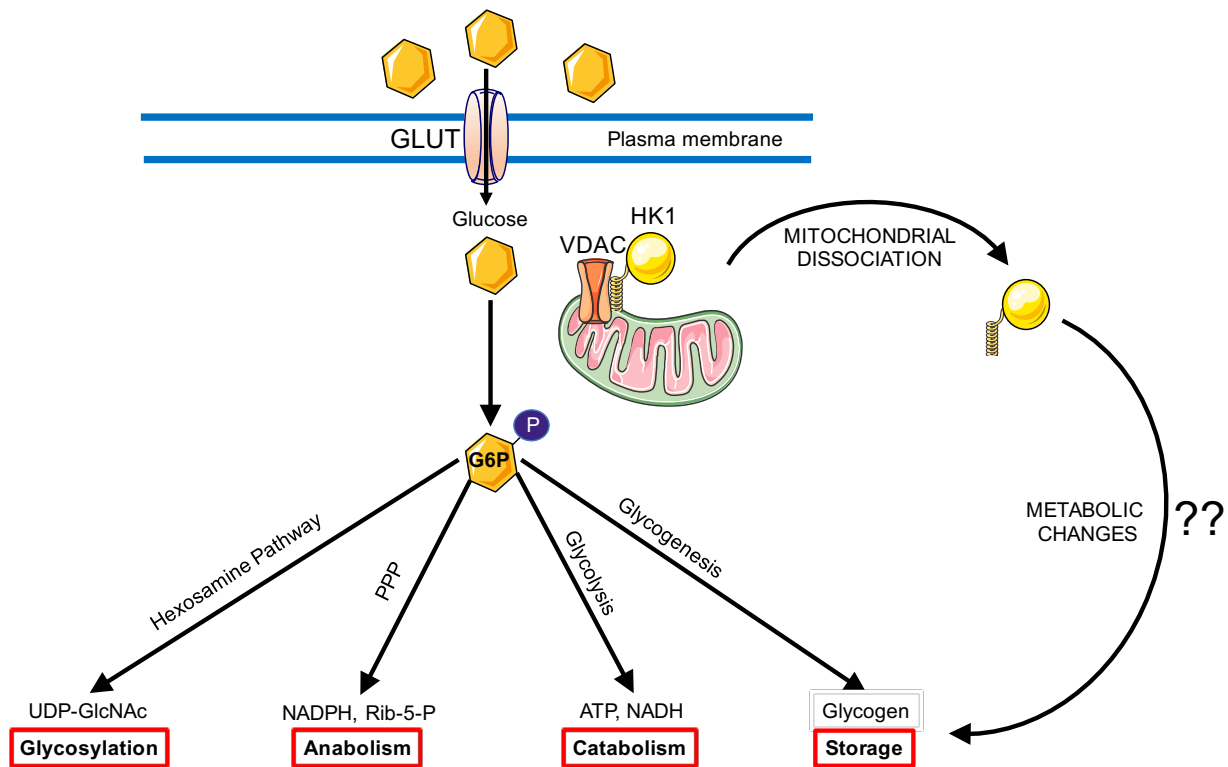


Figure 7. HK mitochondrial binding and metabolic effects.

We hypothesize that HK1 mitochondrial dissociation results in unique metabolic changes that play physiologic roles in regulating cellular function.

CHAPTER 2: ROLE OF HK1 MITOCHONDRIAL BINDING IN HEPG2 CELLS

ABSTRACT

Hexokinases (HKs) catalyze the first committed step in glycolysis by generating G6P, which is shunted down various anabolic and catabolic pathways. Interestingly, HK isoforms 1 and 2 contain a mitochondrial binding domain (MBD) that is thought to allow efficient coupling of glycolytic and oxidative metabolism in the cell. However, there is little research elucidating the impact of HK MBD in the preferential utilization of glucose in the cell toward anabolic or catabolic pathways. We hypothesize that dissociation of HK from the mitochondria shifts the cellular metabolic profile in favor of anabolic processes. Overexpression of HK1 with truncation of the MBD (TrHK1) ablates mitochondrial binding in cells, maintains HK activity same as full length HK1 (FLHK1), and displays no difference in G6P production *in vitro*. However, TrHK1 cells have significantly lower extracellular lactate and reduced intracellular pyruvate production, indicating a shift in glucose handling in the cell. Additionally, metabolomics data from cells overexpressing TrHK1 show reduced glycolytic and tricarboxylic acid (TCA) cycle metabolites (i.e., lactate, pyruvate, and citrate) and increased pentose phosphate pathway and nucleotide metabolites (i.e., ribulose-5P and ribose-5P) as compared to FLHK1. Our findings in cancer cells demonstrate that HK1 dissociation from the mitochondria changes the cells' utilization of glucose from catabolic to anabolic metabolism, which may help elucidate the role of glycolytic enzymes in regulating overall cellular metabolism in various pathologic conditions.

RESULTS

Over-expression of TrHK1 does not change enzymatic activity

HK1 contains a hydrophobic 21-amino acid N-terminal domain that confers outer-mitochondrial membrane (OMM) binding. To determine the cellular consequences of HK1 mitochondrial binding, we generated GFP-tagged constructs of full-length HK1 (FLHK1) and truncated HK1 (TrHK1) that lack the MBD, along with an empty vector (EV) control that lacks an insert (**Figure 8A**). These constructs were transfected into HepG2 cells, and their cellular distribution was assessed by GFP fluorescence. As expected, FLHK1 localized to the mitochondria, while TrHK1 displayed diffuse cellular distribution (**Figure 8B-C**). HepG2 cells expressing TrHK1 displayed similar HK activity as FLHK1 (**Figure 8D-E**), confirming that deletion of the MBD does not affect the ability of HK1 to phosphorylate glucose. These results indicate that altering the subcellular localization of HK1 by removing the MBD does not impair its enzyme activity. These results indicate that altering the subcellular localization of HK1 by removing the MBD does not impair its enzyme activity.

TrHK1 expressing cells have altered glycolytic metabolism

Since there was no difference in glucose phosphorylation with HK1 MBD deletion, we then assessed whether glucose metabolism was altered by the removal of the HK1 MBD. The rate of extracellular lactate production in TrHK1 cells was significantly lower than FLHK1 cells (**Figure 9A**). Furthermore, HepG2 cells expressing TrHK1 displayed lower glycolysis, as assessed by extracellular acidification rate (ECAR), and extracellular lactate production (**Figure 9B**). Together, these results indicate that while removal of the MBD does not impair HK1 enzyme activity, this modification does alter glucose flow through glycolysis.

We then performed $^{13}\text{C}_6$ -glucose flux metabolomics in HepG2 cells with FLHK1 or TrHK1 overexpression and assessed glycolytic metabolic pathways (**Figure 10A**). We saw a significant increase in glycolytic intermediates above the level of GAPDH (glycerol-3P and glycerate) (**Figure 10B**), and an increase in $^{13}\text{C}_6$ -glucose incorporation into the PPP intermediate sedoheptulose-7-P and nucleotides ADP, AMP, ATP, dGDP and GTP were higher in cells overexpressing TrHK1 (**Figure 10C**), in line with increased *de novo* nucleotide synthesis through the PPP. Additionally, we found increased NADPH/NADP⁺ ratio in TrHK1 expressing cells (**Figure 10D**), which is an indicator of increased oxidative PPP flux. Consistent with the observed decrease in glycolytic flux in TrHK1 cells, we found less $^{13}\text{C}_6$ -glucose incorporation into lower glycolytic products such as 2/3-Phosphoglycerate, lactate, and pyruvate (**Figure 10E**) and TCA cycle intermediates citrate, succinate and fumarate (**Figure 10F**) in cells overexpressing TrHK1 compared to FLHK1. Thus, these data suggest that subcellular localization of HK1 shift G6P flux independent of its enzymatic function.

TrHK1 Expressing Cells Have Reduced GAPDH Activity

Our data thus far indicates that there may be a metabolic block at the level of GAPDH. To confirm this, we performed steady-state metabolomics in TrHK1 and FLHK1 cells (**Figure 11A**) and show a metabolic profile consistent with decreased glycolysis below the level of GPADH and increased metabolites above GAPDH (i.e., PPP, nucleotides, and glycerate) (**Figure 11B**). Furthermore, we saw increased NADH/NAD⁺ ratios which is consistent with lower lactate production (**Figure 11C**). Importantly, GAPDH activity was significantly impaired in TrHK1 expressing cells as compared to FLHK1, further supporting our metabolomics findings (**Figure**

11D). Additionally, energy charge of the cell was not significantly altered between TrHK1 and FLHK1 cells (**Figure 11E**).

TrHK1 expression increases cell proliferation

Given the metabolic changes observed in TrHK1 cells, we next assessed whether these perturbations had any consequence on HepG2 cell proliferation. We performed cell proliferation assay over 48hrs and found that TrHK1 cells had higher proliferative capacity as compared to EV or FLHK1 cells (**Figure 12A-D**).

Mitochondrial Depolarization Induces Reversible HK1 Mitochondrial Dissociation

In an attempt to find a more physiologic context for HK1 mitochondrial dissociation, we stimulated FLHK1 cells with LPS and Carbonyl cyanide m-chlorophenyl hydrazone (CCCP), which are known to cause membrane depolarization (164). We confirmed that LPS and CCCP induced mitochondria depolarization as assessed by image analysis of Tetramethylrhodamine (TMRE) intensity (**Figure 13A-B**). Interestingly, FLHK1 was reversibly dissociated from mitochondria after 1hr and returned to baseline after 6 hrs with LPS stimulation, however CCCP maintained both low TMRE signal and FLHK1 mitochondrial dissociation (**Figure 13C**). These findings suggest that mitochondrial membrane potential may play a role in regulating the mitochondrial-to-cytosolic localization dynamics of HK1.

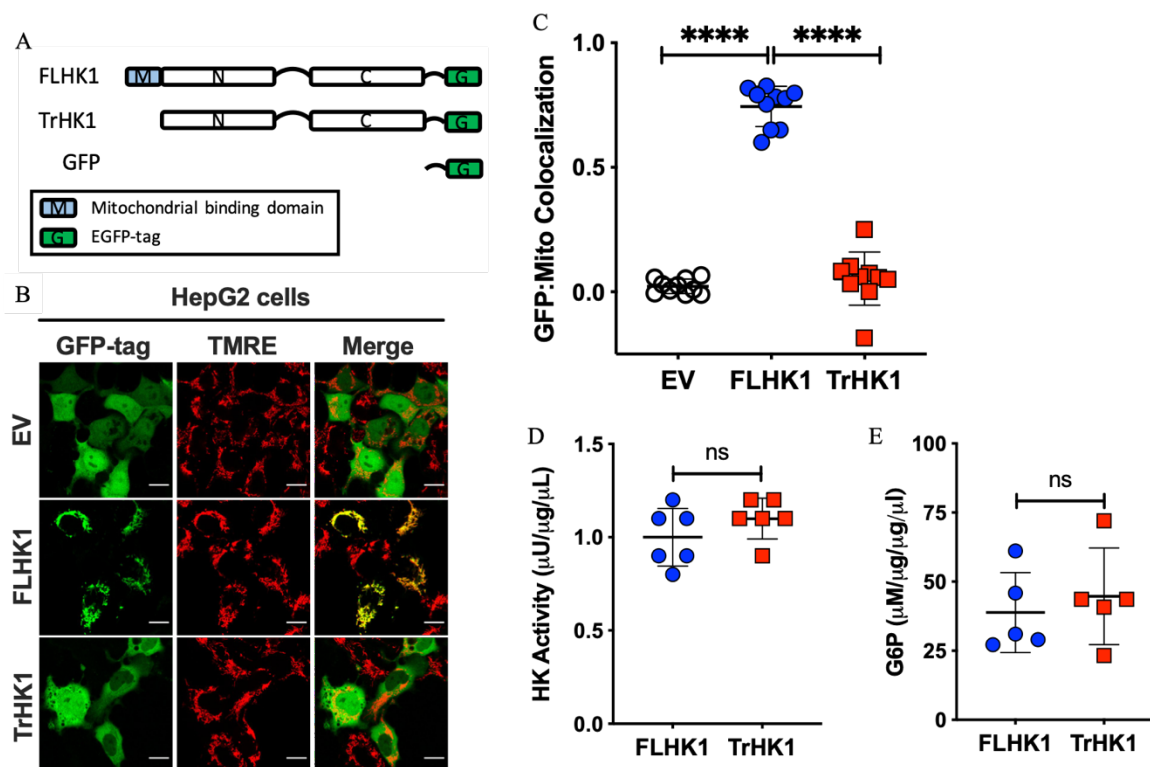


Figure 8. TrHK1 overexpression does not affect intrinsic enzymatic activity.

A. Schematic of EV, FLHK1, and TrHK1 overexpression lentivirus plasmids. **B-C.** Live-cell imaging of GFP-tag fluorescence from EV, FLHK1 and TrHK1 overexpressing HepG2 cells with TMRE (mitochondrial dye) (B) and colocalization analysis of IF images (C) using Pearson's correlation coefficient calculated per cell between GFP-tag (green) and TMRE (red) image channels (n=10 cells per condition, one-way ANOVA and Tukey's post-hoc test, mean \pm SD, colocalization analysis performed using *Coloc-2 macro* on Fiji/ImageJ, scale bar = 15 μm). **D.** HK activity assay normalized to total protein from HepG2 cells (n=6 replicates per condition, unpaired t-test, mean \pm SD). **E.** G6P quantification normalized to total protein from HepG2 cells (n=5 replicates per condition, unpaired t-test, mean \pm SD).

HepG2 cells

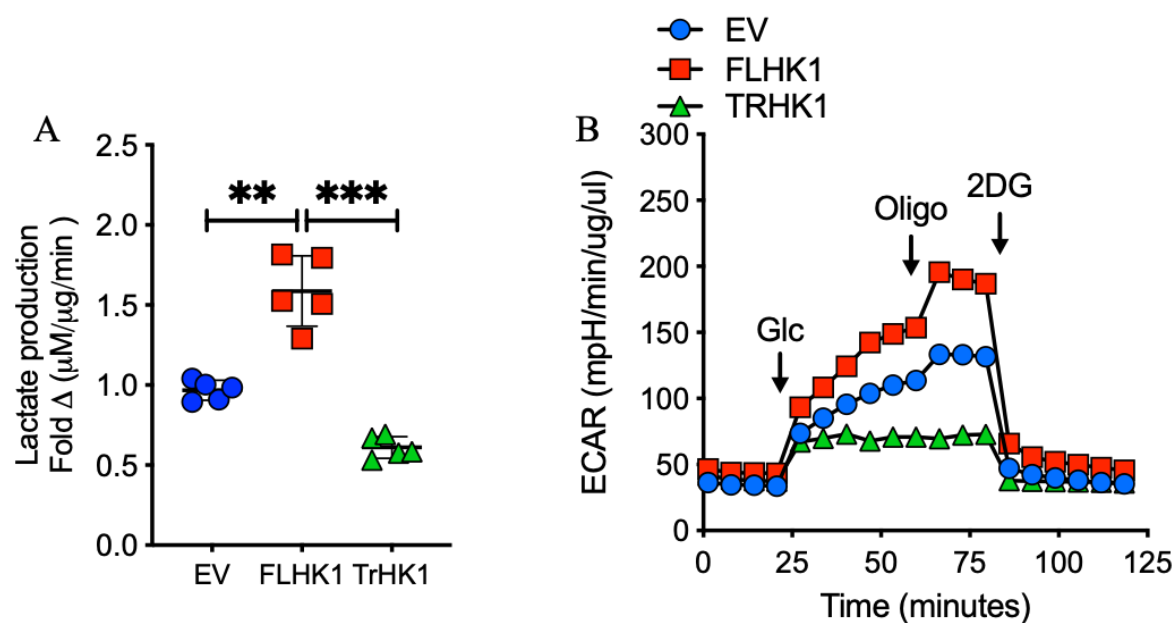


Figure 9. TrHK1 expression reduces lactate production.

A. Extracellular lactate quantification in HepG2 cells with overexpression of FLHK1 or TrHK1 (n=6 replicates per condition, unpaired t-test, mean \pm SD). **B.** ECAR trace of HepG2 cells with overexpression of FLHK1 or TrHK1 (n=5-8 replicates per condition, repeated measures two-way ANOVA, mean \pm SD).

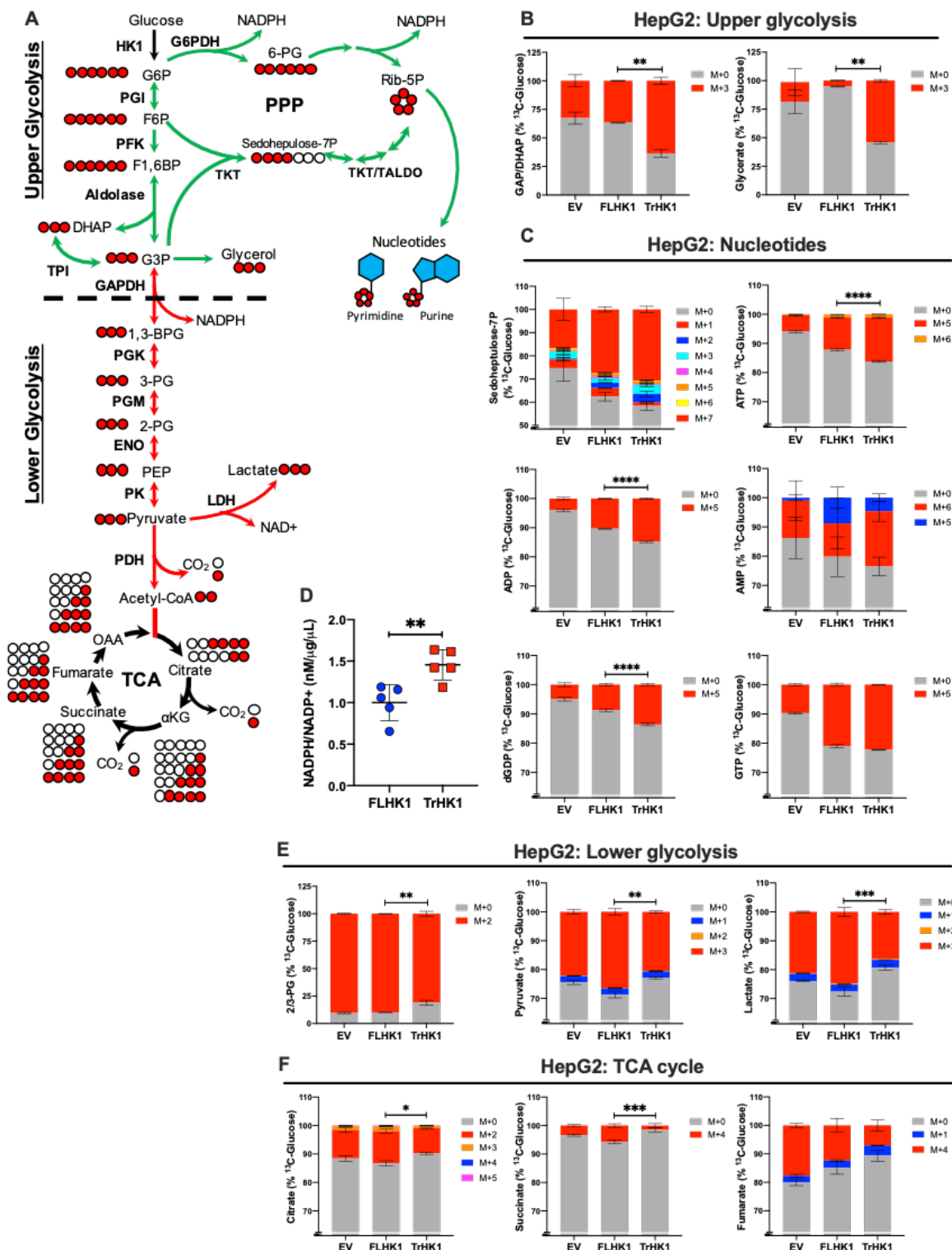
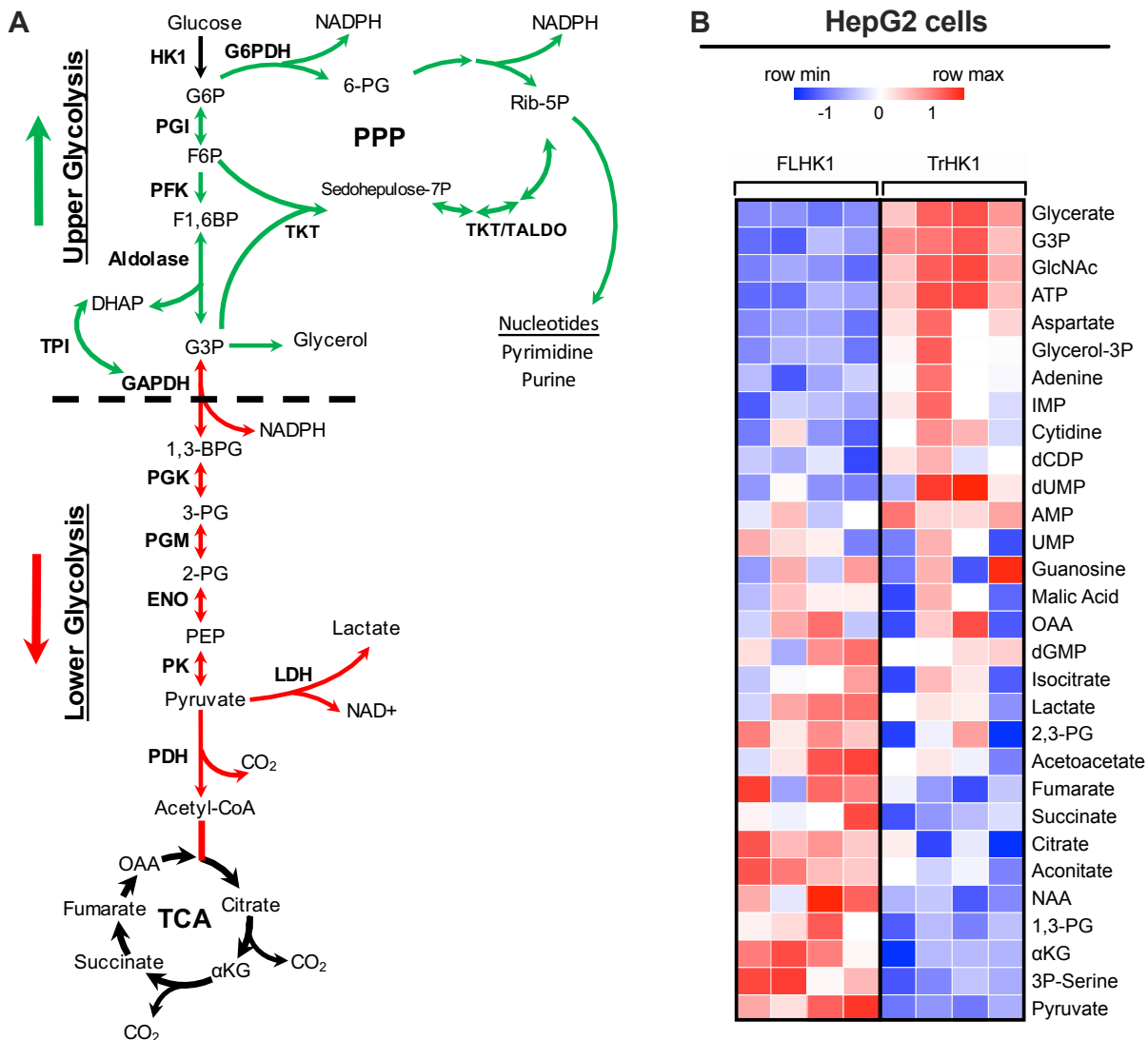


Figure 10. TrHK1 cells have altered glucose flux and increased PPP.

A. Schematic of ^{13}C -glucose carbon labeling through glycolysis (upper and lower glycolysis), PPP,

de novo nucleotide synthesis and TCA cycle. **B.** ^{13}C -glucose incorporation into upper glycolytic metabolites, GAP/DHAP and glycerate in HepG2 cells with overexpression of EV, FLHK1 or TrHK1 (n=3 replicates per condition, two-way ANOVA and Tukey's post-hoc test, mean \pm SEM). **C.** ^{13}C -glucose incorporation into PPP metabolite sedoheptulose-7P and *de novo* nucleotides; ADP, AMP, ATP, dGDP, and GTP in HepG2 cells with overexpression of EV, FLHK1 or TrHK1 (n=3 replicates per condition, two-way ANOVA and Tukey's post-hoc test, mean \pm SEM). **D.** NADPH/NADP⁺ ratio normalized to total protein in HepG2 cells with overexpression of FLHK1 or TrHK1 (N=5 replicates per condition, unpaired t-test, mean \pm SD). **E.** ^{13}C -glucose incorporation into lower glycolytic metabolites, 2/3-PG, pyruvate, and lactate, \pm 4hrs LPS treatment in HepG2 cells with overexpression of EV, FLHK1 or TrHK1 (n=3 replicates per condition, two-way ANOVA and Tukey's post-hoc test, mean \pm SD). **F.** ^{13}C -glucose incorporation into TCA metabolites, citrate, succinate, and fumarate in HepG2 cells with overexpression of EV, FLHK1 or TrHK1 (n=3 replicates per condition, two-way ANOVA and Tukey's post-hoc test, mean \pm SEM).



HepG2 cells

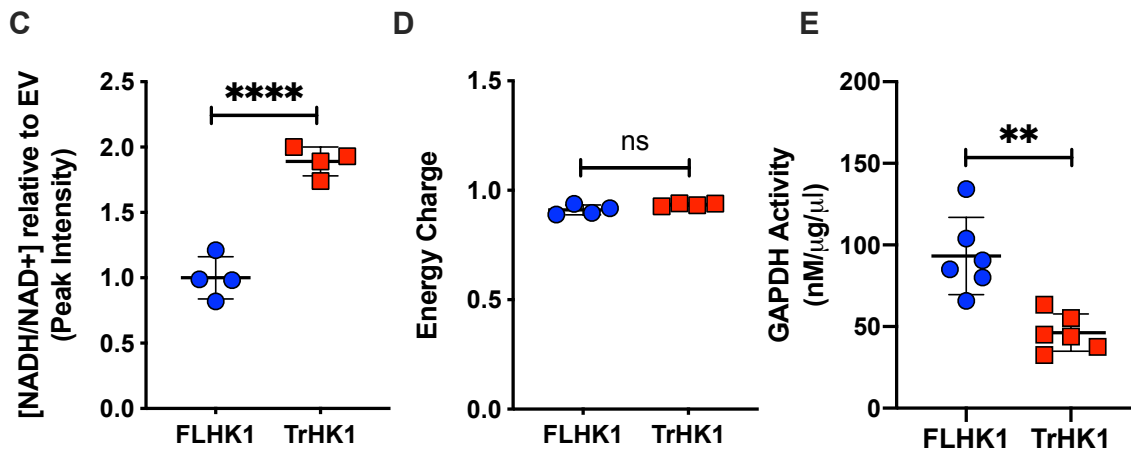


Figure 11. TrHK1 expressing cells display reduced GAPDH enzymatic activity.

A. Schematic of branch points of G6P and glycolytic pathway above and below the level of GAPDH. Green arrow indicates increased metabolites and red depicts reduced levels of metabolites. **B.** Heatmap of steady-state metabolomics performed in HepG2 cells with FLHK1 and TrHK1 overexpression all normalized to EV metabolite levels and total-iron-content in the cells (heatmap generated using MetaboAnalyst). **C.** NADH/NAD⁺ ratio measurement derived from steady-state metabolomics peak-mass-spectrometry (MS) values for NADH and NAD⁺ (n=4 mice per condition, unpaired t-test, mean ± SD). **D.** Energy charge of the cell calculated based on steady-state metabolomics data using ATP, AMP, and ADP metabolite peak-MS values. Formula for energy charge $\frac{[ATP]+0.5[ADP]}{[ATP]+[ADP]+[AMP]}$ (n=4 mice per condition, unpaired t-test, mean ± SD). **E.** GAPDH activity normalized to total protein in HepG2 cells between FLHK1 and TrHK1 normalized to EV (n=6 replicates per condition for, unpaired t-test, mean ± SD).

HepG2 cells

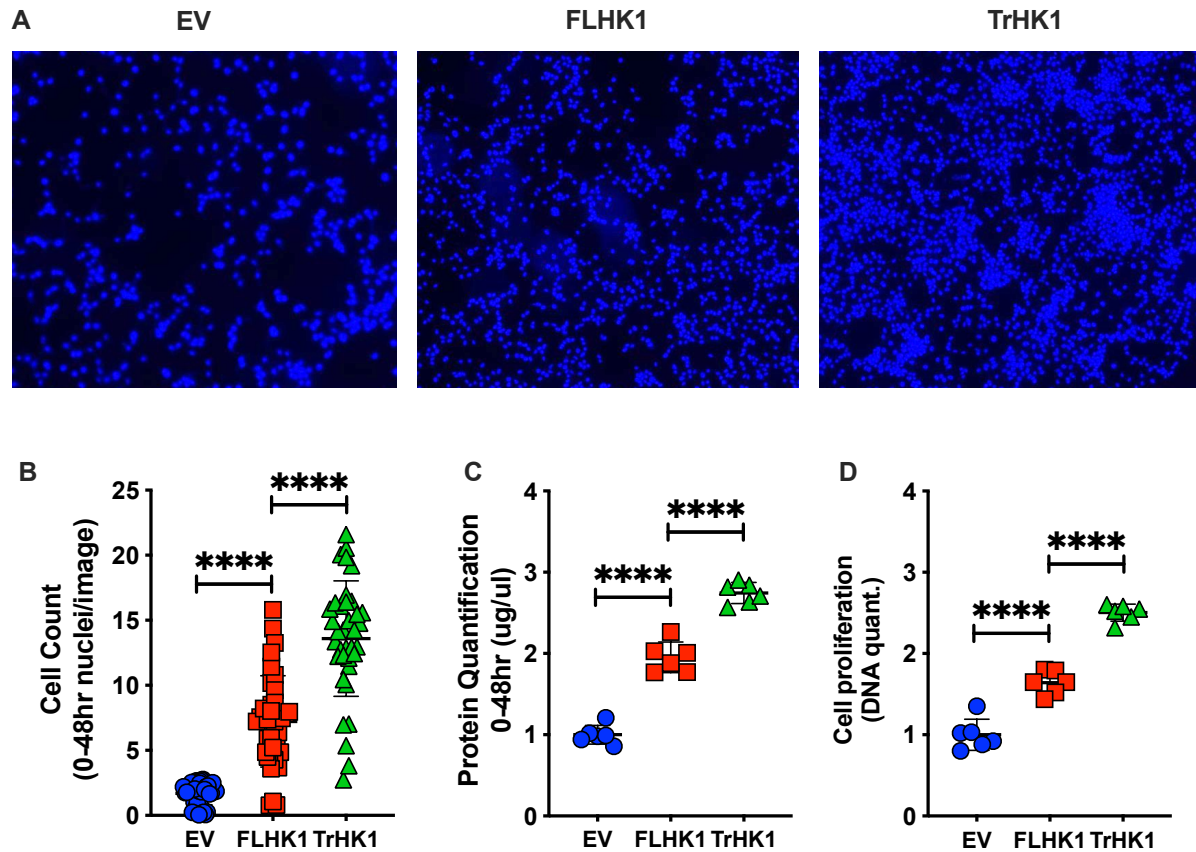


Figure 12. Cells overexpressing TrHK1 have increased proliferation.

A. Epi-fluorescent images of nuclei count stained with Hoechst. **B.** 48hr cell proliferation measured by cell count measured from images in A, normalized to 0hr plate (n=30 images per condition, one-way ANOVA and Tukey's post-hoc test, mean \pm SD) **C.** Protein quantification after 48hrs normalized to 0hr plate (n=6 replicates per condition, one-way ANOVA and Tukey's post-hoc test, mean \pm SD). **D.** Cell proliferation measure on day 0 and day 2 measured by DNA quantification using CyQuant reagent (n=6 replicates per condition, one-way ANOVA and Tukey's post-hoc test, mean \pm SD).

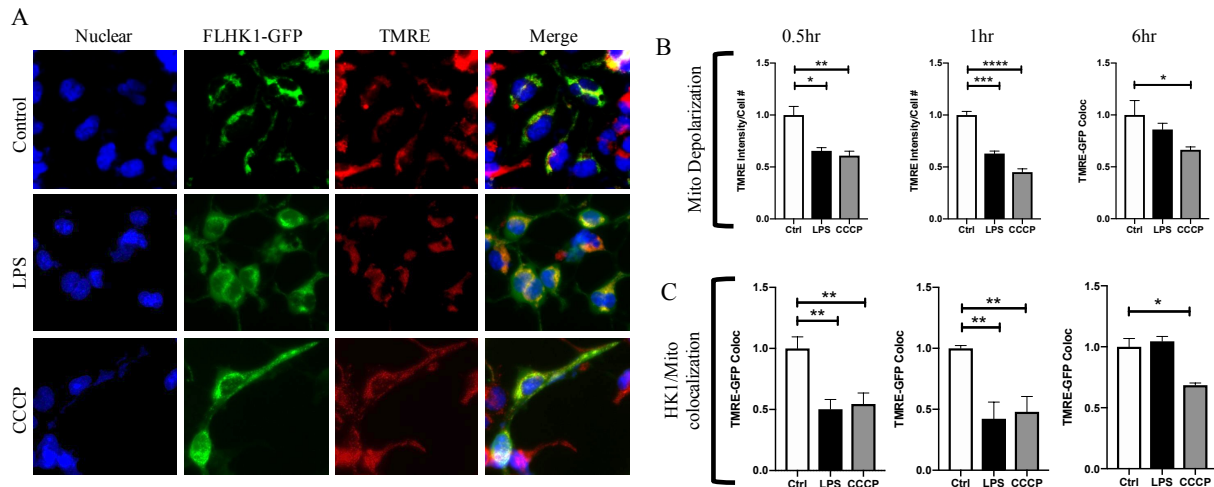


Figure 13. Reversible HK1 mitochondrial dissociation is induced by mitochondrial depolarizing stimuli.

A. Epi-fluorescent images of TMRE stained FLHK1-GFP cells treated with CCCP and LPS. **B.** Mitochondrial depolarization assessed by TMRE intensity measurements from >10 images per condition normalized to total cell number (n=10 replicates per condition, one-way ANOVA and Tukey's post-hoc test, mean \pm SD). **C.** HK1 to mitochondrial colocalization comparing GFP and TMRE signal using Image J (n=10 replicates per condition, one-way ANOVA and Tukey's post-hoc test, mean \pm SD).

**CHAPTER 3: EFFECT OF HK1 MITOCHONDRIAL BINDING ON MACROPHAGE
METABOLISM**

ABSTRACT

Metabolic reprogramming plays a central role in innate immune cell activation and is critical for macrophage mediated inflammation. Lipopolysaccharide (LPS) stimulated macrophages initiate a metabolic switch characterized by reduced mitochondrial respiration and increased glycolytic flux. Mitochondrial bound hexokinase-1 (HK1) catalyzes the first committed step of glycolysis and is critical for inflammatory macrophage activation. We show that HK1 mitochondrial dissociation increases inflammatory cytokine production and secretion in vivo and in vitro, and shifts glycolytic flux in favor of pentose phosphate pathway (PPP) metabolites by inhibiting glyceraldehyde-3-phosphate dehydrogenase (GAPDH) activity. Co-Immunoprecipitation (CoIP) and proteomic analysis of mitochondrial unbound HK1 revealed S100A8 and S100A9 as potential binding partners. S100A8/A9, also called calprotectin, is known to form an enzyme complex with inducible Nitric Oxide Synthase (iNOS) to mediate GAPDH S-nitrosylation and attenuate its enzymatic activity. Our data suggests that HK1 subcellular localization modulates innate immune inflammation by coordinating glycolytic flux in activated macrophages.

RESULTS

Generation of MBD deleted HK1 mouse model

To determine the physiologic function of the HK1 MBD, we generated a mouse model lacking the MBD of the endogenous HK1. The approach to remove the MBD is depicted in **Figure 14**. Guide RNAs (gRNAs) were designed to induce a double strand break (DSB) near the 5' ATG start codon of HK1 in exon 1, and a DNA template containing an M-DYKDDDDK (Methionine-FLAG-tag) sequence with flanking homology arms to the HK1 gene near exon 1 was introduced into fertilized zygotes and implanted into surrogate mice. Homology-directed repair (HDR) of the DSB resulted in replacement of the coding region of the HK1 MBD with the Methionine-FLAG-tag sequence (**Figure 14**). Homozygote mice with this mutation, designated as $\Delta E1HK1$ herein, were born in normal Mendelian ratios (**Figure 15A**) and displayed no overt changes in weight or difference in whole body glucose homeostasis as assessed by glucose tolerance test (GTT) and insulin tolerance test (ITT) compared to wild type (WT) control mice (**Figure 15B-D**). Moreover, hematologic analysis of whole blood from these mice revealed no difference in complete blood cell count (CBC) or white blood cell (WBC) differential (**Figure 15E-F**). To assess whether removal of the endogenous HK1 MBD alters cellular distribution of the protein, we isolated mitochondrial and cytosolic fractions from solid organs with high HK1 expression (brain, kidney and lungs), and showed that HK1 was predominantly present in the cytosolic fraction in organs isolated from $\Delta E1HK1$ mice (**Figure 15G**). We also performed HK activity assay on whole brain and lung tissue lysates and found no difference in activity between the $\Delta E1HK1$ and WT mice (**Figure 15H-I**).

Immunofluorescence (IF) studies in bone marrow-derived macrophages (BMDMs) and peritoneal macrophages (PMs) isolated from WT and $\Delta E1HK1$ mice also confirmed lack of HK1

localization to the mitochondria (**Figure 16A-B and C-D**). Additionally, BMDMs isolated from WT and $\Delta E1HK1$ mice displayed similar glucose uptake and phosphorylating activity, consistent with our findings in solid organs from $\Delta E1HK1$ mice and HepG2 overexpression cells (**Figure 16E-F**). Among the five different HK isoforms, only HK1 and HK3 displayed a dose-dependent increase in their mRNA levels in response to lipopolysaccharide (LPS) in WT BMDMs (**Figure 17**). These results suggest an important role for HK1 in LPS-activated macrophages and provides an ideal system to study the MBD of HK1 in the absence of confounding changes to other mitochondrial bound HKs.

Loss of HK1 Mitochondrial Binding Alters Glucose Flux

Like our overexpression studies in HepG2 cells, $\Delta E1HK1$ BMDMs had significantly lower lactate production (**Figure 18A**). Furthermore, there was a significant reduction in glycolysis upon immediate stimulation with LPS (**Figure 18B-C**) which persisted up to at least 4 hours after LPS treatment (**Figure 20D-E**). Collectively, these results suggest that HK1 mitochondrial dissociation reduces glycolysis independently from its enzymatic activity.

To further elucidate the mechanism responsible for the reduction in glycolysis observed in LPS-activated $\Delta E1HK1$ BMDMs, we performed $^{13}C_6$ -glucose tracing metabolomics in naïve and LPS-stimulated BMDMs derived from WT and $\Delta E1HK1$ mice. We measured ^{13}C -glucose incorporation through glycolysis, tricarboxylic acid (TCA) cycle, and PPP (**Figure 19A**). While there was no difference in G6P levels between WT and $\Delta E1HK1$ BMDMs (**Figure 19B**), $\Delta E1HK1$ BMDMs displayed higher $^{13}C_6$ -glucose incorporation into glyceraldehyde-3-phosphate/dihydroxyacetone phosphate (GAP/DHAP) (**Figure 19C**) and PPP intermediates 6-phosphogluconate and sedoheptulose-7-Phosphate after LPS activation (**Figure 19D-E**).

Consistent with increased PPP metabolism, NADPH/NADP⁺ ratio was significantly increased in Δ E1HK1 BMDMs (**Figure 19F**). Moreover, we observed decreased ¹³C₆-glucose incorporation of glycolytic intermediates below the level of GAPDH including 2/3-phosphoglycerate (2/3-PG), pyruvate, and lactate in LPS-treated BMDMs from Δ E1HK1 as compared to WT controls (**Figure 19G-I**). The TCA cycle intermediate citrate showed decreased ¹³C₆-glucose incorporation (**Figure 19J**), however, we did not observe a change in glucose-derived carbon incorporation into α -ketoglutarate (α KG), succinate, or fumarate between WT and Δ E1HK1 BMDMs (**Fig. 19K-M**). Since unlabeled glutamine can supply carbons into the TCA cycle through anaplerotic conversion to α KG, this may explain the lack of change in ¹³C₆-glucose labeling of TCA cycle metabolites downstream of citrate (153). These results are consistent with our earlier extracellular flux studies in HepG2 cells and BMDMs showing reduced glycolytic rate and extracellular lactate production with HK1 mitochondrial dissociation.

Finally, we performed unbiased metabolomics in whole brain and heart isolates, which are tissues known to have high HK1 expression. Whole brain and heart steady-state metabolomics revealed increased PPP metabolites (i.e., sedoheptulose 7-phosphate, 6-PG, ribose-5-phosphate, GAP, and erythrose 4-phosphate) in tissues from Δ E1HK1 mice compared to WT controls (**Figure 20A-C**).

Constitutive HK1 Mitochondrial Dissociation Increases Inflammation

Glycolysis serves a vital role in the initiation and maintenance of proper effector function of activated macrophages (155,26,165). Our results thus far indicate that HK1 dislocation into the cytoplasm results in increased PPP. To further study this process and its underlying mechanism, we focused our studies on cells with functional PPP. Thus, studies hereafter were done in

macrophages from $\Delta E1HK1$ mice. PPP metabolism has been shown to be upregulated in LPS activated macrophages and is necessary for proper inflammatory activation (166–169). We first assessed the consequence of these changes on the effector function of LPS-activated macrophages. We noted a significant increase in inflammatory cytokines IL-1 β , IL-6 and TNF α mRNA expression in BMDMs from $\Delta E1HK1$ mice compared to WT mice in response to LPS (**Figure 21A-C**). In addition, BMDMs from $\Delta E1HK1$ mice displayed increased IL-1 β protein production after LPS treatment (**Figure 21D**).

PMs isolated from $\Delta E1HK1$ mice also showed increased IL-1 β , IL-6 and TNF α mRNA expression relative to WT cells when stimulated with LPS, similar to BMDMs (**Figure 21E-G**). PMs from $\Delta E1HK1$ mice also had increased IL-1 β protein secretion after LPS treatment, as assessed by ELISA (**Figure 21H**). Furthermore, we extracted mRNA from the spleens of mice treated with LPS or PBS for 4 hours, and found a significant increase in IL-1 β , IL-6, and TNF α mRNA in spleens from $\Delta E1HK1$ mice compared to WT mice treated with LPS (**Figure 21I-K**). Lastly, we performed an *in vivo* LPS-induced endotoxemia survival experiment in these mice (**Figure 21L**). Three-days after sub-lethal LPS administration, $\Delta E1HK1$ mice had significantly reduced survival compared to littermate controls (**Figure 21M**). Collectively, these results indicate that lack of HK1 mitochondrial binding increases inflammatory cytokine production and impairs survival in response to LPS-induced endotoxemia.

As expected, LPS-activated BMDMs from $\Delta E1HK1$ and WT mice showed a similar increase in mRNA expression of HK1, while there was no change in the levels of HK2 mRNA (**Figure 22A-B**). We also assessed mRNA levels of anti-inflammatory cytokines peroxisome proliferator-activated receptor gamma (PPAR γ) and carbohydrate kinase-like protein (CARKL) in BMDMs, and found no difference in their expression between $\Delta E1HK1$ and WT cells (**Figure**

22C-D). Intracellular protein expression of pro-IL-1 β (molecular weight ~35 kDa) in control and LPS-treated BMDMs showed an increase in Δ E1HK1 compared to WT cells, and addition of ATP induced cleavage and secretion of IL-1 β in both groups (**Figure 22E-F**). Moreover, using extracellular media from BMDMs treated with LPS+ATP, we demonstrate that IL-1 β protein secretion increased in Δ E1HK1 BMDMs compared to WT controls (**Figure 22G**).

PPP Inhibition Reverses Hyper-Inflammation Induced by HK1 Mitochondrial Dissociation

PPP is upregulated in pro-inflammatory (M1) macrophages and neutrophils, and the reduction of PPP reduces M1 macrophage cytokine production (168,169). Additionally, the negative regulator of the non-oxidative branch of PPP, carbohydrate kinase-like protein (CARKL) serves as a metabolic regulator of macrophage polarization (170), and the high levels of NADPH produced by the PPP are utilized by M1 macrophages during the phagocytic respiratory burst (171,172). Thus, to determine whether the hyper-inflammatory response seen in Δ E1HK1 mice is dependent on the increased PPP flux, we used two methods to inhibit the PPP: 1) 6-aminonicotinamide (6AN), which is metabolized into an NADP⁺ analog and competitively inhibits NADPH-producing enzymes 6-phosphogluconate dehydrogenase (PGD) and glucose 6-phosphate dehydrogenase (G6PD) enzymes, and 2) oxythiamine (OT), a thiamine antagonist, which suppresses the non-oxidative synthesis of ribose by inhibiting the transketolase (TKT) enzyme (**Figure 23A**) (173,174). Treatment of BMDM from Δ E1HK1 mice with LPS caused a higher release of IL-1 β , as assessed by ELISA, while both 6-AN or OT reversed this increase (**Figure 23B**).

The increase in IL-1 β and IL-6 mRNA levels in BMDM of Δ E1HK1 mice were also reversed with both 6-AN (**Figure 23C**) and OT (**Figure 23D**). To confirm these results, we also

primed BMDM with IFN- γ , followed by LPS treatment and addition of either 6-AN or OT and measured IL-1 β and IL-6 mRNA. The increase in IL-1 β and IL-6 mRNA levels in BMDM of Δ E1(Flag)HK1 mice were reversed with 6-AN and OT (**Figure 23E**). Additionally, we show that there was no significant difference in the mRNA expression of enzymes involved in glycolysis, PPP, pyruvate transport, or TCA cycle metabolism with and without LPS treatment of BMDMs between WT and Δ E1HK1 mice (**Figure 24A-F**), indicating that the mechanism for the glycolytic block causing increased PPP metabolism is not at the transcriptional level. Together, these studies imply that the mechanism by which HK1 dislocation from mitochondria causes an increase in cytokine production is through increased PPP metabolism.

GAPDH Activity is Attenuated in Macrophages with HK1 Mitochondrial Detachment

We next studied the mechanism by which cytosolic HK1 reduces glycolysis and shifts G6P towards the PPP. Analysis of the $^{13}\text{C}_6$ -glucose labeling metabolomics indicated an increase in metabolites in upper glycolysis (i.e., metabolites upstream of the GAPDH-mediated step in glycolysis) and a reduction in metabolites in lower glycolysis (i.e., downstream of GAPDH), suggesting a block in glycolysis at the level of GAPDH. As expected PMs and BMDMs from Δ E1HK1 mice displayed significantly decreased GAPDH activity at baseline and with LPS treatment (**Figure 25A-B**). The difference in GAPDH activity of BMDMs between WT and Δ E1HK1 mice was abolished by the GAPDH inhibitor, CGP3466 (**Figure 25C**). CGP3466 also increased IL-1 β mRNA expression in WT BMDMs to the level of the hyper-inflamed Δ E1HK1 BMDMs (**Figure 25D**).

We next assessed the effects of acute dislocation of HK1 from the mitochondria (as opposed to constitutive dislocation of the protein, as occurs in the Δ E1HK1 mice) on GAPDH

activity. Clotrimazole (CLT), an antifungal drug, is known to dislocate HKs from the mitochondria(175–177). As expected, CLT caused a significant increase in HK1 dislocation from the mitochondria in WT BMDMs (**Figure 25E-F**). Despite minimal change in cytokine mRNA levels with CLT at baseline, stimulation with LPS induced a significant increase in the mRNAs of IL-1 β , IL-6 and TNF α in the CLT-treated cells as compared to vehicle treated controls (**Figure 25G-I**). Finally, CLT also caused a significant decrease in GAPDH activity in RAW264.7 cells after LPS treatment (**Figure 25J**). These results indicate that both acute and constitutive displacement of HK1 from the mitochondria cause a significant reduction in GAPDH activity and accentuates inflammatory cytokine production after LPS treatment.

Moreover, in RAW264.7 cells, GAPDH activity was decreased with the addition of CGP3466 in the presence of LPS (**Figure 26A**), and the increase in IL-1 β mRNA with LPS was amplified with the addition of CGP3466 (**Figure 26B**). Additionally, treatment of RAW264.7 cells with koningic acid (KA), another potent inhibitor of GAPDH, resulted in increased IL-1 β , IL-6 and TNF α mRNA expression after LPS treatment (**Figure 26C-E**).

We also performed steady-state metabolomics in HepG2 cells with TrHK1 overexpression and observed a similar metabolic block at the level of GAPDH (**Figure 27A-B**). While there was an increase in the reductive state of the cell (as assessed by the measurement of NADH/NAD⁺ levels) with overexpression of TrHK1 (**Figure 28A**), the energy charge was not different between FLHK1 and TrHK1 overexpression cells (**Figure 28B**). Consistent with findings in BMDMs, overexpression of TrHK1 was associated with a significant decrease of GAPDH activity (**Figure 28C**).

Cytosolic HK1 Mediates GAPDH Nitrosylation through S100A8/9 Binding

We next studied the mechanism of GAPDH inactivation with HK1 mitochondrial dissociation. We hypothesized that cytosolic HK1 binds to a distinct set of proteins compared to the mitochondrial bound HK1. To test this, we performed an unbiased immunoprecipitation (IP) experiment followed by mass spectrometry (MS) in HepG2 cells with overexpression of FLHK1 and TrHK1. Proteomic analysis yielded 611 unique spectra which corresponded to 175 identified proteins (**Figure 29A**). Biological gene-ontology (GO) term analysis revealed several differences between the two treatments, as depicted in **Figure 29B** (178). VDAC proteins (VDAC1, VDAC2, and VDAC3) were enriched in the FLHK1 pulldown, which is expected since HK1 in its native form binds to these proteins on the OMM (**Figure 29C**) (102,117). Among proteins enriched in cells overexpressing TrHK1, there was an over-representation of the S100 family of proteins, of specific interest were S100A8 and S100A9, which are known to have inflammatory functions (**Figure 29C-D**)(179). We confirmed that S100A8 binds strongly to the truncated HK1 via co-IP in HepG2 cells overexpressing either FLHK1 or TrHK1 (**Figure 30A-B**).

We then confirmed this finding in BMDMs from $\Delta E1HK1$ mice and found S100A8 as a binding partner of cytosolic HK1 in these cells (**Figure 30C-D**). S100A8 and S100A9 form a protein dimer called calprotectin that can bind to iNOS in macrophages and mediate trans-S-nitrosylation of GAPDH (SNO-GAPDH) and inhibition of its glycolytic activity(180). We thus assessed GAPDH nitrosylation in TrHK1 overexpressing cells, and showed that cells with overexpression of TrHK1 display higher GAPDH nitrosylation levels (**Figure 31A**). Importantly, BMDMs from $\Delta E1HK1$ mice also displayed higher GAPDH nitrosylation than WT controls, which was reversible with 1400W treatment, a selective iNOS inhibitor(181) (**Figure 31B-C**).

To assess whether the hyper-inflammation seen in $\Delta E1HK1$ BMDMs is dependent on protein

nitrosylation through iNOS, we administered 1400W to mice 1 hour prior to intraperitoneal injection of a sub-lethal dose of LPS for 3 hours and collected blood and splenic tissue from these mice for analysis (**Figure 32A**). We observed a rescue of the hyper-inflammatory response seen in $\Delta E1HK1$ mice as measured by splenic mRNA (**Figure 32B-D**) and serum ELISA (**Figure 32E-G**) of inflammatory cytokines IL-1 β , IL-6, and TNF α . Additionally, treatment of BMDMs isolated from $\Delta E1HK1$ mice with 1400W caused reversal of the hyper-inflammatory response as measured by mRNA of IL-1 β , IL-6, and TNF α (**Figure 33A-C**). GAPDH activity of $\Delta E1HK1$ BMDMs was also restored to WT levels after 1400W treatment (**Figure 33D**). Next, we assessed whether iNOS inhibition could reverse the altered glycolytic effects seen in $\Delta E1HK1$ BMDMs. We found that iNOS inhibition eliminated the differences in ECAR observed between $\Delta E1HK1$ and WT BMDMs (**Figure 33E-F**). Together, these data indicate that cytosolic HK1 binds to the S100A8 and promotes iNOS mediated nitrosylation and inactivation of GAPDH.

Obesity and Aging Mouse Models Display Increased Inflammation and Cytosolic HK1

Our data thus far indicates that constitutive or acute HK1 dislocation causes an increase in cytokine production through inhibition of GAPDH, which alters glycolysis and subsequently increases PPP metabolism. We next studied whether subcellular localization of HK1 is altered in conditions of chronic low-grade inflammation, such as diabetes and aging. To generate diabetic mice, we fed 4-week-old mice a high fat diet (HFD) consisting of 60% fat, 20% protein, and 20% carbohydrates. Mice given HFD for 27 weeks displayed impaired glucose tolerance and increased body weight as compared to mice fed normal chow (NC) (**Figure 34A-B**). Splenic tissue from HFD mice displayed higher IL-1 β , IL6, and TNF α mRNA levels than NC fed mice, which is consistent with low-grade inflammation (**Figure 35A-C**). Importantly, spleens from HFD mice had an increased cytosolic to mitochondrial HK1 ratio than NC fed mice (**Figure 35D-E**).

To assess whether this elevated inflammation was dependent on GAPDH activity, we isolated PMs from NC and HFD mice and found that the HFD group had lower GAPDH activity before and after LPS stimulation, which could be rescued with 1400W treatment (**Figure 35F**). Furthermore, iNOS inhibition with 1400W reversed the elevation in IL-1 β observed in the HFD PMs back to WT levels (**Figure 35G**). Collectively, these data indicate that HK1 mitochondrial dissociation occurs in diseases of chronic-low grade inflammation, and restoration of GAPDH activity with iNOS inhibition can rescue this phenotype in PMs derived from diabetic mice.

We observed a similar increase in inflammatory mRNA markers in adipose (**Figure 36A-C**) and liver (**Figure 36D-F**) tissues from HFD mice. Furthermore, we observed a similar increase in cytosolic HK1 levels in adipose (**Figure 36G**) and liver (**Figure 36H**) tissue taken from HFD mice. Elevated inflammation was also observed in aged mice, as assessed by measurements of IL-1 β and IL-6 mRNA isolated from spleens of 85-week-old mice (**Figure 37A-B**). Aged mice also displayed increased cytosolic HK1 levels similar to HFD mice (**Figure 37C-D**).

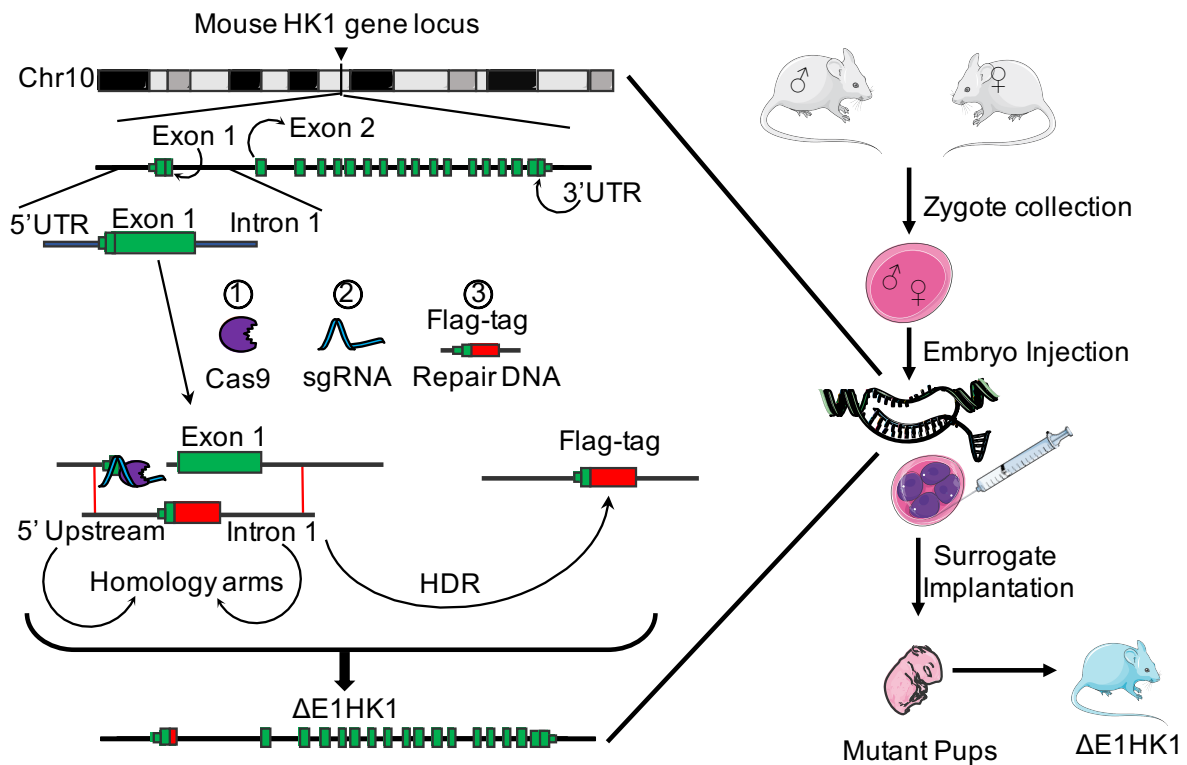


Figure 14. Schematic of $\Delta E1HK1$ mouse model generation.

Guide RNAs (gRNAs) were designed to induce a double strand breakage (DSB) near the 5' ATG start codon of HK1 in exon 1, and a DNA template containing a FLAG sequence in place of the MBD was introduced *in vitro* into fertilized zygotes and implanted into surrogate mice. Subsequent homology-directed repair (HDR) of the DSB resulted in replacement of the coding region of HK1 MBD with a FLAG sequence.

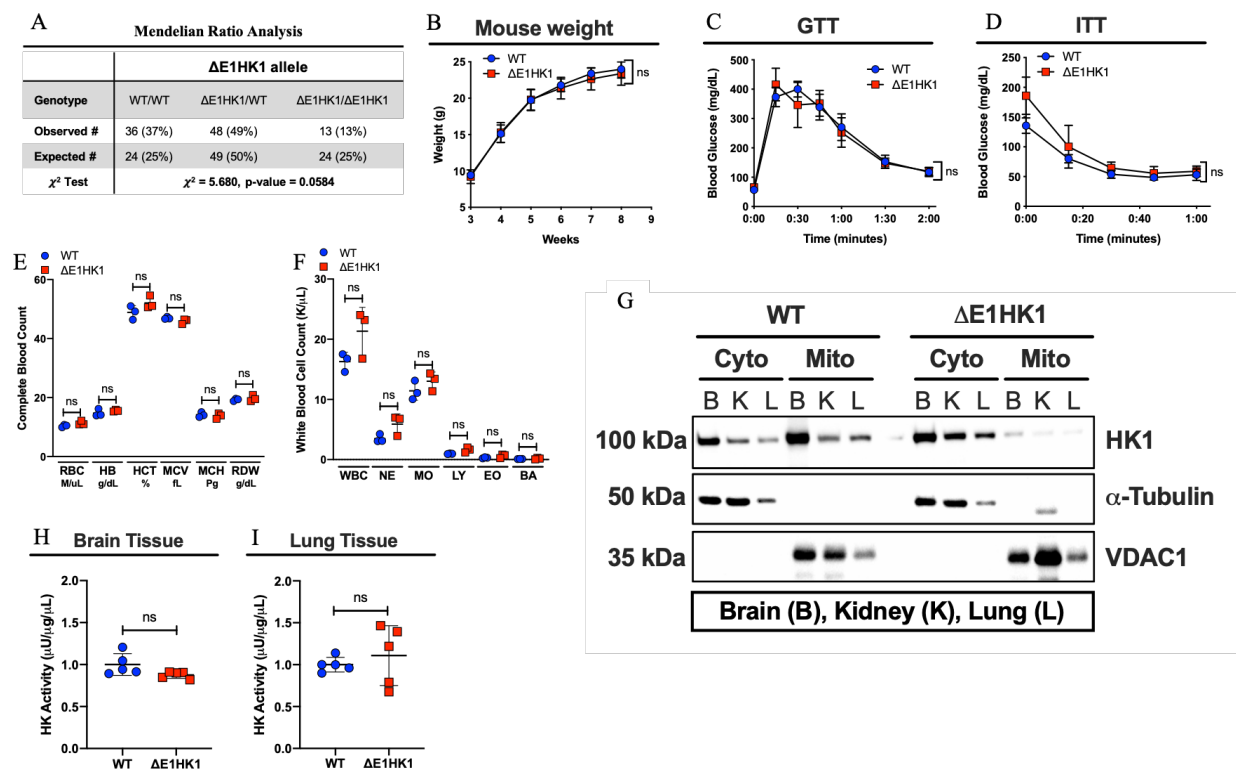


Figure 15. $\Delta E1HK1$ initial mouse model characterization.

A. Mendelian ratio analysis of WT, heterozygous and homozygous ($\Delta E1HK1$) mice (data taken from 4 independent litters, total of 97 mice, Chi-squared test Prism GraphPad). **B.** Mouse weights from 3 to 8 weeks ($n=5$ mice per condition, repeated measures two-way ANOVA, mean \pm SD). **C-D.** Glucose tolerance test (GTT) (c) and insulin tolerance test (ITT) (d) from 10-week-old mice ($n=5$ mice per condition, repeated measures two-way ANOVA, mean \pm SD). **E-F.** CBC (E) and WBC differential (F) in WT and $\Delta E1HK1$ mice, as measured using HEMAVET 950 whole blood analyzer ($n=3$ mice per condition, two-way ANOVA and Tukey's post-hoc test, mean \pm SD). **G.** Mitochondria and cytosolic protein fractionation and western blot of brain, kidney and lung tissue, VDAC1 is a mitochondrial marker and α -tubulin is a cytosolic marker. **H-I.** HK activity assay normalized to total protein from brain (H) and lung (I) tissue ($n=4$ mice per condition, unpaired t-test, mean \pm SD).

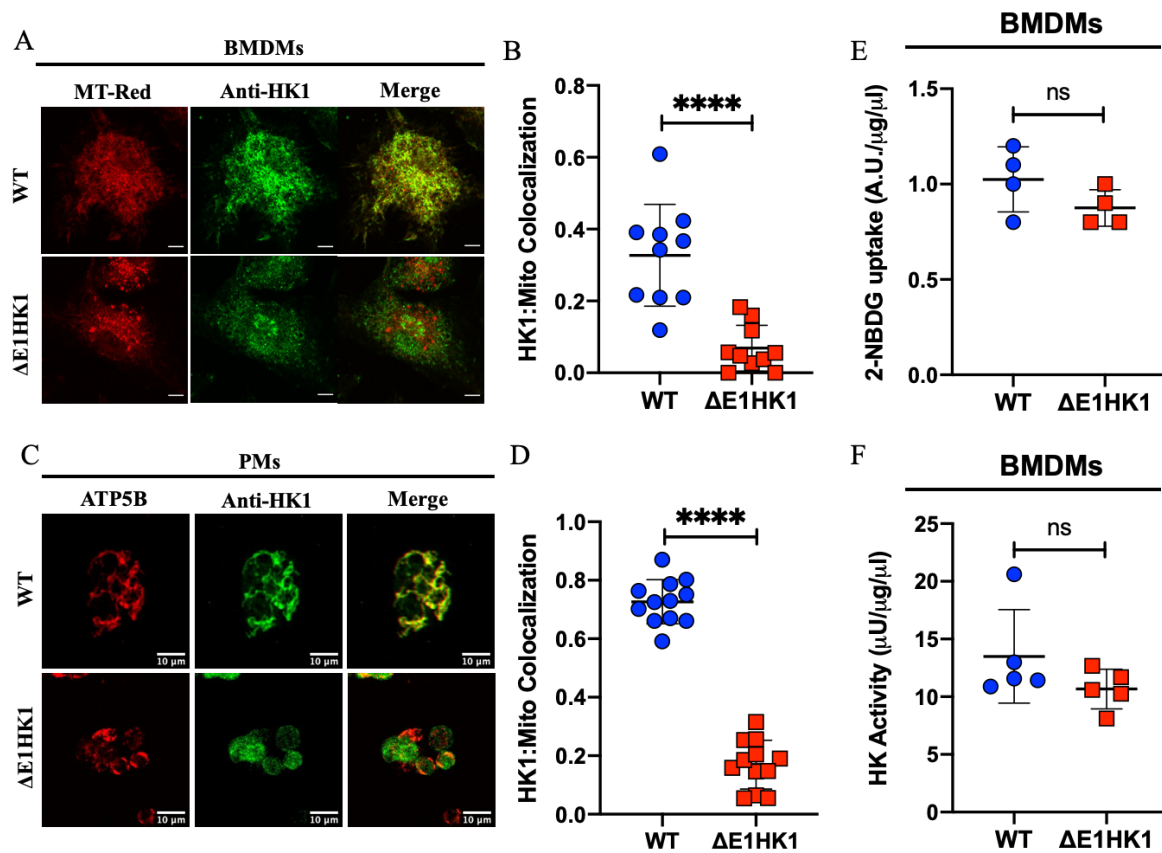


Figure 16. $\Delta E1HK1$ BMDM and PMs have mitochondrial dissociation of HK1

A. Representative immunofluorescence (IF) images probing for HK1 and mitochondria (MT-Red) in isolated BMDMs. **B.** Colocalization analysis of IF images (A) using Pearson's correlation coefficient calculated per cell between MT-Red (red) and HK1 (green) image channels (n=10 cells per condition, unpaired t-test, mean \pm SD, colocalization analysis performed using *Coloc-2 macro* on ImageJ, scale bar = 15 μ m). **C-D.** Representative IF images probing for HK1 and mitochondria (ATP5B) in isolated PMs (C). Colocalization analysis of IF images (D) using Pearson's correlation coefficient calculated per cell between ATP5B (red) and HK1 (green) image channels (n=12 cells per condition, unpaired t-test, mean \pm SD, colocalization analysis performed using *Coloc-2 macro* on Fiji/ImageJ). **E.** 2-NBDG glucose uptake assay normalized to total protein of LPS (200ng/ml)-

activated BMDMs (n=4 mice per condition, unpaired t-test, mean \pm SD). **F.** HK activity assay normalized to total protein of LPS (200ng/ml)-activated BMDMs (n=5 mice per condition, unpaired t-test, mean \pm SD).

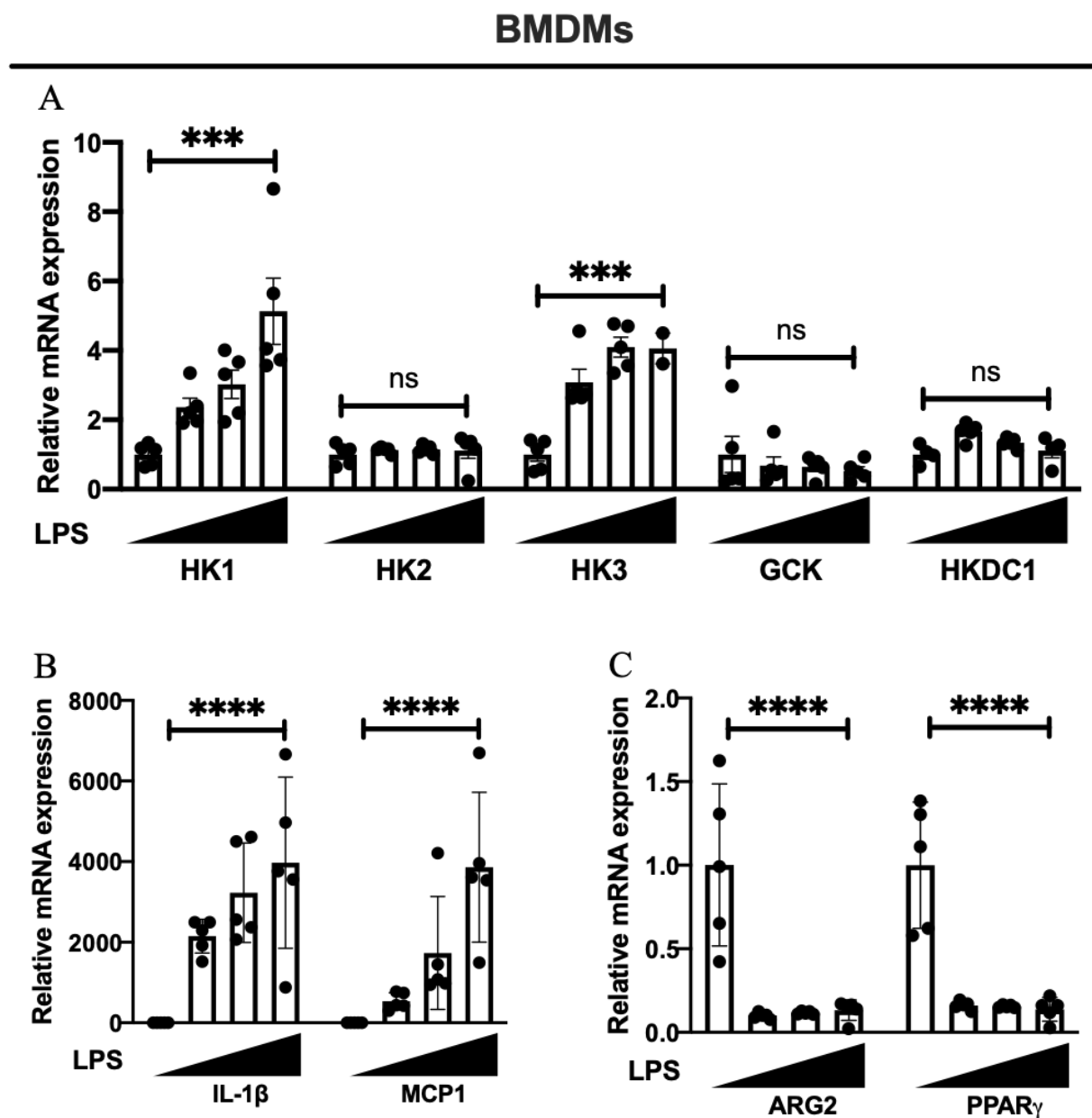


Figure 17. BMDMs have high HK1 and HK3 expression after LPS treatment.

A. mRNA expression of all known HK isozymes (HK1, HK2, HK3, GCK, HKDC1) in WT BMDMs (n=5 mice per condition, repeated measures two-way ANOVA and Tukey's post-hoc test, mean \pm SD). **B-C.** mRNA expression of inflammatory (IL-1 β and MCP1) (B) and anti-inflammatory markers (ARG2 and PPAR γ) (C) in WT BMDMs (n=5 mice per condition, repeated

measures two-way ANOVA and Tukey's post-hoc test, mean \pm SD).

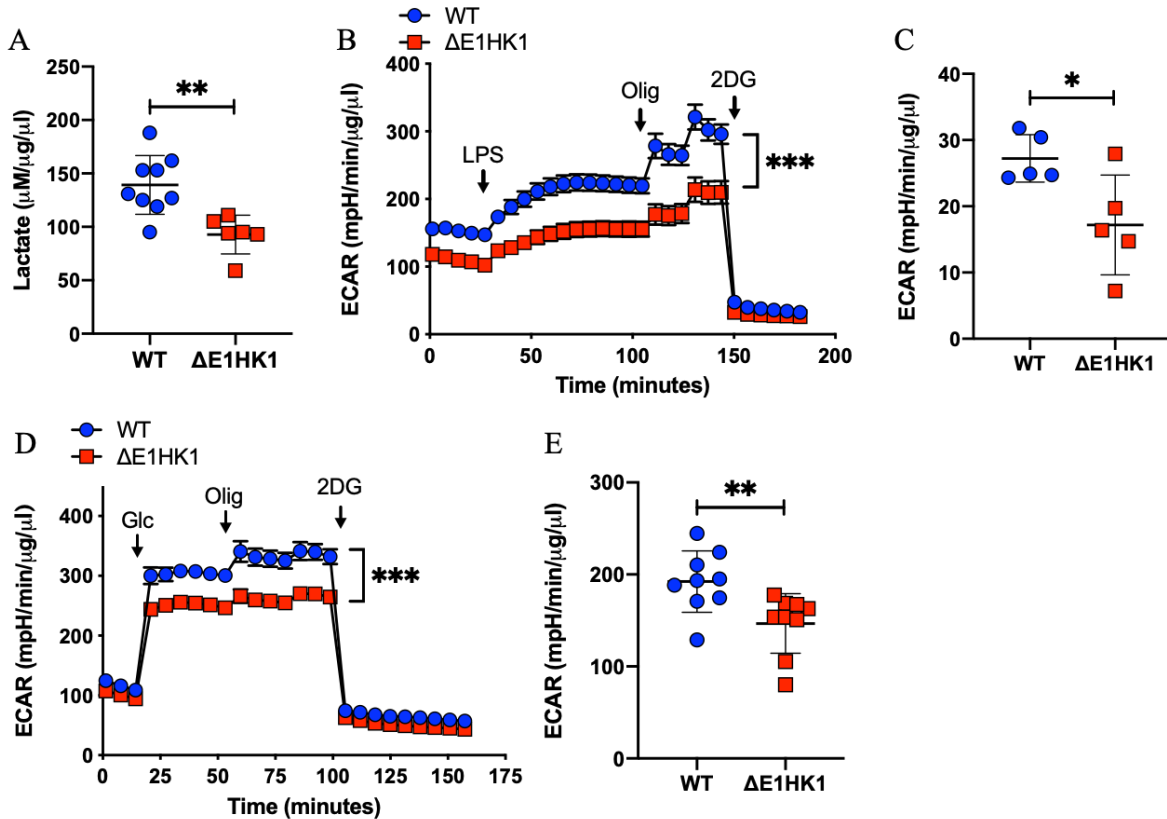


Figure 18. Loss of HK1 mitochondrial binding alters glycolytic metabolism.

A. Extracellular lactate quantification in LPS-activated BMDMs (n=6-9 mice per condition, unpaired t-test, mean \pm SD). **B-C.** ECAR trace of unstimulated BMDMs \pm acute LPS (200ng/ml) stimulation for 2hrs (B) and ECAR quantification at 60min time point (C) (n=9 mice per condition, repeated measures two-way ANOVA, mean \pm SEM). **D-E.** ECAR trace of BMDMs \pm 5hrs LPS (200ng/ml) stimulation (D) and ECAR quantification at 60min time point (E) (n=5 mice per condition, repeated measures two-way ANOVA, mean \pm SEM).

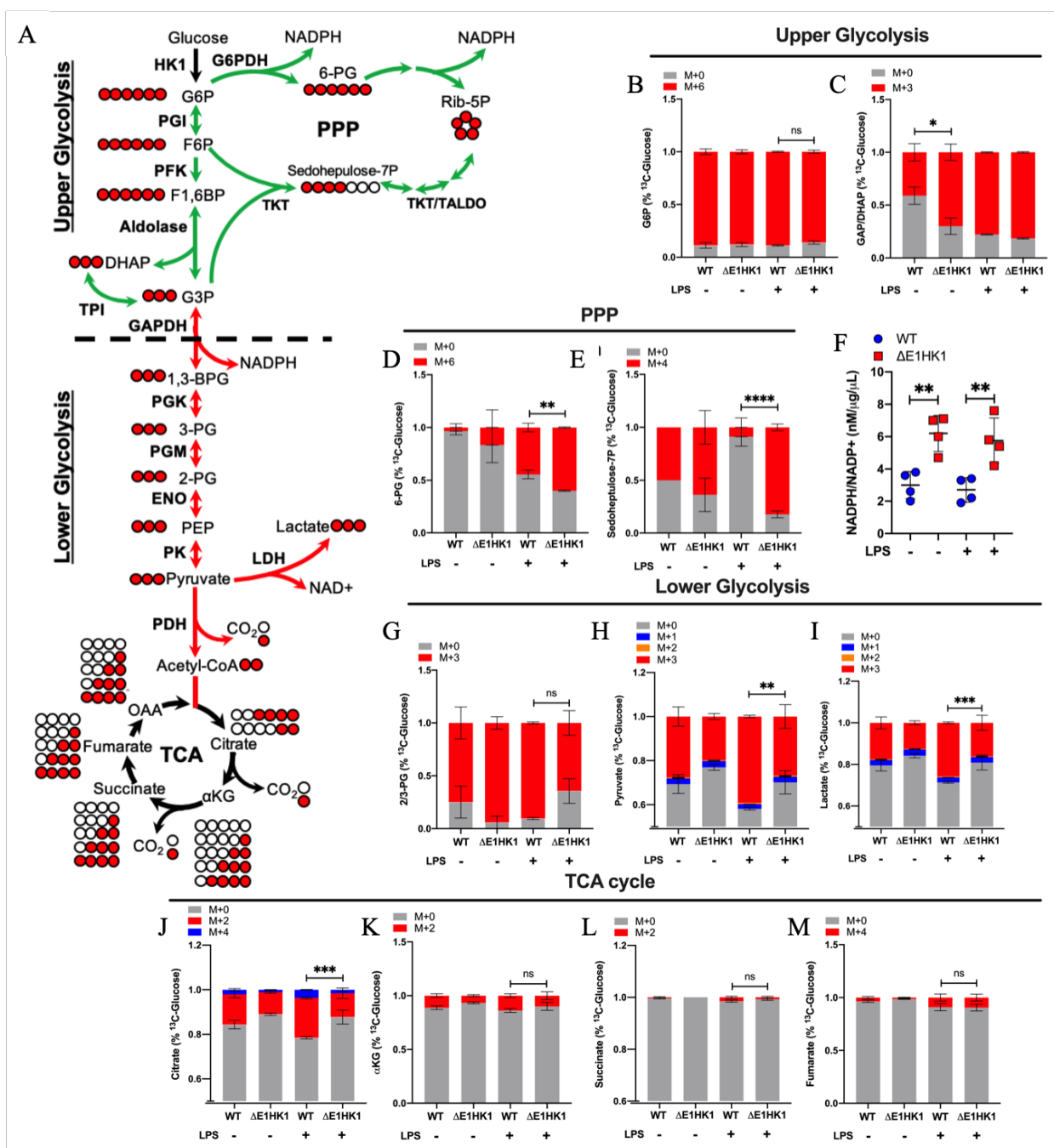


Figure 19. HK1 mitochondrial dissociation decreases lower glycolytic flux and increases PPP metabolism.

A. Schematic of ^{13}C -glucose carbon labeling through glycolysis (upper and lower glycolysis), PPP, and TCA cycle. Green arrow indicates increased metabolites and red depicts reduced levels of metabolites. **B-C.** ^{13}C -glucose incorporation into upper glycolytic metabolites, G6P (**B**) and GAP

(C), \pm 4hrs LPS treatment (n=5 mice per condition, two-way ANOVA, mean \pm SEM). **D-E.** ^{13}C -glucose incorporation into PPP metabolites, 6-PG (D) and sedoheptulose-7P (E), \pm 4hrs LPS treatment (n=5 mice per condition, two-way ANOVA, mean \pm SEM). **F.** NADPH/NADP⁺ ratio normalized to total protein in isolated BMDMs \pm 4hr LPS treatment (N=4 mice per condition, one-way ANOVA and Tukey's post-hoc test, mean \pm SD). **G-I.** ^{13}C -glucose incorporation into lower glycolytic metabolites, 2/3-PG (G), pyruvate (H), and lactate (I), \pm 4hrs LPS treatment (n=5 mice per condition, two-way ANOVA, mean \pm SEM). **J-M,** ^{13}C -glucose incorporation into TCA metabolites, citrate (J), α KG (K), succinate (L), and fumarate (M) \pm 4hrs LPS treatment (n=5 mice per condition, two-way ANOVA, mean \pm SEM).

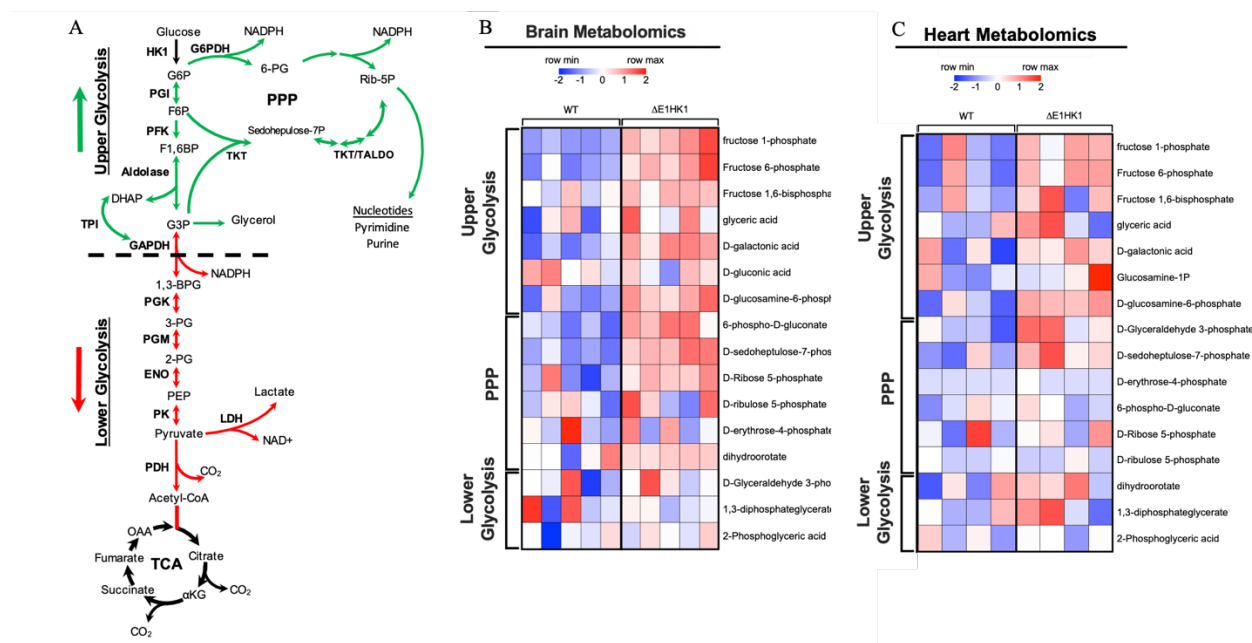


Figure 20. Brain and heart tissue metabolomics analysis shows higher PPP metabolites.

A. Schematic of upper and lower glycolysis including PPP metabolic shunt off G6P. Heatmap of steady-state metabolomics performed on whole mouse brain (B) and heart (C) normalized to total-iron-content in the cells (Heatmap generated using MetaboAnalyst).

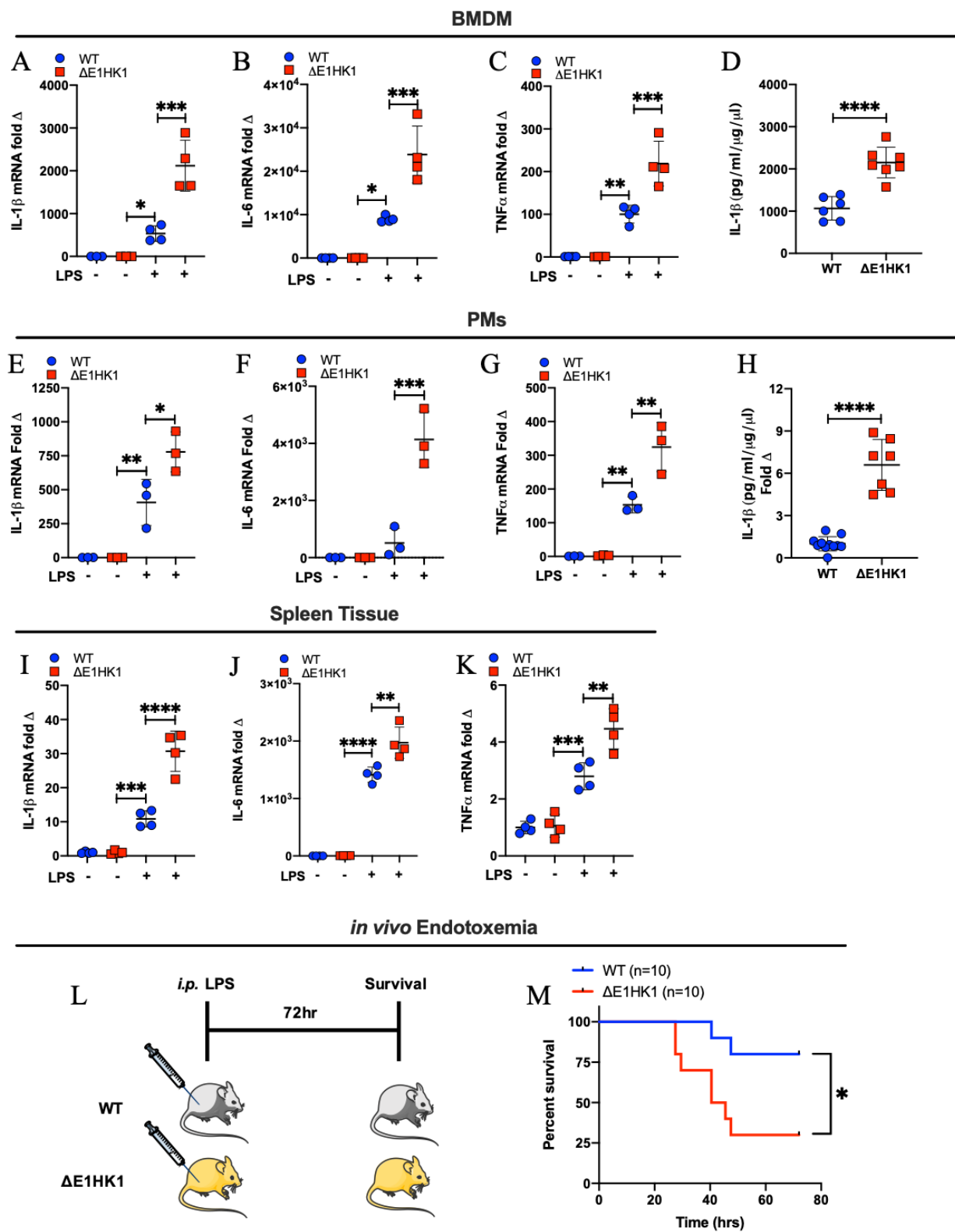


Figure 21. Constitutive HK1 mitochondrial dissociation increases inflammation.

A-C. Inflammatory cytokine mRNA expression of IL-1 β (A), IL-6 (B), and TNF α (C) from

isolated BMDMs \pm 6hrs LPS (200ng/ml) (n=4 mice per condition, one-way ANOVA and Tukey's post-hoc test, mean \pm SD). **D.** IL-1 β ELISA from BMDM media \pm 6hrs of LPS (200ng/ml) followed by 30min ATP (2.5mM), normalized to total protein (n=6-7 mice per condition, unpaired t-test, mean \pm SD). **E-G.** mRNA expression of IL-1 β (E), IL-6 (F), and TNF α (G) from isolated PMs \pm 6hrs LPS (300ng/ml) (n=3 mice per condition, one-way ANOVA and Tukey's post-hoc test, mean \pm SD). **H.** IL-1 β ELISA from PM media \pm 6hrs of LPS (300ng/ml) followed by 30min of ATP (2.5mM), normalized to total protein (n=7-10 mice per condition, unpaired t-test, mean \pm SD). **I-K.** mRNA expression of IL-1 β (I), IL-6 (J), and TNF α (K) from splenic tissue after i.p. injection of mice with LPS (15mg/kg) for 4hrs. (n=4 mice per condition, one-way ANOVA and Tukey's post-hoc test, mean \pm SD). **L.** Schematic of LPS-induced endotoxemia model. Mice were given i.p. injection of LPS (15mg/kg) and observed over 72hrs for survival. **M.** Survival curve of mice in LPS-induced endotoxemia model (n=10 mice per condition, survival curve log-rank (Mantel-Cox) test).

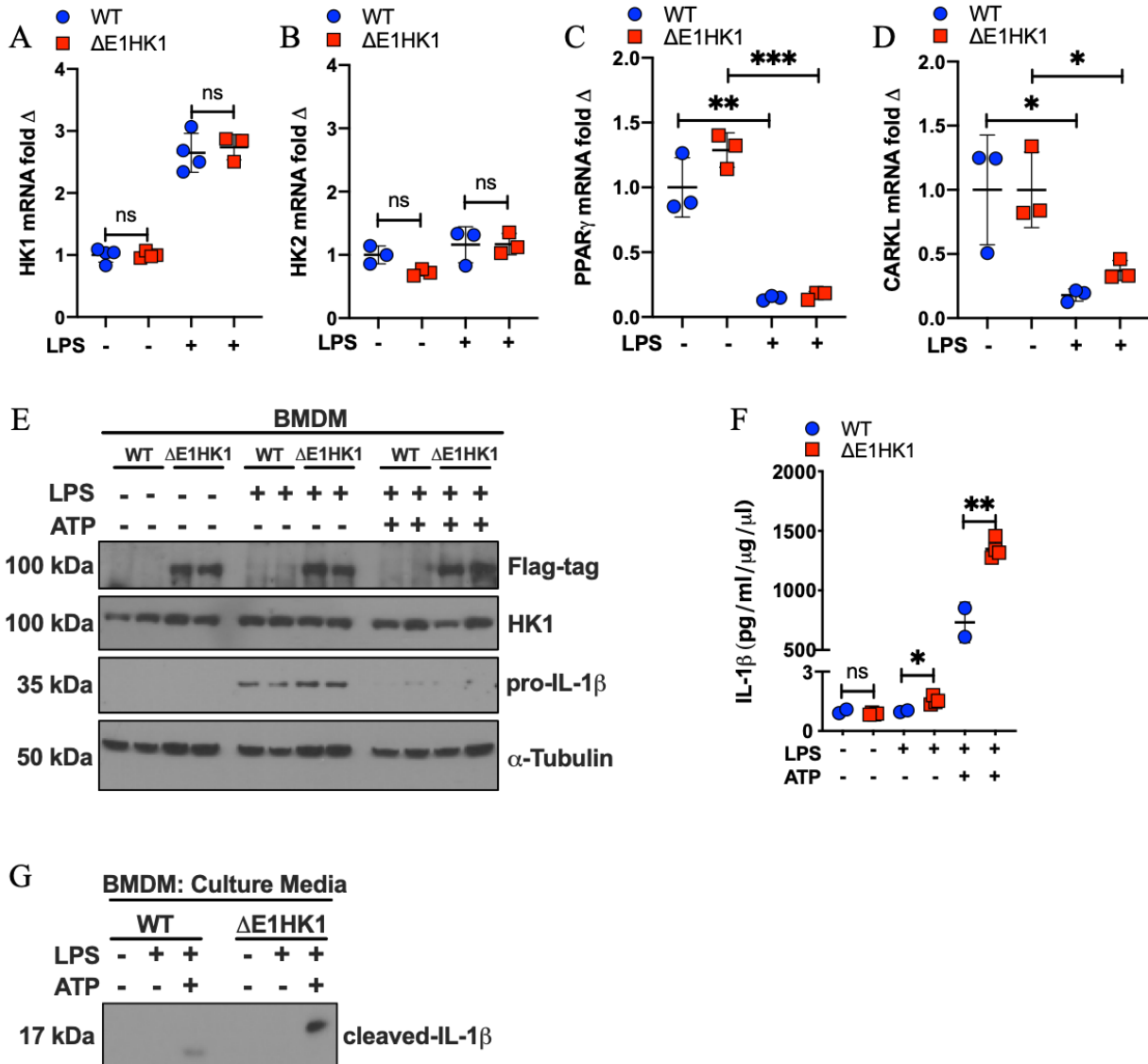


Figure 22. HK1 mRNA expression is not significantly altered between Δ E1HK1 and WT BMDMs.

A-B. HK1 (A) and HK2 (B) mRNA expression in isolated BMDMs \pm 6hrs LPS (200ng/ml) (n=3-4 mice per condition, one-way ANOVA and Tukey's post-hoc test, mean \pm SD). **C-D.** Anti-inflammatory cytokine mRNA expression of PPAR γ (C) and CARL (D) from isolated BMDMs \pm 6hrs LPS (200ng/ml) (n=3-4 mice per condition, one-way ANOVA and Tukey's post-hoc test, mean \pm SD). **E.** Western blot analysis of BMDMs treated with LPS or LPS+ATP probing for Flag-

tag, HK1 and pro-IL-1 β . **F.** IL-1 β ELISA from BMDM media \pm 6hrs of LPS (200ng/ml) followed by 30min ATP (2.5mM), normalized to total protein (n=2-4 mice per condition, one-way ANOVA and Tukey's post-hoc test, mean \pm SD). **G.** Western blot of cleaved-IL-1 β from media of LPS or LPS+ATP treated cells.

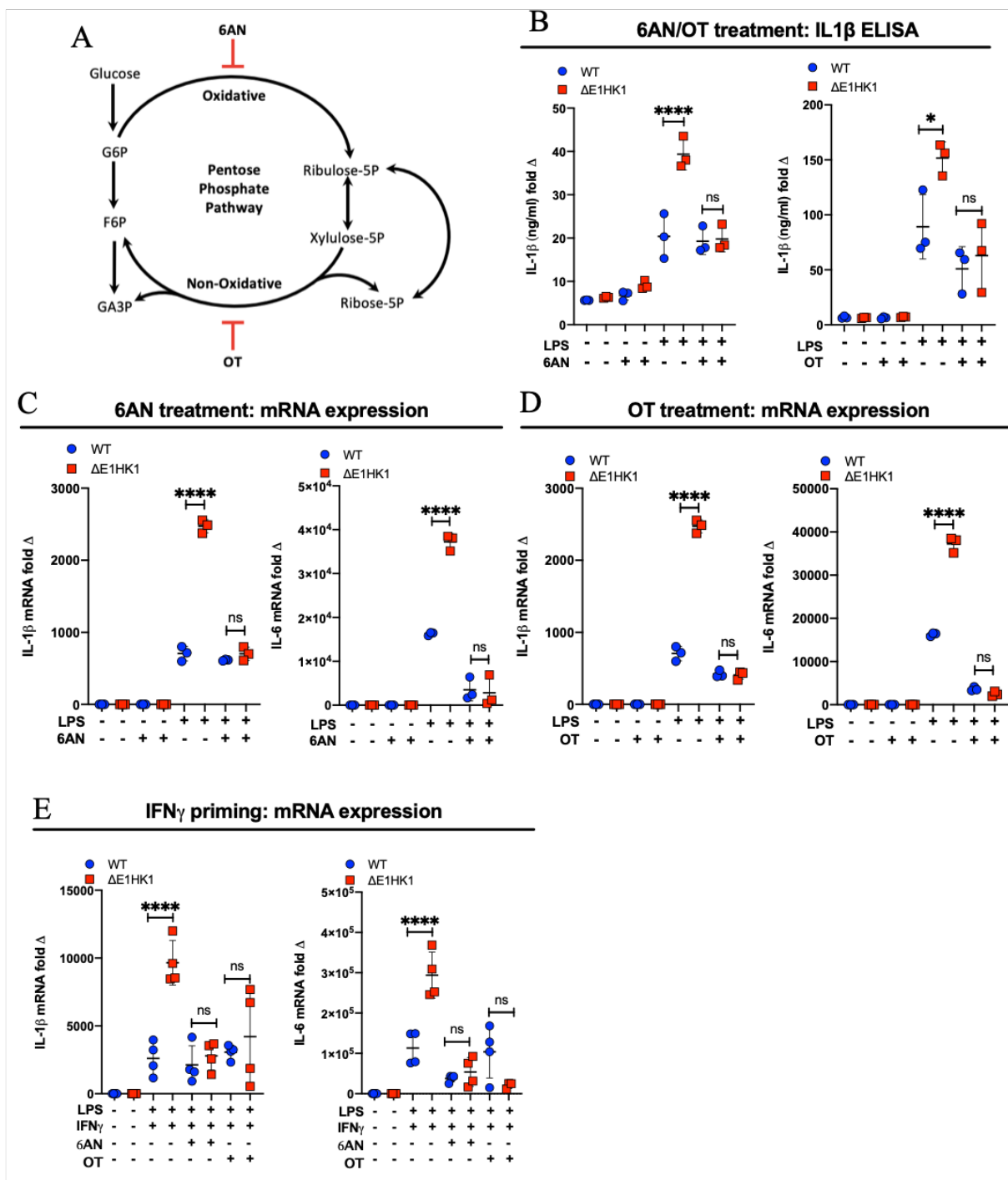


Figure 23. PPP inhibition reverses hyper-inflammation induced by HK1 mitochondrial dissociation.

A. Schematic of oxidative and non-oxidative branch of PPP with 6AN blocking the oxidative

branch and OT blocking the non-oxidative branch. **B-C.** IL-1 β ELISA from BMDM media after 4hrs of LPS (200ng/ml) \pm 6AN (1mM) (B) or OT (50 μ M) (C) followed by 30min of ATP (2.5mM), normalized to total protein (n=3 mice per condition, two-way ANOVA and Tukey's post-hoc test, mean \pm SD). **D-E.** mRNA expression of IL-1 β (D) and IL-6 (E) \pm 4hr 6AN (1mM) or \pm LPS (200ng/ml) (n=3 mice per condition, two-way ANOVA and Tukey's post-hoc test, mean \pm SD). **F-G.** mRNA expression of IL-1 β (F) and IL-6 (G) \pm 4hr OT (50 μ M) or \pm LPS (200ng/ml) (n=3 mice per condition, two-way ANOVA and Tukey's post-hoc test, mean \pm SD). **H-I.** mRNA expression of IL-1 β (H) and IL-6 (I) with \pm 16hrs IFN γ priming followed by \pm 4hrs of LPS (200ng/ml) \pm 6AN (1mM) and \pm OT (50 μ M) (n=4 mice per condition, two-way ANOVA and Tukey's post-hoc test, mean \pm SD).

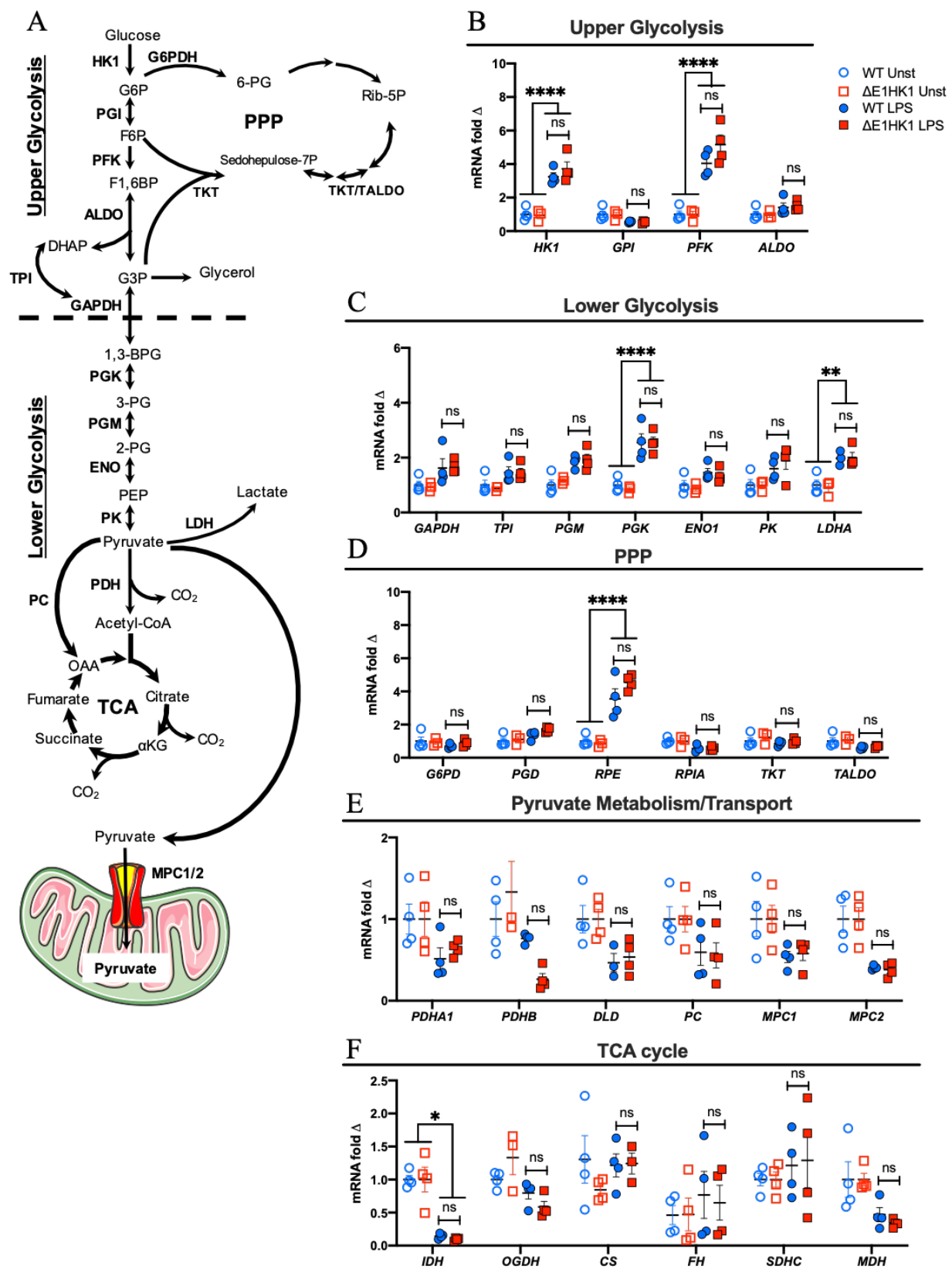


Figure 24. mRNA expression of glycolytic, PPP and TCA cycle genes in BMDMs from WT and Δ E1HK1 mice.

A. Schematic of upper and lower glycolysis, PPP, TCA cycle, and pyruvate metabolic pathways. **B.** mRNA expression of upper glycolytic genes HK1, glucose-6-phosphate isomerase (GPI), phosphofructokinase (PFK), and aldolase (ALDO) from isolated BMDMs \pm 6hrs LPS (200ng/ml) (n= mice per condition, one-way ANOVA and Tukey's post-hoc test, mean \pm SD). **C.** mRNA expression of lower glycolytic genes GAPDH, triosephosphate isomerase (TPI), Phosphoglucomutase (PGM), phosphoglycerate kinase (PGK), enolase (ENO1), pyruvate kinase (PK) and lactate dehydrogenase A (LDHA) from isolated BMDMs \pm 6hrs LPS (200ng/ml) (n= mice per condition, one-way ANOVA and Tukey's post-hoc test, mean \pm SD). **D.** mRNA expression of PPP genes glucose-6-phosphate dehydrogenase (G6PD), phosphogluconate dehydrogenase (PGD), ribulose-5-phosphate-3-epimerase (RPE), ribose-5-phosphate isomerase A (RPIA), transketolase (TKT), and transaldolase (TALDO) from isolated BMDMs \pm 6hrs LPS (200ng/ml) (n= mice per condition, one-way ANOVA and Tukey's post-hoc test, mean \pm SD). **E.** mRNA expression of pyruvate metabolism genes pyruvate dehydrogenase E1 alpha 1 subunit (PDHA1), pyruvate dehydrogenase E1 beta subunit (PDHB), dihydrolipoamide dehydrogenase (DLD), (PC), mitochondrial pyruvate carrier 1 (MPC1), and mitochondrial pyruvate carrier 2 (MPC2) from isolated BMDMs \pm 6hrs LPS (200ng/ml) (n= mice per condition, one-way ANOVA and Tukey's post-hoc test, mean \pm SD). **F.** mRNA expression of TCA cycle genes iso-citrate dehydrogenase (IDH), oxoglutarate dehydrogenase (OGDH/ α KGD), citrate synthase (CS), fumarate hydratase (FH), succinate dehydrogenase complex subunit C (SDHC), and malate dehydrogenase (MDH) from isolated BMDMs \pm 6hrs LPS (200ng/ml) (n= mice per condition, one-way ANOVA and Tukey's post-hoc test, mean \pm SD).

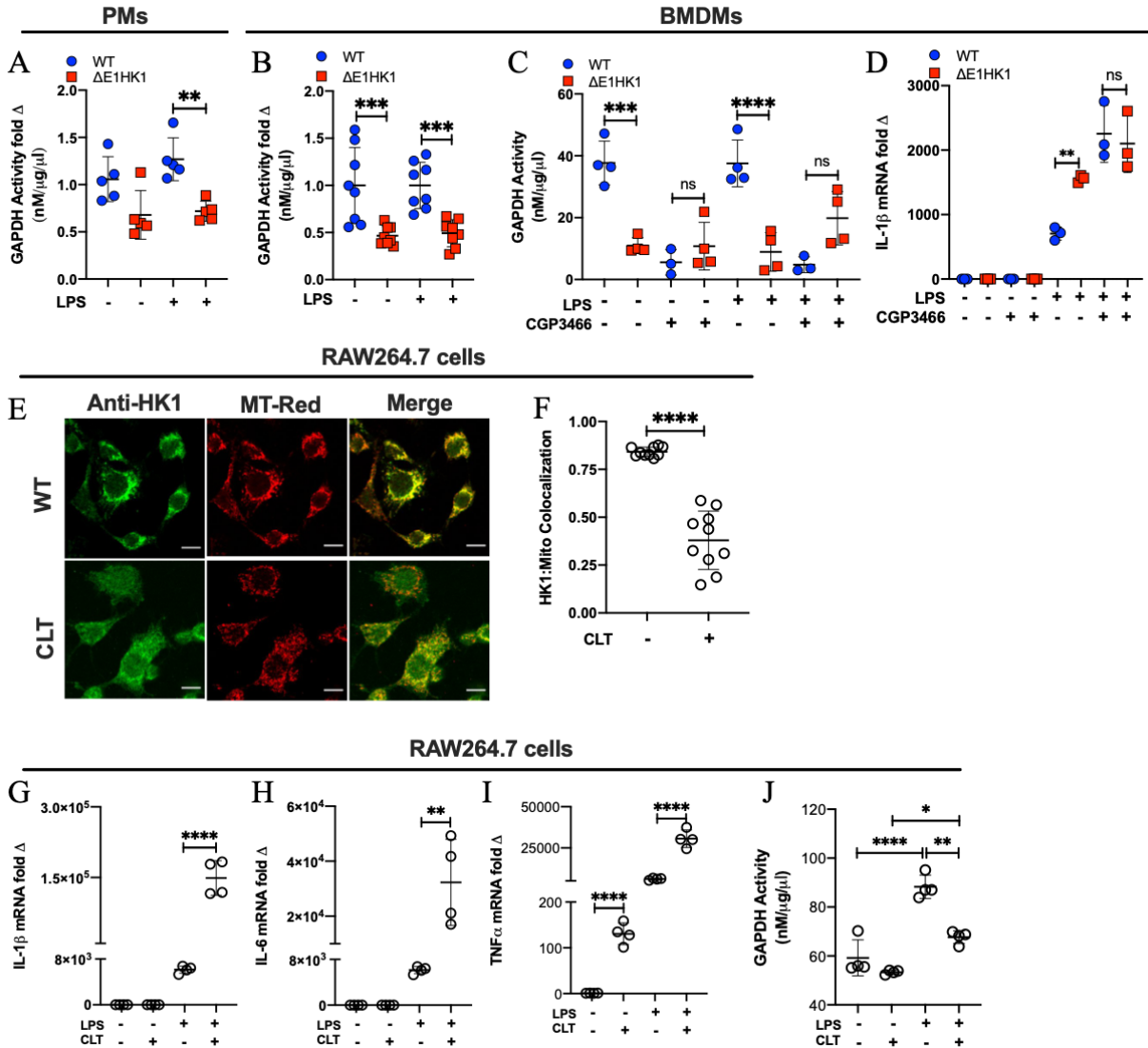


Figure 25. GAPDH activity is attenuated in macrophages with HK1 mitochondrial detachment.

A. GAPDH activity normalized to total protein in PMs treated with \pm LPS (300ng/ml) ($n=5$ mice per condition, two-way ANOVA and Tukey's post-hoc test, mean \pm SD). **B-C.** GAPDH activity normalized to total protein in BMDMs \pm LPS (200ng/ml) (B) and \pm CGP3466 (GAPDH inhibitor) for 4hrs (C) ($n=8$ mice per condition for panel B and $n=4$ mice per condition for panel C, two-way ANOVA and Tukey's post-hoc test, mean \pm SD). **D.** IL-1 β mRNA expression in BMDMs \pm LPS and \pm CGP3466 for 4hrs ($n=3$ mice per condition, two-way ANOVA and Tukey's post-hoc test, mean \pm SD). **E-F.** IF of HK1 and mitochondria (MT-Red) imaging in RAW264.7 cells \pm

clotrimazole (CLT) (20 μ M) (E) and mitochondrial to HK1 colocalization analysis (F) (n=10 cells per condition, unpaired t-test, mean \pm SD, colocalization analysis performed using *Coloc-2* macro on ImageJ, scale bar = 15 μ m). **G-I** mRNA expression of IL-1 β (G), IL-6 (H), and TNF α (I) in RAW264.7 cells \pm CLT (20 μ M) (n=4 replicates per condition, two-way ANOVA and Tukey's post-hoc test, mean \pm SD). **J.** GAPDH activity normalized to total protein in RAW264.7 cells \pm CLT (20 μ M) (n=4 replicates per condition, two-way ANOVA and Tukey's post-hoc test, mean \pm SD).

RAW264.7

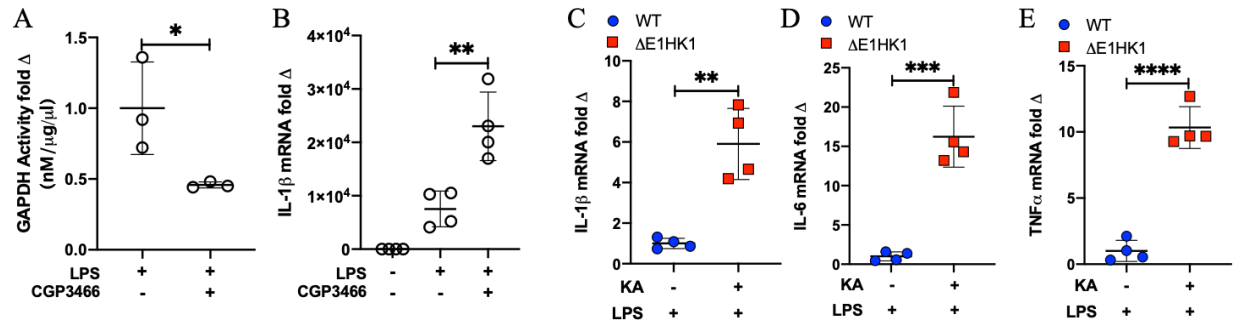


Figure 26. Inhibition of GAPDH activity in RAW264.7 cells.

A. GAPDH activity normalized to total protein in RAW264.7 cells treated with LPS (200ng/ml) and \pm CGP3466 (n=3 replicates per condition, unpaired t-test, mean \pm SD). **B.** IL-1 β mRNA expression in RAW264.7 cells \pm LPS (200ng/ml) and \pm CGP3466 for 4hrs (n=4 replicates per condition, one-way ANOVA and Tukey's post-hoc test, mean \pm SD). **C-E.** Expression of IL-1 β (C), IL-6 (D), and TNF α (E) from isolated BMDMs treated with 6hrs LPS (200ng/ml) (n=4 replicates per condition, one-way ANOVA and Tukey's post-hoc test, mean \pm SD).

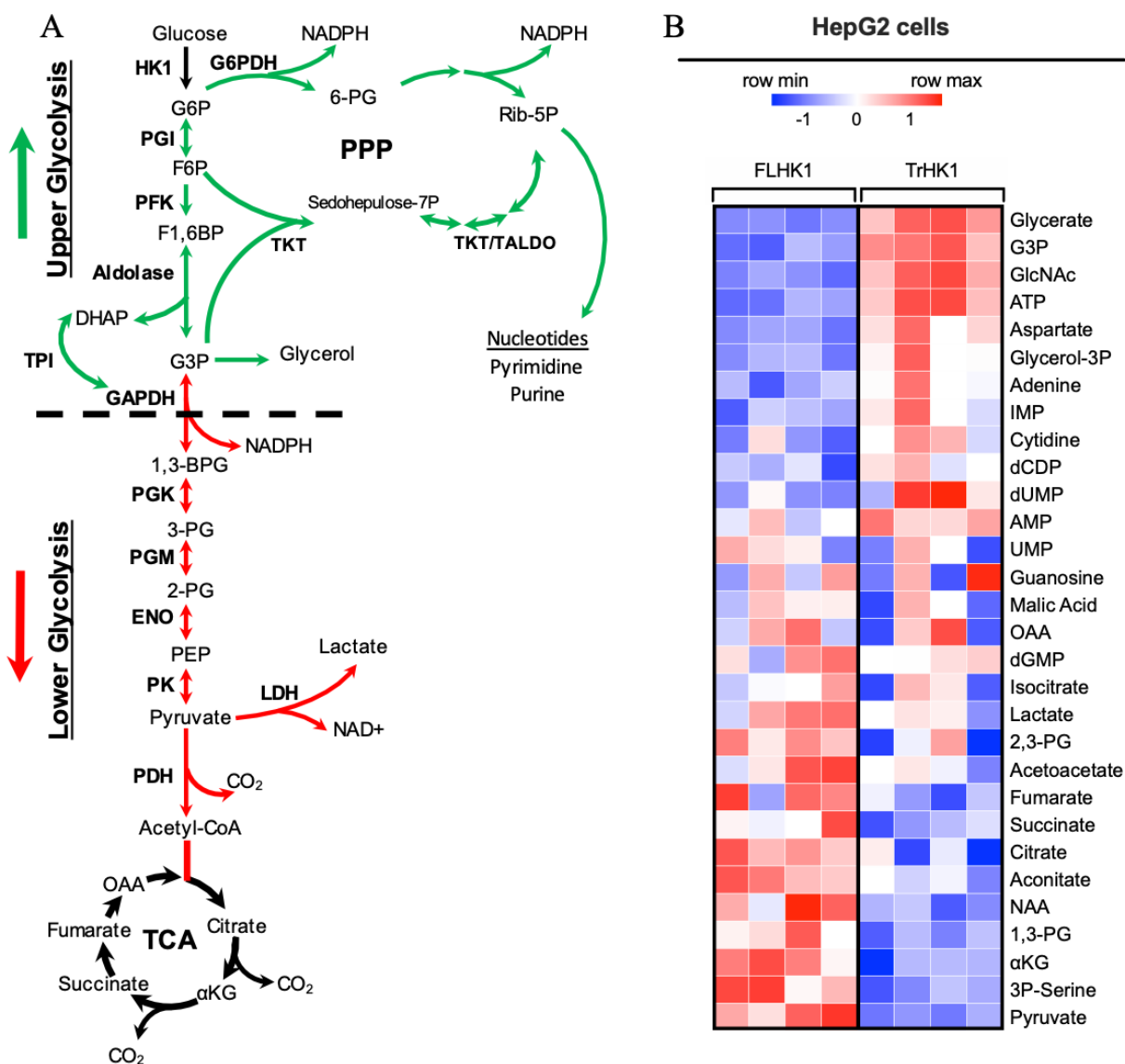


Figure 27. Steady-state metabolomics in HepG2 cells.

A. Schematic of branch points of G6P and glycolytic pathway above and below the level of GAPDH. Green arrow indicates increased metabolites and red depicts reduced levels of metabolites. **B.** Heatmap of steady-state metabolomics performed in HepG2 cells with FLHK1 and TrHK1 overexpression all normalized to EV metabolite levels and total-iron-content in the cells (Heatmap generated using MetaboAnalyst).

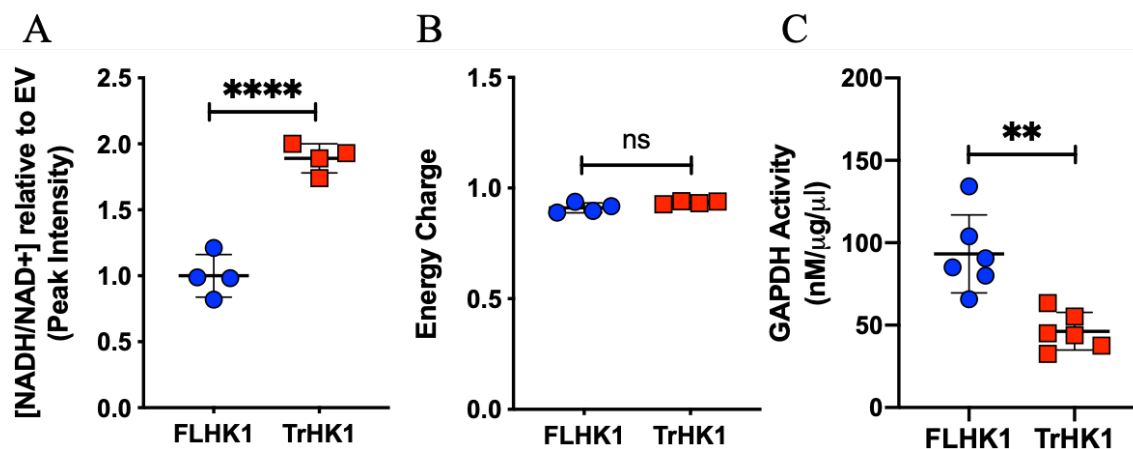


Figure 28. Metabolic studies and GAPDH activity measurement in HepG2 cells.

A. NADH/NAD⁺ ratio measurement derived from steady-state metabolomics peak-mass-spectrometry (MS) values for NADH and NAD⁺ (n=4 mice per condition, unpaired t-test, mean ± SD). **B.** Energy charge of the cell calculated based on steady-state metabolomics data using ATP, AMP, and ADP metabolite peak-MS values. Formula for energy charge $\frac{[ATP]+0.5[ADP]}{[ATP]+[ADP]+[AMP]}$ (n=4 mice per condition, unpaired t-test, mean ± SD). **C.** GAPDH activity normalized to total protein in HepG2 cells between FLHK1 and TrHK1 normalized to EV (n=6 replicates per condition for, unpaired t-test, mean ± SD).

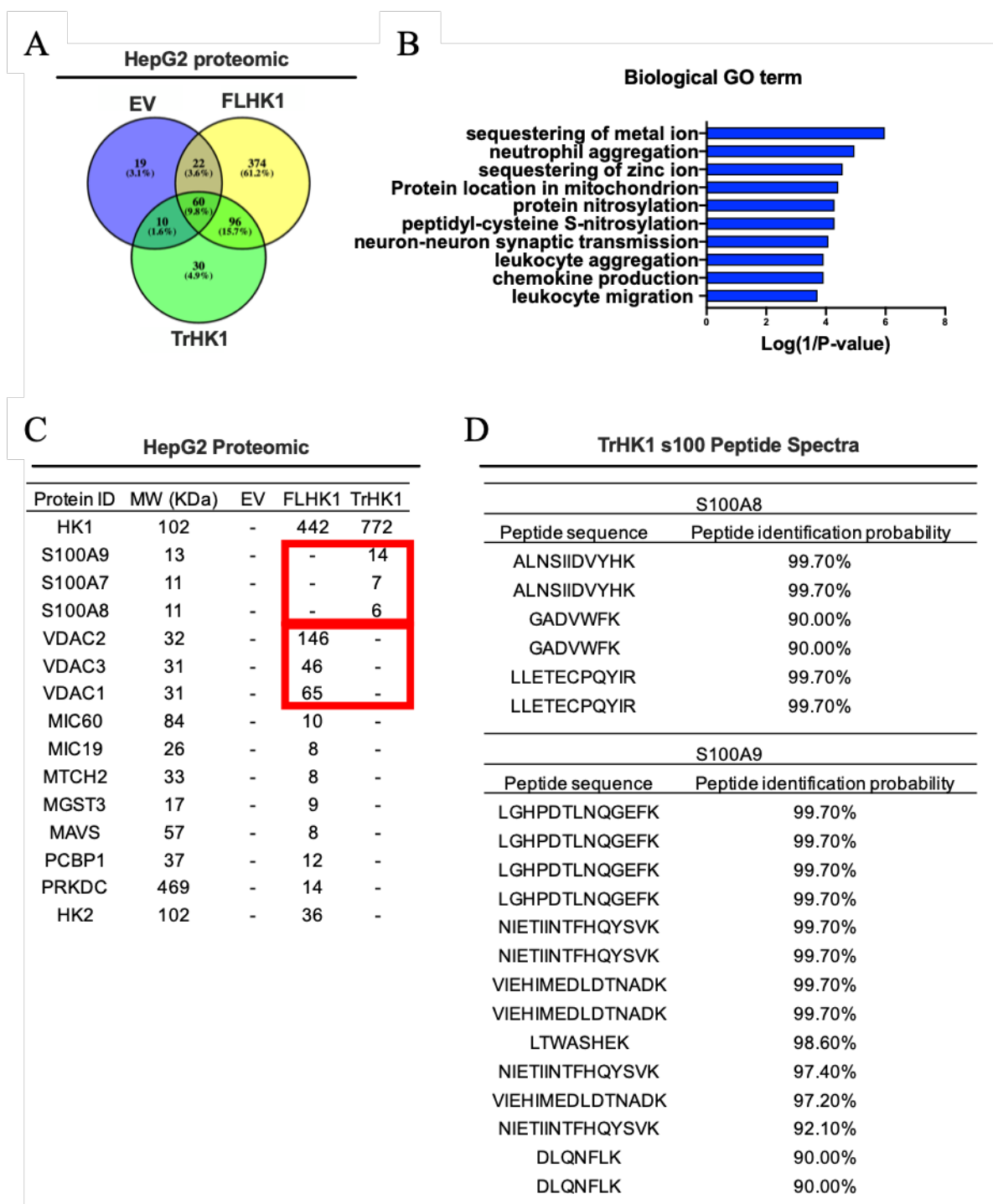


Figure 29. Proteomic analysis of HepG2 cells with FLHK1 and TrHK1 overexpression.

A. Venn diagram of total unique spectra identified in co-IP and MS proteomics of HepG2 cell with overexpression of EV, FLHK1, and TrHK1. **B.** PANTHER Biological GO-enrichment analysis of proteins identified by proteomics. **C.** Table of selected proteins identified by MS with HK1, VDAC

and S100 family proteins highlighted with red borders (threshold of >5 Unique Spectral Counts).

D. Peptide spectra of S100A8 and S100A9 identified by MS. All HepG2 co-IP and MS data was analyzed using Scaffold Proteome Software.

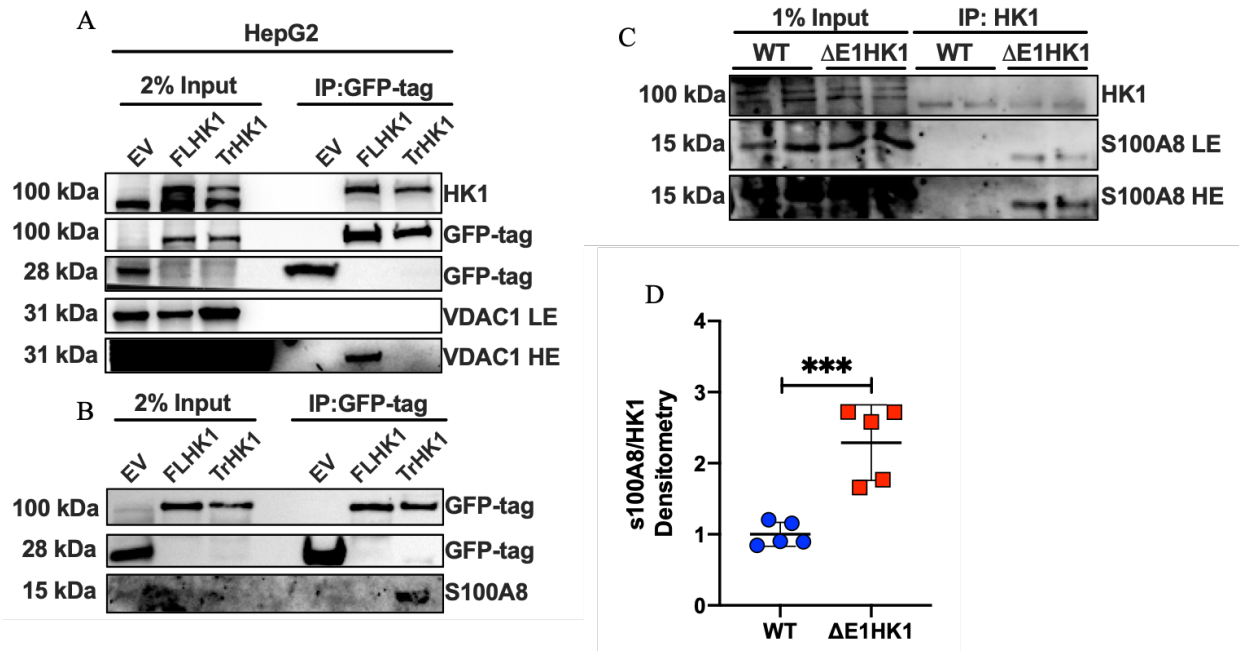


Figure 30. Co-IP of cytosolic HK1 with S100A8/9.

A-B. Co-IP of GFP-tagged EV, FLHK1, and TrHK1 proteins in HepG2 cells and western blot analysis probing for S100A8. **C.** Western blot of HK1 co-IP from BMDMs treated with LPS (200ng/ml) for 3hrs and probing for S100A8 binding. LE = Low-exposure and HE = high-exposure (also see Fig. S6G). **D.** HK1 co-IP western blot densitometry analysis of S100A8 divided by total HK1 eluted (n=5 mice per condition, unpaired t-test, mean ± SD, densitometry analysis performed using *Gel Analyzer* on ImageJ).

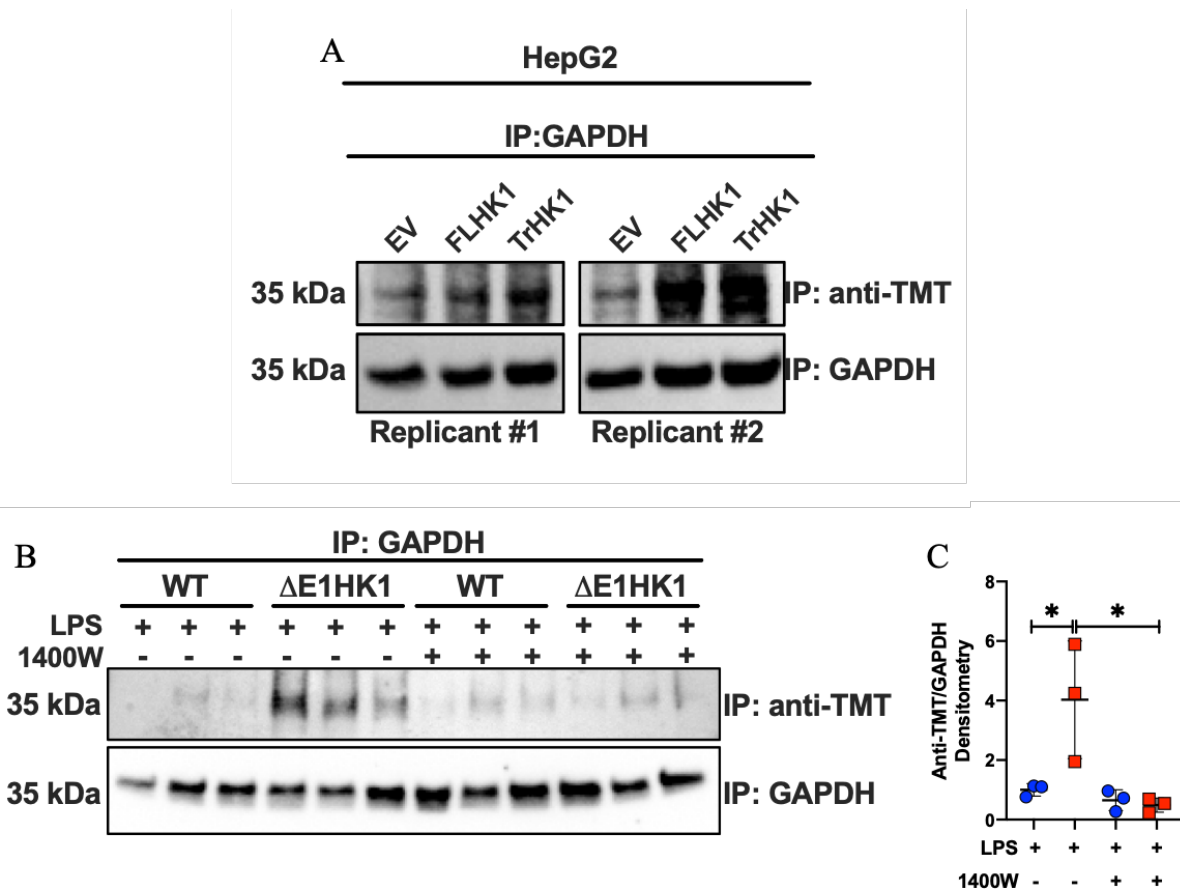
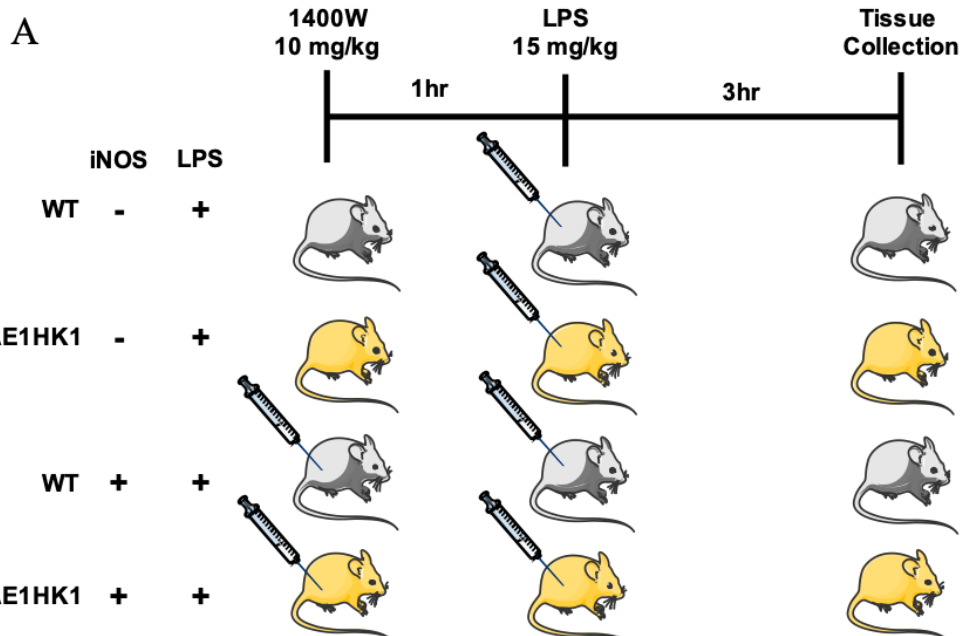
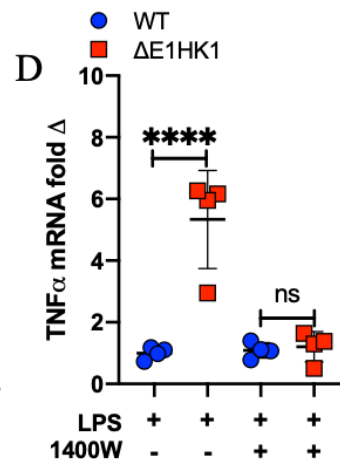
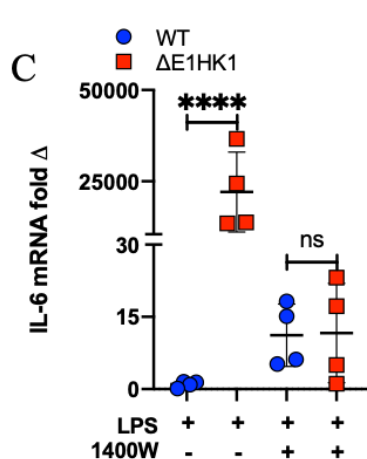
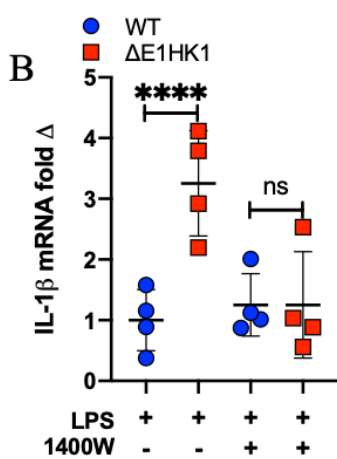


Figure 31. Cytosolic HK1 mediates GAPDH nitrosylation through S100A8/9 binding.

A. Western blot of GAPDH IP and TMT switch nitrosylation assay in HepG2 cells (n=2 replicates per condition). **B-C.** Western blot of GAPDH IP and TMT switch nitrosylation assay of LPS (200ng/ml) treated BMDMs \pm 1400W (10mg/kg) and Western blot densitometry of anti-TMT normalized to total GAPDH eluted (n=3 mice per condition, one-way ANOVA and Tukey's post-hoc test, mean \pm SD, densitometry analysis performed using *Gel Analyzer* on ImageJ).



in vivo iNOS inhibition: Spleen Tissue



Serum Cytokines

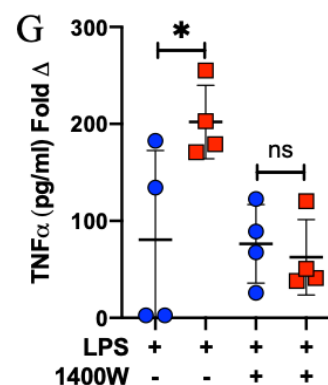
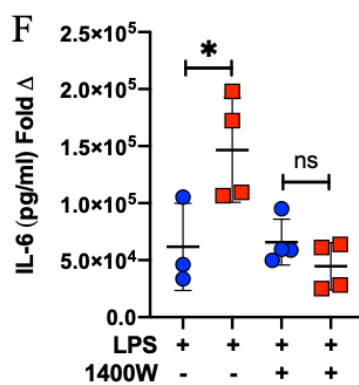
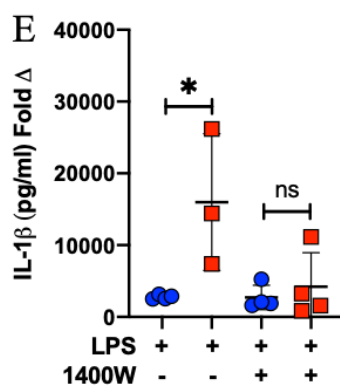


Figure 32. *In vivo* inhibition of iNOS reverse Δ E1HK1 hyper-inflammation.

A. Schematic of *in vivo* LPS (15mg/kg) \pm 1400W (10mg/kg) i.p. injection experiment. **B-D.** Spleen tissue mRNA expression of IL-1 β (A), IL-6 (B), and TNF α (C) from mice after i.p. injection of LPS \pm 1400W (n=4 mice per condition, one-way ANOVA and Tukey's post-hoc test, mean \pm SD). **E-G.** Mouse serum cytokine analysis using ELISA for IL-1 β (E), IL-6 (F), and TNF α (G) from *in vivo* LPS treated mice \pm 1400W (10mg/kg) (n=3-4 mice per condition, two-way ANOVA, mean \pm SD).

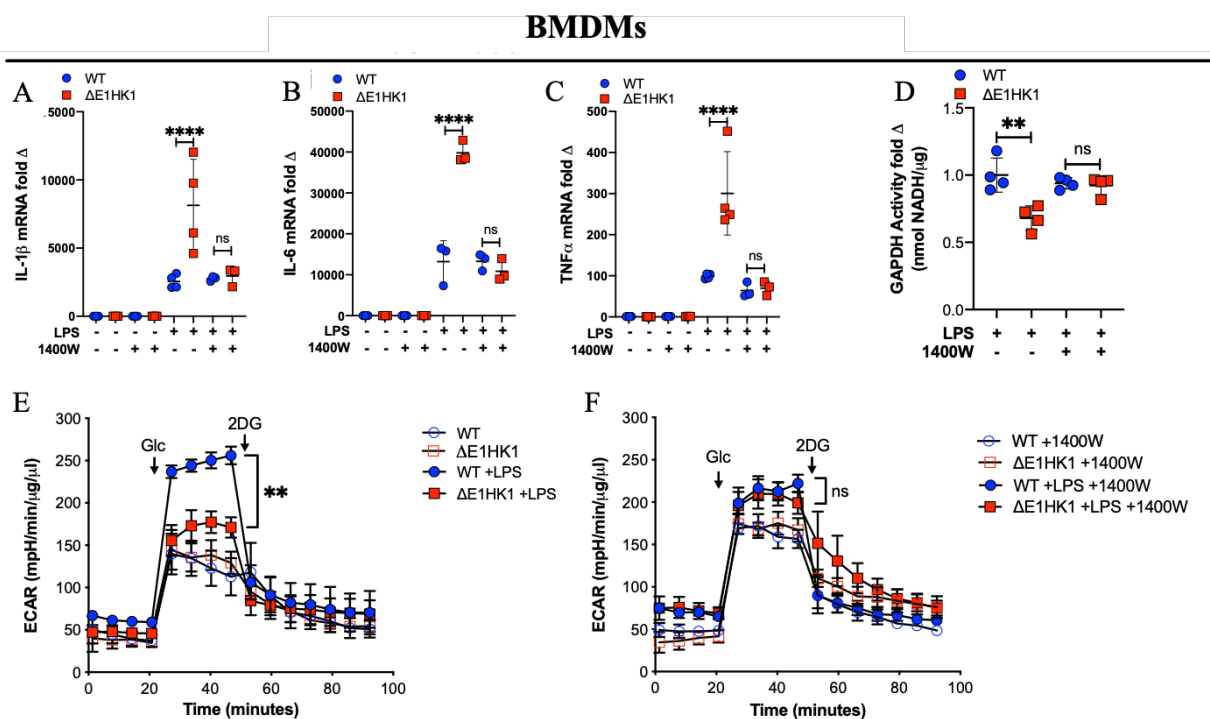


Figure 33. BMDMs with iNOS inhibition eliminates hyper-inflammation in Δ E1HK1 mice.
A-C. mRNA expression of IL-1 β (A), IL-6 (B), and TNF α (C) from isolated BMDMs \pm 4hrs LPS (200ng/ml) \pm 1400W (50 μ M) (n=4 mice per condition, one-way ANOVA and Tukey's post-hoc test, mean \pm SD). **D.** GAPDH activity normalized to total protein from BMDMs treated with LPS (200ng/ml) \pm 1400W (50 μ M) (n=4 mice per condition, one-way ANOVA and Tukey's post-hoc test, mean \pm SD). **E-F** ECAR trace of BMDMs \pm 5hrs of LPS (200ng/ml) (E) or \pm 5hrs LPS \pm 1400W (50 μ M) (F) (n=3-4 mice per condition, repeated measures two-way ANOVA and Tukey's post-hoc test, mean \pm SEM).

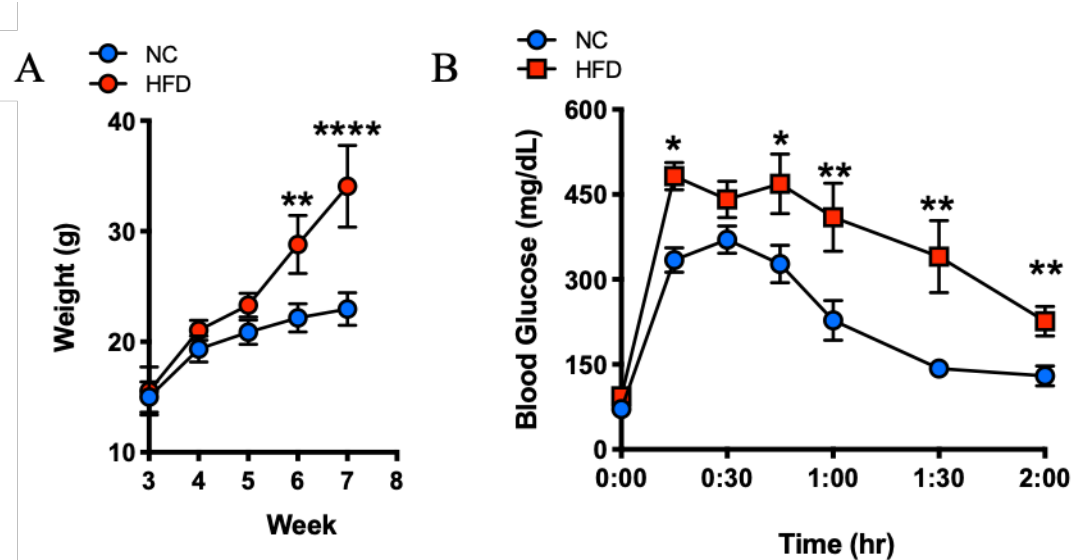


Figure 34. Weight and blood glucose in mice after 27-weeks of NC and HFD.

A. Mouse weights from 3 to 8 weeks after NC and HFD (n=4-7 mice per condition, repeated measures two-way ANOVA, mean \pm SD). **B.** Glucose tolerance test (GTT) from NC and HFD mice (n=5 mice per condition, repeated measures two-way ANOVA, mean \pm SD).

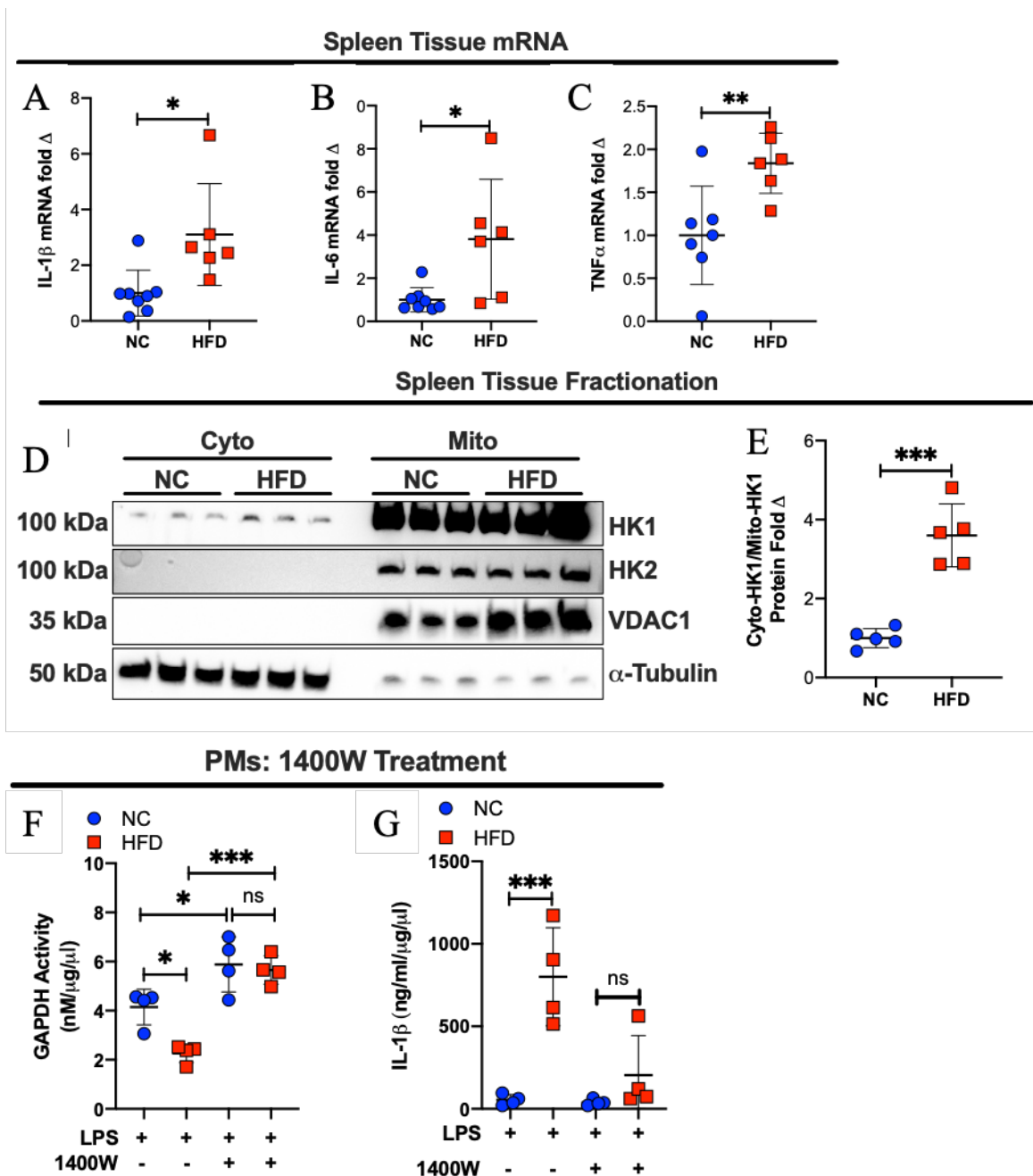


Figure 35. Diabetes and aging are associated with HK1 mitochondrial dislocation and increased cytokine production.

A-C. Spleen tissue mRNA expression of IL-1 β (A), IL-6 (B), and TNF α (C) from NC and HFD mice (n=6-8 mice per condition, unpaired t-test, mean \pm SD). **D-E.** Western blot analysis of HK1 and HK2 from mitochondrial and cytosolic subcellular fractionation of spleen tissue from NC and HFD mice (D). Cytosolic HK1 to mitochondrial HK1 densitometry quantification (E) (n=5 mice

per condition, unpaired t test, mean \pm SD, densitometry analysis performed using *Gel Analyzer* on ImageJ). **F.** GAPDH activity normalized to total protein in PMs isolated from NC and HFD treated with LPS (300ng/ml) \pm 1400W (50 μ M) for 4hrs (n=4 mice per condition, unpaired t-test, mean \pm SD). **G.** IL-1 β ELISA from media of PMs treated with LPS (300ng/ml) for 6hrs and ATP (2.5mM) for 30min (n=4 mice per condition, one-way ANOVA and Tukey's post-hoc test, mean \pm SD).

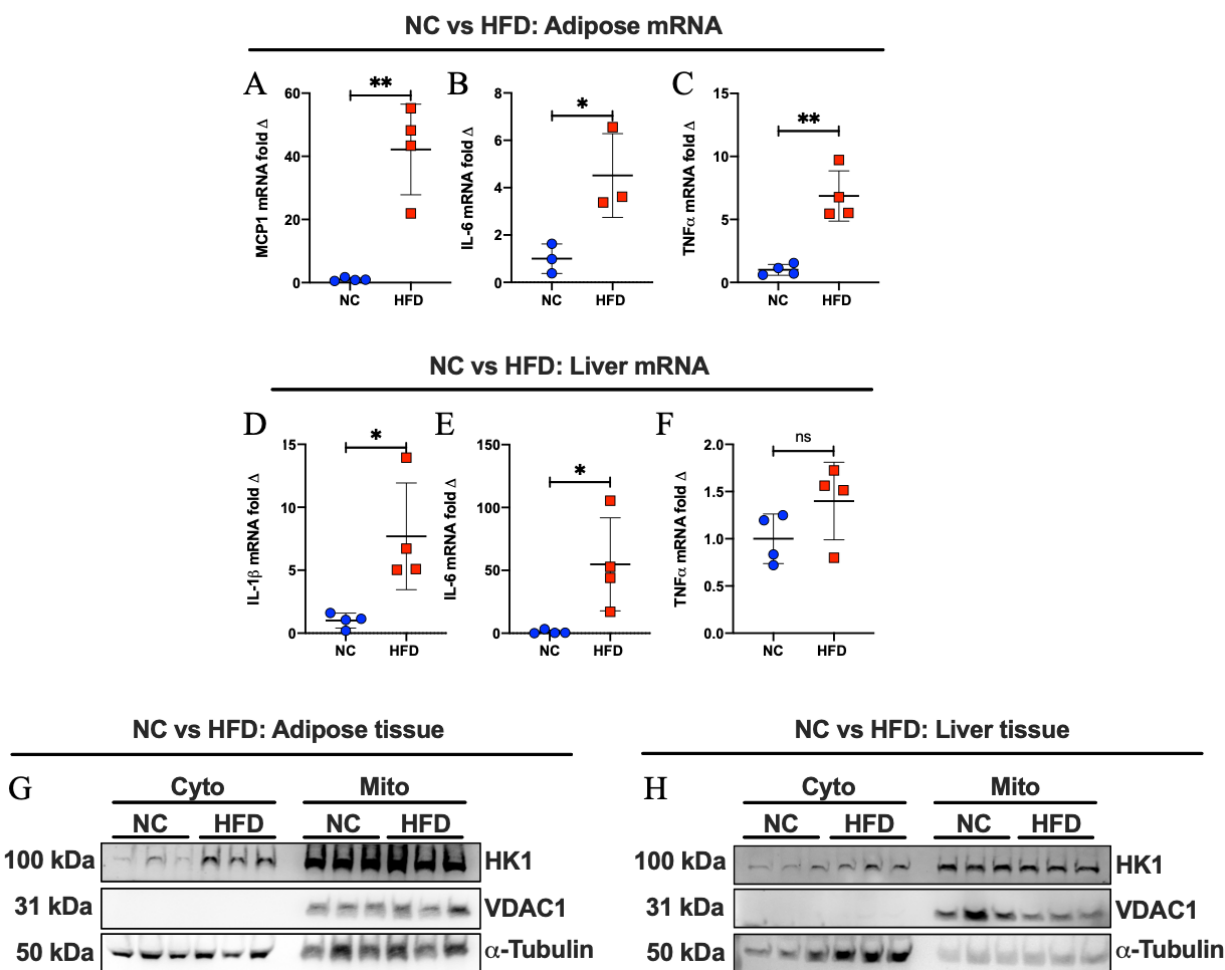


Figure 36. Cytokine production and HK1 subcellular localization in mice after NC and HFD.

A-C. mRNA analysis of MCP1 (a), IL-6 (b), and TNF α (c) in adipose tissue (n=3-4 mice per condition, unpaired t-test, mean \pm SD). **D-F.** mRNA analysis of IL-1 β (d), IL-6 (e), and TNF α (f) in liver tissue (n=3-4 mice per condition, unpaired t-test, mean \pm SD). **G-H.** Western blot analysis of HK1 from mitochondrial and cytosolic subcellular fractionation of adipose (g) and liver (h) tissue from NC and HFD mice (n=3 mice per condition).

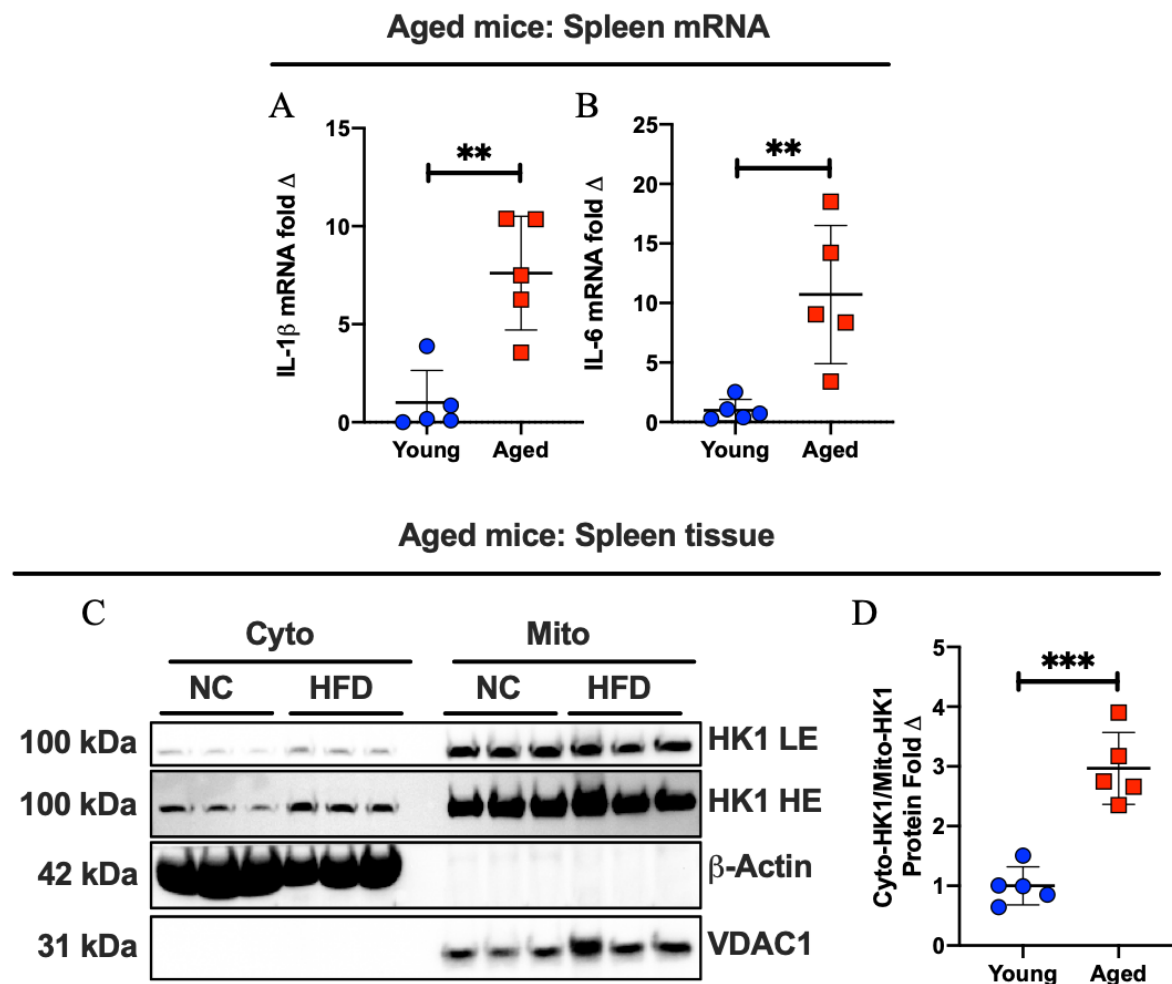


Figure 37. Cytokine production and HK1 subcellular localization in aging mice.

A-B. mRNA expression of IL-1 β (A) and IL-6 (B) in spleen tissue from young and aged mice (85-weeks-old) (n=5 mice per condition, unpaired t-test, mean \pm SD). **C-D.** Representative western blot of mitochondrial and cytosolic subcellular fractionation of spleen tissue from young and aged mice (C) and cytosolic HK1 to mitochondrial HK1 densitometry quantification (D) (n=5 mice per condition, unpaired t-test, mean \pm SD, densitometry analysis performed using *Gel Analyzer* on Fiji/ImageJ).

CHAPTER 4: CONCLUSION

DISCUSSION AND FUTURE DIRECTIONS

We previously showed that the mitochondrial binding of HK1 and HK2 are needed for their protective effects against cell death(182). Other reports have suggested that the binding of HK1 and HK2 to the mitochondrial allows preferential access of these enzymes to mitochondrial-produced ATP that is transported through VDAC, in addition to effective delivery of ADP that is produced by glucose phosphorylation to ANT for transport to mitochondrial matrix(65,183,184). However, the K_m for ATP of these enzymes is significantly lower than cytosolic ATP(65,185), making the validity of this hypothesis dubious. Thus, the physiological significance of HK1 binding to the mitochondria is not clear. G6P can shuttle through different pathways(5), and despite extensive work on glucose metabolism, there is a paucity in our understanding of how the metabolic fate of G6P is determined. Here, we identify the mechanism by which the localization of HK1, independent of its enzymatic activity, regulates the metabolic fate of its enzymatic product, G6P, and increases its shunting into the PPP. These data highlight how subcellular localization of a metabolic enzyme determines the fate of its product, and provides physiological significance for the mitochondrial binding of HK1.

We also showed that the mechanism by which cytosolic HK1 increases PPP in macrophages is through GAPDH nitrosylation and its enzymatic inhibition. A role for GAPDH nitrosylation in inflammation has been previously reported (168,169,180,186,187). Our results provide a biological context and mechanism for GAPDH regulation and links these steps to HK1 mitochondrial binding. GAPDH is a critical step in glycolysis in that the substrates above this step can enter the PPP, and thus its inhibition would block glycolysis, while allowing shuttling of upstream intermediates into PPP. We suspect that this system was developed in mammalian cells to serve as a means of regulating the metabolic fate of G6P into ancillary pathways off glycolysis,

such as the PPP. Since the metabolic block at GAPDH increases metabolite levels above this point, it would be interesting to investigate how other metabolic branch points of G6P (i.e., glycogenesis and hexosamine pathway) are affected in other contexts.

In light of our findings, it is now important to determine both physiological and pharmacological factors that modulate HK1 binding to the mitochondria and its release into the cytoplasm. HK1 dislocation from the mitochondria has been reported to occur in response to a number of pathways and processes, including senescence, reactive oxygen species, CLT, inhibition of AKT, and activation of GSK(188,111,177,189–192,38). Thus, there is shuttling of HK1 from the mitochondria to the cytoplasm under physiological and pathological conditions. In addition, a synthetic peptide with sequence homology to the N-terminus of HK1 can be used to displace the proteins from the mitochondria(193). This peptide can therefore potentially be used in clinical settings to induce HK1 displacement from mitochondria and increase the inflammatory response in conditions of impaired inflammation, such as immunosuppressive disorders. We also showed that in the setting of conditions associated with low-grade inflammation, such as aging and diabetes, there is endogenous HK1 dislocation from the mitochondria, increased production of inflammatory markers, and diminished GAPDH activity with LPS stimulation. These results indicate that HK1 mitochondrial binding may mediate the inflammation underlying the pathogenesis of diabetes and aging. Thus, it would be important to devise strategies to maintain HK1 on the mitochondria to reduce or ablate the inflammation (either low-grade or fulminant) that contributes to the negative sequelae of these and other inflammation-associated disorders.

In summary, we have shown that HK1 mitochondrial dissociation produces a metabolic block at the level of GAPDH, which increases PPP metabolism. This feature of HK1 regulation is dependent on its localization between the cytosol and mitochondria and is independent of its

enzymatic activity, since removal of HK1 MBD does not change its enzymatic function. We also demonstrate that the increased PPP metabolism has functional consequences, as dislocation of HK1 to the cytoplasm results in higher cytokine production and exaggerated inflammatory response to endotoxemia *in vivo*. Additionally, we show that the mechanism for the altered G6P metabolism by HK1 cellular distribution is through increased GAPDH S-nitrosylation and subsequent attenuation of its enzymatic activity. Our data suggest that cytosolic HK1 binds to S100A8/A9, leading to S-nitrosylation of GAPDH through iNOS. Furthermore, we find that inhibition of iNOS is sufficient to reverse the metabolic alterations and elevated cytokine production seen with mitochondrial dissociation of HK1. Therefore, HK1 subcellular localization is a critical modulator of glycolysis, and regulates the inflammatory response in macrophages **(Figure 38)**.

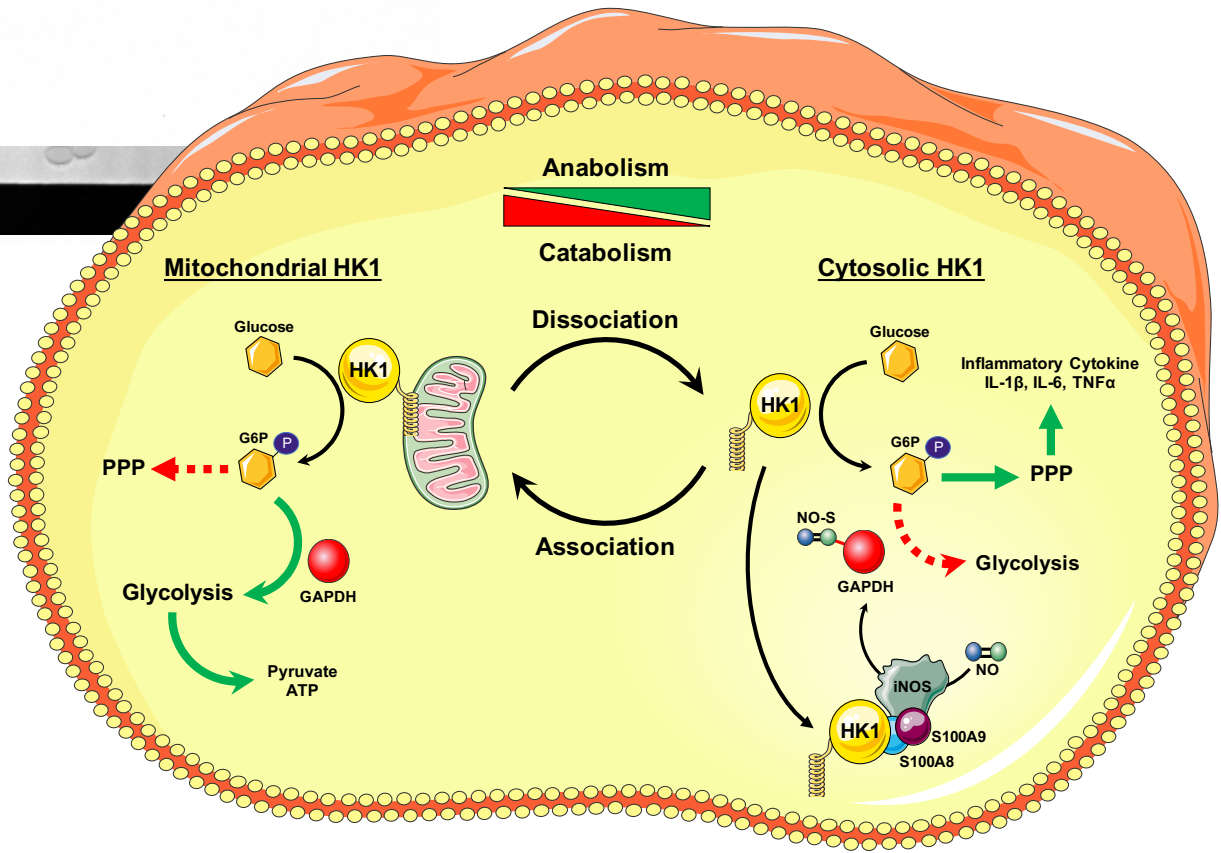


Figure 38. HK1 mitochondrial dissociation induced hyper-inflammation mechanism

METHODS

Cell Lines and Culture

RAW264.7 cells were a gift from Jason A. Wertheim MD, PhD. HepG2 and HEK293T cells were obtained from ATCC. RAW264.7, HEK293T, and HepG2 cells were cultured in Dulbecco's Modified Eagle's Medium (DMEM) (Corning) supplemented with 10% FBS (Atlanta Biologicals), 2mM glutamine (HyClone), and 1mM sodium pyruvate (Corning). RAW264.7 cells were treated with 300ng/ml LPS for 4-6hrs with or without CLT (50 μ M).

Mouse Line

HK1 ^{Δ E1HK1/ Δ E1HK1} (Δ E1HK1) and HK1^{WT/WT} wild type (WT) control mice were generated by the Northwestern Mutagenesis and Transgenic core. Mouse genetic background is C57BL/6J. Mice were maintained in the barrier facility at Northwestern University under specific pathogen-free conditions in accordance with Federal and University guidelines and protocols approved by Institutional Animal Care and Use Committee (IACUC) with 12hr light and 12hr dark cycle, and received normal chow. Male and female mice were used at 8-12 weeks of age. HFD and NC diet mice were maintained on respective diets for 27 weeks. All animal studies were approved by the IACUC at Northwestern University and were performed in accordance with guidelines from the National Institutes of Health.

Peritoneal Macrophages Isolation and Cell Culture

Peritoneal macrophages were isolated from 8-10-week-old Δ E1HK1 and littermate control WT mice by peritoneal lavage as described previously (194). Briefly, mice were euthanized and the peritoneal cavity was injected with PBS supplemented with 5% FBS using a 27g needle. The abdominal wall was gently agitated to dislodge peritoneal cells. Using a fresh 25g needle, the

peritoneal lavage (PBS and peritoneal cells) was aspirated and collected. Cells were then centrifuged at 500g for 10min and re-suspended in 1mL of complete RPMI (Corning) supplemented with 10% FBS (Atlanta Biologicals), 2mM glutamine (HyClone), 1mM HEPES (Corning) and 1mM pyruvate (Corning). Stimulation with LPS (Invivogen) was performed the next day. 300ng/ml of LPS was given to the cells for 4-6hrs with or without the following drugs; OT (50 μ M), 6-AN (1mM), 1400W (50 μ M), or CGP3466 (50nM).

BMDM Isolation and Cell Culture

BMDMs were isolated from Δ E1HK1 and WT mice as previously reported (134). Briefly, bone marrow was isolated from the tibia and femur of 8-10-week-old mice by puncturing one end of the femur and tibia with a 27g needle and placing it in a 0.5ml tube with a hole punched in the bottom. The 0.5ml tube containing the bone was then placed in a 1.75ml tube and centrifuged at 5,000xg for 3.5 minutes. Bone marrow was then collected into the 1.75ml tube and resuspend in 1ml of RBC lysis buffer (abcam) for 1 minute and then transferred to a 50ml tube with 4ml RBC lysis buffer and incubated for 4 minutes. Next, 35ml of PBS was added and centrifuged at 300xg for 5min and supernatant was then decanted and cell pellet was re-suspended in complete RPMI with 20ng/ml mCSF (Preprotech). Cells were counted using a hemocytometer and plated in 10cm tissue culture plates at a density of 3-million cells/plate. Cells were cultured with 20ng/mL mCSF to induce differentiation into BMDMs. Media was changed every 2 days and BMDMs were harvested by scraping on day 6 and plated in 12 well plates at a density of 1-million cells/well for mRNA extraction experiments. BMDMs were stimulated in the same manner as peritoneal macrophages (LPS dose for BMDMs was 200ng/ml).

Generation of HK1 Lentivirus Gene Overexpression Constructs

Lentivirus C-terminal GFP-tag fusion over-expression constructs for EV, FLHK1, and TrHK1 were cloned into the pHIV-Puro vector (generated in our lab) using InFusion-HD cloning method. Lentiviral particles were produced in HEK293T cells co-transfected with pSPAX2 and pMD2.G packaging vectors using standard protocols. To generate the full-length and truncated HK1-GFP fusion plasmids, In-Fusion cloning PCR primers were designed to the first or second exon of the 2754-bp fragment from the EGFP-N3 plasmid containing FLHK1 or TrHK1. To perform the In-Fusion reaction, the PCR primers also contained overhang regions containing *XhoI* and *BamHI*-HF restriction enzyme sites and a 15-bp homology portion to the pHIV-Puro vector to facilitate recombination.

RNA Isolation, Reverse Transcription and Quantitative RT-PCR

RNA was isolated from cells or tissues using RNA-STAT60 (Teltest) followed by chloroform extraction and precipitation. Reverse transcription was carried out using qScript cDNA Synthesis Kit (Quanta Bio). The resulting cDNA was amplified quantitatively using PerfeCTa SYBR Green Mix (Quanta Bio) on a 7500 Fast Real-time PCR System (Applied Biosystems). The relative gene expression was determined using differences in Ct values between gene of interest and house-keeping control genes. Complete list of primers can be found in Key Reagents Table.

Western Blots

Cells and tissue were lysed in radio-immunoprecipitation assay (RIPA) buffer supplemented with 1x protease inhibitor (G-Bioscience). Protein concentration in samples was determined using the BCA Protein Quantification Kit (Pierce). Equal amounts of protein were loaded on a tris-glycine

polyacrylamide gel (Life Technologies) and transferred to nitrocellulose membrane. After blocking with tris-buffered saline containing 0.05% Tween 20 (DOT Scientific Inc) and 5% BSA, the membrane was incubated with primary antibody against indicated proteins. A complete list of antibodies is included in Key Resources Table. For low molecular weight protein S100A8 western blots, 16% tricine protein gels (ThermoFisher) were used and western blots run as previously described (195). Western blot densitometry was performed using Fiji/ImageJ *Gel analyzer* macro (196).

Confocal Imaging

Glass-bottom confocal dishes (35 mm; VWR) were coated with 60nM fibronectin (Sigma-Aldrich), diluted in 0.1% gelatin overnight. Before plating cells, coated confocal dishes were washed twice with PBS. BMDMs (100,000 cells/well), PMs (100,000 cells/well), HepG2 (50,000 cells/well), or RAW264.7 (50,000 cells/well) cells were plated in their respective growth media (complete DMEM or RPMI) and allowed to settle overnight before immunofluorescence (IF) staining. For fixed cell immunofluorescence (IF), cells were plated in 6-well plates (Corning) containing 15mm glass coverslips (Fisher-Scientific) coated in gelatin and fibronectin. Prior to fixation, growth media was removed and cells were washed 2x with PBS. Cells were fixed with 1ml of ice-cold 4% formaldehyde for 10min at room temperature (4% formaldehyde prepared from 16% stock and diluted in PBS). After fixing the cells, plates were washed with PBS 2x and permeabilized with 0.3% triton-X-100 in PBS for 10min at room temperature. Then, cells were blocked with 10% FBS/PBS for 1 hour at room temperature and subsequently treated with primary antibody diluted in 10% FBS/PBS solution over-night. The next day, secondary antibody was diluted in 10% FBS/PBS at 1:1000 and incubated for 2hrs at room temperature. Cells were then

washed 3x with PBS and mounted on glass slides (Fisher-Scientific) using ProLong Gold Antifade Mountant with DAPI and imaged using confocal microscope. HK1 antibody diluted at 1:100, ATP Synthase-beta (ATP5B) Monoclonal-Alexa Fluor 555 antibody diluted at (1:200), and MitoTracker Deep Red FM (1 μ M). All images were acquired on a Zeiss LSM 510 Meta confocal microscope. Images were quantified using ImageJ.

TMRE Colocalization

HepG2 cells with EV, FLHK1, or TrHK1 overexpression were washed with PBS and changed to confocal buffer (25mM D-glucose, 1.8 mM CaCl₂, 2.5 mM KCl, 140 mM NaCl, 2 mM sodium pyruvate, 2 mM glutamine, 20 mM HEPES, pH 7.5, 1 mM MgCl₂). Cells were stained with 5nM TMRE (for mitochondrial stain) for 20 minutes. Cells were then washed with PBS, and fresh confocal buffer was added. TMRE (red channel) and GFP (green channel) signals were analyzed for colocalization using ImageJ Coloc-2 function to determine Pearson correlation coefficient between green and red channel for confocal images.

¹³C₆-glucose Tracing and Steady-State Metabolomics

Cultured BMDMs or HepG2 cells were treated with ¹³C₆-glucose for 4hrs \pm LPS (200ng/ml) and mass-spectrometry and metabolite identification was performed on 80% methanol & 20% ultrapure water extracted metabolites. Whole brain tissues were harvested from mice and immediately flash frozen in liquid nitrogen until harvested for metabolites using 80% methanol & 20% ultrapure water extraction protocol. Metabolomics services were performed by the Metabolomics Core Facility at Robert H. Lurie Comprehensive Cancer Center of Northwestern University. Samples were analyzed by High-Performance Liquid Chromatography and High-

Resolution Mass Spectrometry and Tandem Mass Spectrometry (HPLC-MS/MS). Specifically, system consisted of a Thermo Q-Exactive in line with an electrospray source and an Ultimate3000 (Thermo) series HPLC consisting of a binary pump, degasser, and auto-sampler outfitted with an Xbridge Amide column (Waters; dimensions of 4.6 mm × 100 mm and a 3.5 μm particle size). The mobile phase A contained 95% (vol/vol) water, 5% (vol/vol) acetonitrile, 20 mM ammonium hydroxide, 20 mM ammonium acetate, pH = 9.0; B was 100% Acetonitrile. The gradient was as following: 0 min, 15% A; 2.5 min, 30% A; 7 min, 43% A; 16 min, 62% A; 16.1-18 min, 75% A; 18-25 min, 15% A with a flow rate of 400 μL/min. The capillary of the ESI source was set to 275 °C, with sheath gas at 45 arbitrary units, auxiliary gas at 5 arbitrary units and the spray voltage at 4.0 kV. In positive/negative polarity switching mode, an m/z scan range from 70 to 850 was chosen and MS1 data was collected at a resolution of 70,000. The automatic gain control (AGC) target was set at 1×10^6 and the maximum injection time was 200 ms. The top 5 precursor ions were subsequently fragmented, in a data-dependent manner, using the higher energy collisional dissociation (HCD) cell set to 30% normalized collision energy in MS2 at a resolution power of 17,500. The sample volumes of 10 μl were injected. Data acquisition and analysis were carried out by Xcalibur 4.0 software and Tracefinder 2.1 software, respectively (both from Thermo Fisher Scientific).

Glucose Uptake Assay

2-NBDG glucose uptake assay of LPS-activated BMDMs from WT and ΔE1HK1 mice was performed based on previous reports (197). Briefly, cells were cultured overnight in 96 well plates and treated the next day with 300μM 2NBDG for 1hr and then quickly washed 3x with PBS. Cells were then re-suspended in RIPA buffer and imaged in a fluorescent plate reader.

Extracellular IL-1 β Western Blot

BMDMs were stimulated with O5:B55 LPS (Invivogen) for 6 hours with addition of 2mM ATP (Sigma) for 30 minutes to activate the cleavage of pro-IL-1 β (35kDa) to cleaved-IL-1 β (17kDa). Cell supernatant was collected and analyzed by ELISA according to manufacturer's instructions for IL-1 β (DY401), IL-6 (DY406), and TNF α (DY410).

S-Nitrosylation Western Blot of GAPDH Immunoprecipitation

GAPDH immunoprecipitation of HepG2 and BMDM cells was performed and nitrosylated cysteines were replaced with covalent binding of TMT using Pierce S-Nitrosylation western blot kit according to manufacturer's protocol. Briefly, free cysteines were blocked with MMTS reagent, lysates were treated with iodoTMT/ascorbate to induce replacement of unstable S-NO with stable S-TMT moiety. Western blot was then run on the TMT-replaced lysates and probed with GAPDH (dilution 1:8,000) and anti-TMT (dilution 1:1000).

Seahorse Assay

The day before the assay, the Seahorse cartridge was placed in the XF calibrant and incubated overnight at 37°C. On the day of the assay, cells were seeded into the Seahorse 96-well plate at 15,000 cells/80 μ l per well for HepG2 cells or 100,000 cells/80 μ l per well for BMDMs. The plates were incubated at RT for 1 hour in glucose free complete DMEM or RPMI without bicarbonate or phenol-red to allow even distribution of cells across the well floor. Before placing the sample plates in the Seahorse XF96 Analyzer, medium volume was adjusted to 175 μ l in each well. 11mM or 25mM glucose for HepG2 cells or BMDMs respectively, Oligomycin at 2 μ M, CCCP at 10 μ M,

and 2DG at 2 μ M each, diluted in DMEM, were injected sequentially into each well including control wells, containing only medium, following the standard Seahorse protocol. For acute injection of LPS, the first port of the drug cartridge was replaced with LPS at 200ng/ml.

Endotoxin-Induced Model of Sepsis

LPS induced sepsis model in mice was approved by Northwestern University Institutional Animal Care and Use Committee. For short term LPS induced cytokine quantification, C57/Bl6 mice (aged 10-12 weeks) were treated i.p. with or without 1400W (10mg/kg) for 2hrs prior to i.p. treatment with ultrapure O5:B55 LPS from Invivogen (15mg/kg) i.p. for 4 hours. Whole blood samples were harvested via cardiac puncture after mice were euthanized. Cytokine production in serum from whole blood was measured using the Mouse IL-1 β (DY401), IL-6 (DY406), and TNF α (DY410) ELISAs from R&D. For survival studies, Crude O5:B55 LPS (Sigma) was administrated i.p. at a sub-lethal dose of 15 mg/kg and mice were monitored over 72hrs, every 2-4hrs for survival and signs of deterioration to determine humane endpoints (198).

Commercial Assay Kits

The following kits were used according to the manufacturer's instructions: Promega NADP/NADPH quantification kit (G9081) and NAD/NADPH quantification kit (G9071); Glyceraldehyde-3-Phosphate Dehydrogenase Activity Assay kit (abcam); ELISAs for IL-1 β (DY401), IL-6 (DY410), and TNF α (DY406).

CBC and WBC from Whole Blood

A HEMEVET blood cell analyzer was used on whole blood from mice using mouse standard blood as a control for comparing readouts.

Co-Immunoprecipitation- Western Blot

Anti-HK1 magnetic beads IP kit (Sino Biological) was used to IP HK1 from BMDMs. BMDMs were plated in 15cm culture dishes and lysed using NP40 cell lysis buffer (Sino Biological-provided in kit) and sonicated for 5 pulses for 1sec each. Lysate was centrifuged at 8,000xg and supernatant was collected in a fresh tube. 50 μ L of HK1-magnetic beads was added to a fresh 1.7mL tube and washed with 150 μ L 1xTBS (10xTBS: 60.6g Tris, 87.6g NaCl, 1M HCl, 7.5pH) with 0.5% Tween-20 (DOT Scientific Inc) and beads were precipitated with magnetic separator (Sino Biological-provided in kit). 1,000ug of lysate from Δ E1HK1 and WT BMDMs was added to the precipitated magnetic HK1 beads and incubated overnight at 4 $^{\circ}$ in rotator. Next day, beads were magnetically precipitated and washed 3x with 1xTBST. Bound protein from precipitated beads was eluted using acidity elution buffer (Sino Biological-provided in kit) and western blot analysis was performed.

Co-Immunoprecipitation- Mass Spectrometry

HepG2 cells were plated to confluency on 15cm dishes and scrapped in 10-mL PBS and collected into 15mL conical tube. Cells in PBS were then centrifuged at 500xg for 15min at 4 $^{\circ}$ C. Supernatant was then aspirated and cell pellet was re-suspended in 300 μ L co-IP lysis buffer (100mM HEPES-pH 7.7, 250mM KCl, 2mM MgCl₂, 2mM EDTA, 10% glycerol, 1% digitonin) and then transferred to 1.7mL tubes. The lysate was then sonicated for five pulses of 1 second each and incubated on

ice for 30 minutes. Lysates were then centrifuged at 16,000xg for 15min and supernatant was collected in fresh 1.7mL tube. Protein quantification was performed using BCA (Pierce) and 2,000µg of protein was used for co-IP. Co-IP was performed using GFP-Trap-Agarose beads (Chromotek) according to manufacturer's protocol. Eluted samples were given to the Northwestern Proteomics Core using the 100-minute gradient tandem mass spectrometry Orbitrap.

Lactate Quantification Assay

Lactate quantification adapted from previous work (Gandhi et al., 2009). The lactate reporter system contained 200 µmol/L Amplex red (Molecular Probes), 4 units/mL lactate oxidase (Sigma), and 0.8 units/mL horseradish peroxidase (Sigma) in 50 mmol/L Tris-HCl, pH 7.4, which was deoxygenated with helium to reduce oxidation of Amplex red. The assays were incubated for 30 min, followed by measurement of fluorescence at 590 nm using excitation at 530 nm.

Glucose-6-phosphate Quantification Assay

Glucose-6-phosphate (G6P) quantification assay adapted from previous work (Zhu et al., 2009). Ten µl of G6P standards and extraction samples were pipetted to a 96-well plate, followed by the addition of 90 µl of a cocktail of 50 mM triethanolamine (pH 7.6), 1.0 mM MgCl₂, 100 µM NADP⁺, 10 µM resazurin, 0.1 U/ml G6PD, and 0.2 U/ml diaphorase. The assays were incubated for 30 min, followed by measurement of fluorescence at 590 nm using excitation at 530 nm.

***In vivo* Metabolic Studies**

For all *in vivo* metabolic studies, age-matched WT and ΔE1HK1 littermates were used. For the glucose-tolerance test (GTT), mice were fasted for 16 hours and injected via an i.p. approach with

a 20% dextrose (Millipore Sigma) solution in PBS at 2g/kg body weight. For the insulin-tolerance test (ITT), mice were fasted for 4 hours and injected via an i.p. approach with a 0.1 U Humulin/ml PBS solution at 0.75 U/kg body weight (Lily).

Mitochondrial and Cytosolic Subcellular Fractionation

Mitochondrial Isolation Kit for Tissue (Pierce) was used to purify mitochondrial and cytosolic protein subcellular fractions according to the Pierce manufacturer's protocol.

HK Activity Assay

HK activity was determined, as previously described (199). In brief, cells were plated on 12cm dishes and allowed to attach overnight. The next day, cells were washed once with PBS and harvested by scraping and pelleted at 4000 rpm for 5 minutes. Cells were lysed by sonication, five pulses of 1 second, in 100 μ l homogenization buffer: 0.2% Triton X-100, 0.5 mM EGTA, 10 mM D-(+)-glucose, 11.1 mM monothioglycerol, 45 mM Tris-HCl (pH 8.2), and 50 mM KH_2PO_4 . After sonication, lysates were centrifuged at 8000 rpm for 5 minutes. HK activity was determined by the whole-cell lysate's ability to phosphorylate glucose over 2 minutes in an assay mixture with final concentrations of 50 mM triethanolamine chloride, 7.5 mM MgCl_2 , 0.5 mM EGTA, 11 mM monothioglycerol, 0.5 to 25 mM glucose, 6.6 mM ATP, 0.5 mg/mL NADP, and 0.5 U/mL G6PDH, pH 8.5. G6P formation was measured indirectly by NADPH production from G6PDH by measuring absorbance at 340 nm on a spectrophotometer and was normalized to protein concentration as determined by BCA protein assay kit (Fisher Scientific).

Statistical Analysis

Data are presented as mean \pm SEM or SD as indicated. For a two-group comparison unpaired two-

tailed Student's t-tests was used. For data with multiple groups (>2) or multiple treatments a one- or two-way ANOVA was used as indicated followed by Tukey's post-hoc test to determine p-values for individual comparisons. No statistical methods were used to predetermine sample size. All statistical analysis was performed using Graphpad Prism 8.0. $p < 0.05$ was statistically significant and is presented as * $p < 0.05$, ** $p < 0.01$, *** $p < 0.001$, **** $p < 0.0001$, or ns = not significant). Survival experiment was performed in Prism 8 using comparison of survival curves with Log-rank (Mantel-Cox) test. For *in vivo* experiments, animals were assigned to experimental groups using simple randomization, without investigator blinding. Hierarchical clustering and heatmaps for metabolomics data were generated using MetaboAnalyst 4.0 statistical software (200).

KEY RESOURCES TABLE

REAGENT or RESOURCE	SOURCE	IDENTIFIER
Antibodies		
S100A8 Rabbit Polyclonal Antibody	Proteintech	15792-1-AP
ATP Synthase Beta Monoclonal-Alexa Fluor 555	Thermo Fisher Scientific	MA1930A555
GFP-tag Mouse Monoclonal Antibody	Proteintech	66002-1-Ig
VDAC1/Porin Rabbit Polyclonal Antibody	Proteintech	55259-1-AP
Hexokinase I (C35C4) Rabbit mAb	Cell Signaling Technologies	2024S
Hexokinase II (C64G5) Rabbit mAb	Cell Signaling Technologies	2867
IL-1 β (3A6) Mouse mAb	Cell Signaling Technologies	12242
GAPDH (14C10) Rabbit mAb	Cell Signaling Technologies	2118S
GFP-Trap Agarose	Chromotek	gta-20
Binding Control Agarose Beads	Chromotek	bab-20
Alpha-Tubulin Antibody	Proteintech	66031-1-Ig

TMT Monoclonal Antibody (25D5)	Thermo Fisher Scientific	90075
Beta-Actin Antibody	Proteintech	60008-1-Ig
FLAG M2 mouse	Sigma-Aldrich	F1804
Goat anti-Rabbit IgG (H+L), Superclonal™ Secondary Antibody, Alexa Fluor 488	Thermo Fisher Scientific	A27034
Donkey Anti-Mouse IgG (H+L) Antibody Horseradish Peroxidase (HRP)	Jackson ImmunoResearch	715-035-150
Donkey Anti-Rabbit IgG (H+L) Antibody Horseradish Peroxidase (HRP)	Jackson ImmunoResearch	711-035-152
Bacterial and Virus Strains		
pHIV-Puro-EGFP (lentivirus)	This paper	N/A
pHIV-Puro-FLHK1-EGFP (lentivirus)	This paper	N/A
pHIV-Puro-TrHK1-EGFP (lentivirus)	This paper	N/A
Chemicals, Peptides, and Recombinant Proteins		
Lactate Oxidase from Aerococcus Viridans	Sigma-Aldrich	L9795

β -Nicotinamide adenine dinucleotide phosphate sodium salt	Sigma-Aldrich	N8035-15VL
Pierce 16% formaldehyde	Thermo Fisher Scientific	28906
Clotrimazole	Sigma-Aldrich	C6019
2-Deoxy-D-glucose	Sigma-Aldrich	D8375
IFN gamma mouse recombinant protein	PeptoTech	315-05-100ug
RNA stat 60	Tel Test Inc	CS-502
Novex™ 16% Tricine Protein Gels, 1.0 mm, 12-well	Thermo Fisher Scientific	EC66952BO X
Accutase	Sigma-Aldrich	A6964
Red Blood Cell (RBC) Lysis Buffer	Abcam	Ab204733
Macrophage-Colony Stimulating Factor (mCSF)-mouse	GenScript	Z02930
Methyl pyruvate	Sigma-Aldrich	371173
CGP 3466B maleate	Tocris	2966
Heptelidic Acid (Koningic Acid)	Cayman Chemical Company	14079

1400W dihydrochloride	Tocris	1415
6-Aminonicotinamide	Sigma-Aldrich	A68203
Oxythiamine chloride hydrochloride	Sigma-Aldrich	04000
DMEM with L-Glutamine	Corning	MT-10-017- CV
RPMI 1640 with L-Glutamine	Sigma-Aldrich	R1383
Digitonin	Sigma-Aldrich	D141
ProLong Gold Antifade Mountant with DAPI	Life Technologies	P36931
MitoTracker Deep Red FM	Thermo Fisher Scientific	M22426
Tetramethylrhodamine, Ethyl Ester, Perchlorate (TMRE)	Thermo Fisher Scientific	T669
Ultrapure O5:B55 LPS	Invivogen	tlr1-pb5lps
Crude O5:B55 LPS	Sigma	L2880
D-Glucose (U-13C6)	Cambridge Isotope Laboratories	CLM-1396-1
2-NBDG	Cayman Chemical Company	11046

Glucose-6-Phosphate Dehydrogenase (G6P-DH) from <i>Leuconostoc mesenteroides</i>	Sigma	10165875001
ATP	Sigma-Aldrich	A2383
Tween-20	DOT Scientific Inc	DSP20370- 0.5
TRUE Metrix Blood Glucose Test Strips 5	Trividia Health Inc.	N/A
Critical Commercial Assays		
NADP/NADPH-Glo kit	Promega	G9081
NAD/NADH-Glo kit	Promega	G9071
Duoset ELISA IL-1beta-mouse kit	R&D	DY401-05
Duoset ELISA TNFalpha-mouse kit	R&D	DY410-05
Duoset ELISA IL-6-mouse kit	R&D	DY406-05
Anti-HK1 Magnetic Beads IP kit	Sino Biological	MB101347- T38
Infusion HD kit	Clontech	638910
Glyceraldehyde 3 Phosphate Dehydrogenase Activity Assay kit	Abcam	ab204732

Thermo Scientific Pierce S-Nitrosylation Western Blot kit	Fisher Scientific	PI90105
Pierce BCA Protein Assay kit	Fisher Scientific	PI23225
Mitochondria Isolation Kit for Cultured Cells	Fisher Scientific	PI-89874
Experimental Models: Cell Lines		
Human: HEK293T	ATCC	Cat# CRL-3216
Human: HepG2	ATCC	Cat# HB-806
Mouse: RAW264.7	Prof. Jason Albert Wertheim (Northwestern University)	N/A
Mouse: primary bone marrow-derived macrophages	This paper	N/A
Mouse: primary peritoneal macrophages	This paper	N/A
Experimental Models: Organisms/Strains		
Δ E1HK1-C57BL/6J mice	This paper	N/A
WT C57BL/6J mice	This paper	N/A

Oligonucleotides		
IL-1 β mouse primers	IDT	Fwd: GTGGACGGGACGCTCTAC Rev: TTCACTGTTTGGTGCATGATT
TNF α 1 β mouse primers	IDT	Fwd: GCCTCTTCTCATTCTGCTTG Rev: CTGATGAGAGGGAGGCCATT
IL-6 mouse primers	IDT	Fwd: CCTCTGGTCTTCTGGAGTACC Rev: ACTCCTTCTGTGACTCCAGC
MCP1 mouse primers	IDT	Fwd: AGCCAACCTCTCACTGAAGCC Rev: GCGTAACTGCATCTGGCTG
ARG2 mouse primers	IDT	Fwd: GGAAAGCCAATGAAGAGCTGG Rev: GCTTCCAACCTGCCAGACTGT
PPAR γ mouse primers	IDT	Fwd: GCTGGGGTATTGGGTTCGC Rev: TTCCATCACGGAGAGGTCCA
CARKL mouse primers	IDT	Fwd: CACTTGGTCACATGGCAGGA Rev: CTCAGAACTCCGGGCTGT
HK1 mouse primers	IDT	Fwd: GTGGACGGGACGCTCTAC Rev: TTCACTGTTTGGTGCATGATT
HK2 mouse primers	IDT	Fwd: GAATGGGAAGTGGGGTGGAG Rev: TGTGGTCAAAGAGCTCGTCC

HK3 mouse primers	IDT	Fwd: CTGAGATGGAGGACACCGC Rev: CCACGCACACATATTGCACC
GCK mouse primers	IDT	Fwd: AGGGAACAACATCGTGGGAC Rev: TGGACTGGGAGCATTGTGG
HKDC1 mouse primers	IDT	Fwd: AGATGGCTCAGAAAACGGGG Rev: GGGCCAGCTTCTTGTTCTCT
GPI mouse primers	IDT	Fwd: AAGGAGGTGATGCAGATGCT Rev: GCCCGATTCTCGGTGTAGT
PFK mouse primers	IDT	Fwd: TGGCAGACTATGTGTCTGGGGAGC Rev: GCTAGCACTGGGAGGGTGAGAGTC
ALDO mouse primers	IDT	Fwd: GCCGCAGCCAGTGAATCTCTCTTC Rev: TTCACAGACAACACCGCACACGAG
G6PD mouse primers	IDT	Fwd: TTTGTCCTATGCTGCTGCCACTGC Rev: GGCTGGAAGGGAGGTGATTCAGGT
PGD mouse primers	IDT	Fwd: CCGTCACCCTCATTGGAG Rev: GGACCACCTTAGGACCCTTC
RPE mouse primers	IDT	Fwd: TCTGTCATTCCCTCCTGCCCTGG Rev: TCCAACCCAGTGGCACTTCCAAGA

RPIA mouse primers	IDT	Fwd: TCAATCTCATCAAGGGTGGA Rev: CATAACCAGCCACGATCTTCT
TKT mouse primers	IDT	Fwd: GGGCTGGTGTA ACTCTGCAT Rev: CCCGGATGCTGATCTTATCT
TALDO mouse primers	IDT	Fwd: CCACAGAAGTTGATGCAAGG Rev: AGCTTCTTTGTAAAGCTCGATGA
GAPDH mouse primers	IDT	Fwd: TGGTGGACCTCATGGCCTACATGG Rev: TGAGGGAGATGCTCAGTGTTGGGG
TPI mouse primers	IDT	Fwd: TGAGCCGTTTCCACCGCCCTATTA Rev: GCTCCAACCATGAGTTTCCAGCCC
PGM mouse primers	IDT	Fwd: GTTCTCGGACCACATCGAGGGACA Rev: TGCAGGACAGGTTCCAGGGACAAA
PGK mouse primers	IDT	Fwd: AAGTCCTTCCTGGGGTGGATGCTC Rev: AGGGTTCCTGGTGCCACATCTCAG
ENO1 mouse primers	IDT	Fwd: TAGGCATCCACACCTGACCACCAG Rev: GGGCTCCAGACACTAGCTGGGAAG
PK mouse primers	IDT	Fwd: TTAGGCCAGCAACGCTTG TAGTGC Rev: AGATGCTGCCGCCCTTCTGTGATA

LDHA mouse primers	IDT	Fwd: CACTGACTCCTGAGGAAGAGGCC Rev: AGCTCAGACGAGAAGGGTGTGGTC
PDHA1 mouse primers	IDT	Fwd: TGTGTGATGGTCAGGAAGCC Rev: CCGAGTGAAGGTGAAGCCAT
PDHB mouse primers	IDT	Fwd: AGTTGCCCAGTATGACGGTG Rev: CCAGCAAAGCCCATCTCTGA
DLG mouse primers	IDT	Fwd: TGGCAAAGACTTGGTGCAGA Rev: AAGCAGCTTCGACAGACACA
PC mouse primers	IDT	Fwd: GGGCGGAGCTAACATCTACC Rev: TATACTCCAGACGCCGGACA
MPC1 mouse primers	IDT	Fwd: CGGTAGATGCACTTCTGGGG Rev: GAAAGTCATCCGCCCACTGA
MPC2 mouse primers	IDT	Fwd: ACCTACCACCGACTCATGGA Rev: AGCACACACCAATCCCCATT
IDH mouse primers	IDT	Fwd: GGCACTGTCACACGTCACTA Rev: ATGGAAGCAATGGGGTTGGT
OGDH mouse primers	IDT	Fwd: CAGATGTCCTGCCTGACCTG Rev: TCGCAGCACATGGAAGAAGT

CS mouse primers	IDT	Fwd: CGGTTTGTCTACCCTTCCCC Rev: GGCAGGATGAGTTCTTGGCT
FH mouse primers	IDT	Fwd: GCAGCATCATGCCAGGAAAG Rev: ATTCCCATGACTTGGGCTG
SDHC mouse primers	IDT	Fwd: ATAGCCTTGAGTGGAGGGGT Rev: CAGACCTGGGGTATTGCCAG
MDH mouse primers	IDT	Fwd: GACCTGTTCAACACCAACGC Rev: GGATGGTGGAGTTCCTGGG
18s mouse primers	IDT	Fwd: AGTCCCTGCCCTTTGTACACA Rev: CGATCCGAGGGCCTCACTA
ACTB mouse primers	IDT	Fwd: CCGTGAAAAGATGACCCAGAT Rev: GTACATGGCTGGGGTGTTG
Recombinant DNA		
FLHK1-pGFPN3	This lab	N/A
TrHK1-pGFPN3	This lab	N/A
Software and Algorithms		
MetaboAnalyst 4.0	Xia, Wishart, & Chong, 2019	https://www.metaboanalyst.c a/

Scaffold	Proteome Software	http://www.proteomesoftware.com/products/scaffold/
Prism 8.0	Graphpad	https://www.graphpad.com/
PANTHER classification system	Gene ontology Unifying Biology	http://pantherdb.org/geneListAnalysis.do
Fiji/ImageJ	NIH	https://imagej.net/Fiji/Downloads RRID: SCR_002285
Other		
High Fat Diet (HFD; 60% kcal fat)	Research diets	Cat# D12492

REFERENCES

1. Gould GW, Holman GD. The glucose transporter family: structure, function and tissue-specific expression. *Biochem. J.* 1993;295(Pt 2):329–341.
2. Bell GI, Burant CF, Takeda J, Gould GW. Structure and function of mammalian facilitative sugar transporters. *J. Biol. Chem.* 1993;268(26):19161–19164.
3. Mueckler M. Facilitative glucose transporters. *Eur. J. Biochem.* 1994;219(3):713–725.
4. Printz RL, Osawa H, Ardehali H, Koch S, Granner DK. Hexokinase II gene: structure, regulation and promoter organization. *Biochem. Soc. Trans.* 1997;25(1):107–112.
5. Adeva-Andany MM, Pérez-Felpete N, Fernández-Fernández C, Donapetry-García C, Pazos-García C. Liver glucose metabolism in humans. *Biosci. Rep.* 2016;36(6):e00416.
6. Puleston DJ, Villa M, Pearce EL. Ancillary Activity: Beyond Core Metabolism in Immune Cells. *Cell Metab.* 2017;26(1):131–141.
7. Middleton RJ. Hexokinases and glucokinases. *Biochem. Soc. Trans.* 1990;18(2):180–183.
8. Ureta T. The comparative isozymology of vertebrate hexokinases. *Comp. Biochem. Physiol. B* 1982;71(4):549–555.
9. Wilson JE. Isozymes of mammalian hexokinase: structure, subcellular localization and metabolic function. *J. Exp. Biol.* 2003;206(12):2049–2057.
10. Cárdenas ML, Cornish-Bowden A, Ureta T. Evolution and regulatory role of the hexokinases. *Biochim. Biophys. Acta BBA - Mol. Cell Res.* 1998;1401(3):242–264.
11. Ardehali H, Yano Y, Printz RL, Koch S, Whitesell RR, May JM, Granner DK. Functional organization of mammalian hexokinase II. Retention of catalytic and regulatory functions in both the NH₂- and COOH-terminal halves. *J. Biol. Chem.* 1996;271(4):1849–1852.
12. Rose IA, Warms JVB. Mitochondrial Hexokinase RELEASE, REBINDING, AND LOCATION. *J. Biol. Chem.* 1967;242(7):1635–1645.
13. Sui D, Wilson JE. Structural Determinants for the Intracellular Localization of the Isozymes of Mammalian Hexokinase: Intracellular Localization of Fusion Constructs Incorporating Structural Elements from the Hexokinase Isozymes and the Green Fluorescent Protein. *Arch. Biochem. Biophys.* 1997;345(1):111–125.
14. Fiek C, Benz R, Roos N, Brdiczka D. Evidence for identity between the hexokinase-binding protein and the mitochondrial porin in the outer membrane of rat liver mitochondria. *Biochim. Biophys. Acta* 1982;688(2):429–440.
15. Lindén M, Gellerfors P, Nelson BD. Pore protein and the hexokinase-binding protein from the outer membrane of rat liver mitochondria are identical. *FEBS Lett.* 1982;141(2):189–192.

16. Aflalo C, Azoulay H. Binding of Rat Brain Hexokinase to Recombinant Yeast Mitochondria: Effect of Environmental Factors and the Source of Porin. *J. Bioenerg. Biomembr.* 1998;30(3):245–255.
17. Azoulay-Zohar H, Israelson A, Abu-Hamad S, Shoshan-Barmatz V. In self-defence: hexokinase promotes voltage-dependent anion channel closure and prevents mitochondria-mediated apoptotic cell death. *Biochem. J.* 2004;377(Pt 2):347–355.
18. Printz RL, Ardehali H, Koch S, Granner DK. Human Hexokinase II mRNA and Gene Structure. *Diabetes* 1995;44(3):290–294.
19. Andreoni F, Ruzzo A, Magnani M. Structure of the 5' region of the human hexokinase type I (HKI) gene and identification of an additional testis-specific HKI mRNA. The nucleotide sequence data reported in this paper will appear in DDBJ, EMBL and GenBank nucleotide sequence databases under the accession numbers AF163908–AF163913. *Biochim. Biophys. Acta BBA - Gene Struct. Expr.* 2000;1493(1):19–26.
20. Calmettes G, John S, Weiss JN, Ribalet B. Hexokinase Isoforms and Glucose Metabolism in Adult and Neonatal Cardiac Myocytes. *Biophys. J.* 2013;104(2, Supplement 1):314a.
21. John S, Weiss JN, Ribalet B. Subcellular Localization of Hexokinases I and II Directs the Metabolic Fate of Glucose. *PLoS ONE* 2011;6(3). doi:10.1371/journal.pone.0017674.
22. Pastorino JG, Hoek JB, Shulga N. Activation of Glycogen Synthase Kinase 3 β Disrupts the Binding of Hexokinase II to Mitochondria by Phosphorylating Voltage-Dependent Anion Channel and Potentiates Chemotherapy-Induced Cytotoxicity. *Cancer Res.* 2005;65(22):10545–10554.
23. Roberts DJ, Tan-Sah VP, Smith JM, Miyamoto S. Akt phosphorylates HK-II at Thr-473 and increases mitochondrial HK-II association to protect cardiomyocytes. *J. Biol. Chem.* 2013;288(33):23798–23806.
24. Wilson JE. Hexokinases. *Rev. Physiol. Biochem. Pharmacol.* 1995;126:65–198.
25. Preller A, Wilson JE. Localization of the type III isozyme of hexokinase at the nuclear periphery. *Arch. Biochem. Biophys.* 1992;294(2):482–492.
26. Pearce EL, Pearce EJ. Metabolic Pathways in Immune Cell Activation and Quiescence. *Immunity* 2013;38(4):633–643.
27. Sancho D, Enamorado M, Garaude J. Innate Immune Function of Mitochondrial Metabolism. *Front. Immunol.* 2017;8. doi:10.3389/fimmu.2017.00527.
28. Stienstra R, Netea-Maier RT, Riksen NP, Joosten LAB, Netea MG. Specific and Complex Reprogramming of Cellular Metabolism in Myeloid Cells during Innate Immune Responses. *Cell Metab.* 2017;26(1):142–156.
29. Cheng S-C, Quintin J, Cramer RA, Shepardson KM, Saeed S, Kumar V, Giamarellos-

- Bourboulis EJ, Martens JHA, Rao NA, Aghajani-refah A, Manjeri GR, Li Y, Ifrim DC, Arts RJW, van der Veer BMJW, van der Meer BMJW, Deen PMT, Logie C, O'Neill LA, Willems P, van de Veerdonk FL, van der Meer JWM, Ng A, Joosten LAB, Wijmenga C, Stunnenberg HG, Xavier RJ, Netea MG. mTOR- and HIF-1 α -mediated aerobic glycolysis as metabolic basis for trained immunity. *Science* 2014;345(6204):1250684.
30. Everts B, Amiel E, Huang SC-C, Smith AM, Chang C-H, Lam WY, Redmann V, Freitas TC, Blagih J, van der Windt GJW, Artyomov MN, Jones RG, Pearce EL, Pearce EJ. TLR-driven early glycolytic reprogramming via the kinases TBK1- $IKK\epsilon$ supports the anabolic demands of dendritic cell activation. *Nat. Immunol.* 2014;15(4):323–332.
 31. Garaude J, Acín-Pérez R, Martínez-Cano S, Enamorado M, Ugolini M, Nistal-Villán E, Hervás-Stubbs S, Pelegrín P, Sander LE, Enríquez JA, Sancho D. Mitochondrial respiratory-chain adaptations in macrophages contribute to antibacterial host defense. *Nat. Immunol.* 2016;17(9):1037–1045.
 32. O'Neill LAJ, Pearce EJ. Immunometabolism governs dendritic cell and macrophage function. *J. Exp. Med.* 2016;213(1):15–23.
 33. Pavlova NN, Thompson CB. The Emerging Hallmarks of Cancer Metabolism. *Cell Metab.* 2016;23(1):27–47.
 34. Andrejeva G, Rathmell JC. Similarities and Distinctions of Cancer and Immune Metabolism in Inflammation and Tumors. *Cell Metab.* 2017;26(1):49–70.
 35. Hughes MM, O'Neill LAJ. Metabolic regulation of NLRP3. *Immunol. Rev.* 2018;281(1):88–98.
 36. Nishizawa T, Kanter JE, Kramer F, Barnhart S, Shen X, Vivekanandan-Giri A, Wall VZ, Kowitz J, Devaraj S, O'Brien KD, Pennathur S, Tang J, Miyaoka RS, Raines EW, Bornfeldt KE. Testing the Role of Myeloid Cell Glucose Flux in Inflammation and Atherosclerosis. *Cell Rep.* 2014;7(2):356–365.
 37. Moon J-S, Hisata S, Park M-A, DeNicola GM, Ryter SW, Nakahira K, Choi AMK. mTORC1 induced HK1-dependent glycolysis regulates NLRP3 inflammasome activation. *Cell Rep.* 2015;12(1):102–115.
 38. Mogilenko DA, Haas JT, L'homme L, Fleury S, Quemener S, Levavasseur M, Becquart C, Wartelle J, Bogomolova A, Pineau L, Molendi-Coste O, Lancel S, Dehondt H, Gheeraert C, Melchior A, Dewas C, Nikitin A, Pic S, Rabhi N, Annicotte J-S, Oyadomari S, Velasco-Hernandez T, Cammenga J, Foretz M, Viollet B, Vukovic M, Villacreces A, Kranc K, Carmeliet P, Marot G, Boulter A, Tavernier S, Berod L, Longhi MP, Paget C, Janssens S, Staumont-Sallé D, Aksoy E, Staels B, Dombrowicz D. Metabolic and Innate Immune Cues Merge into a Specific Inflammatory Response via the UPR. *Cell* 2019;177(5):1201-1216.e19.
 39. Barnett JA. A history of research on yeasts 6: the main respiratory pathway. *Yeast Chichester Engl.* 2003;20(12):1015–1044.

40. Cori CF. Embden and the glycolytic pathway. *Trends Biochem. Sci.* 1983;8(7):257–259.
41. Wilson JE. An introduction to the isoenzymes of mammalian hexokinase types I-III. *Biochem. Soc. Trans.* 1997;25(1):103–107.
42. Raja M, Puntheeranurak T, Hinterdorfer P, Kinne R. Chapter Two - SLC5 and SLC2 Transporters in Epithelia—Cellular Role and Molecular Mechanisms. In: Bevenssee MO, ed. *Current Topics in Membranes*. Vol 70. Co-Transport Systems. Academic Press; 2012:29–76.
43. Boyle J. Lehninger principles of biochemistry (4th ed.): Nelson, D., and Cox, M. *Biochem. Mol. Biol. Educ.* 2005;33(1):74–75.
44. Stincone A, Prigione A, Cramer T, Wamelink MMC, Campbell K, Cheung E, Olin-Sandoval V, Grüning N-M, Krüger A, Alam MT, Keller MA, Breitenbach M, Brindle KM, Rabinowitz JD, Ralser M. The return of metabolism: biochemistry and physiology of the pentose phosphate pathway. *Biol. Rev. Camb. Philos. Soc.* 2015;90(3):927–963.
45. Adeva-Andany MM, González-Lucán M, Donapetry-García C, Fernández-Fernández C, Ameneiros-Rodríguez E. Glycogen metabolism in humans. *BBA Clin.* 2016;5:85–100.
46. Zachara N, Akimoto Y, Hart GW. The O-GlcNAc Modification. In: Varki A, Cummings RD, Esko JD, Stanley P, Hart GW, Aebi M, Darvill AG, Kinoshita T, Packer NH, Prestegard JH, Schnaar RL, Seeberger PH, eds. *Essentials of Glycobiology*. 3rd ed. Cold Spring Harbor (NY): Cold Spring Harbor Laboratory Press; 2015. Available at: <http://www.ncbi.nlm.nih.gov/books/NBK453063/>.
47. Pusec CM, De Jesus A, Khan MW, Terry AR, Ludvik AE, Xu K, Giancola N, Pervaiz H, Smith ED, Ding X, Harrison S, Chandel NS, Becker TC, Hay N, Ardehali H, Cordoba-Chacon J, Layden BT. Hepatic HKDC1 expression contributes to liver metabolism. *Endocrinology* 2018. doi:10.1210/en.2018-00887.
48. Zhang L, Sun Z, Zhao P, Huang L, Xu M, Yang Y, Chen X, Lu F, Zhang X, Wang H, Zhang S, Liu W, Jiang Z, Ma S, Chen R, Zhao C, Yang Z, Sui R, Zhu X. Whole-exome sequencing revealed HKDC1 as a candidate gene associated with autosomal-recessive retinitis pigmentosa. *Hum. Mol. Genet.* 2018;27(23):4157–4168.
49. Irwin DM, Tan H. Molecular evolution of the vertebrate hexokinase gene family: Identification of a conserved fifth vertebrate hexokinase gene. *Comp. Biochem. Physiol. Part D Genomics Proteomics* 2008;3(1):96–107.
50. Robey RB, Hay N. Mitochondrial hexokinases, novel mediators of the antiapoptotic effects of growth factors and Akt. *Oncogene* 2006;25(34):4683–4696.
51. Griffin LD, Gelb BD, Wheeler DA, Davison D, Adams V, McCabe ERB. Mammalian hexokinase 1: Evolutionary conservation and structure to function analysis. *Genomics* 1991;11(4):1014–1024.

52. Lenzen S. A Fresh View of Glycolysis and Glucokinase Regulation: History and Current Status. *J. Biol. Chem.* 2014;289(18):12189–12194.
53. Caro JF, Triester S, Patel VK, Tapscott EB, Frazier NL, Dohm GL. Liver Glucokinase: Decreased Activity in Patients with Type II Diabetes. *Horm. Metab. Res.* 1995;27(01):19–22.
54. Irwin DM, Tan H. Evolution of glucose utilization: Glucokinase and glucokinase regulator protein. *Mol. Phylogenet. Evol.* 2014;70:195–203.
55. Agius L. Glucokinase and molecular aspects of liver glycogen metabolism. *Biochem. J.* 2008;414(1):1–18.
56. Weinhouse S. Regulation of glucokinase in liver. *Curr. Top. Cell. Regul.* 1976;11:1–50.
57. Matschinsky FM. Glucokinase as glucose sensor and metabolic signal generator in pancreatic beta-cells and hepatocytes. *Diabetes* 1990;39(6):647–652.
58. Nawaz MH, Ferreira JC, Nedyalkova L, Zhu H, Carrasco-López C, Kirmizialtin S, Rabeh WM. The catalytic inactivation of the N-half of human hexokinase 2 and structural and biochemical characterization of its mitochondrial conformation. *Biosci. Rep.* 2018;38(1). doi:10.1042/BSR20171666.
59. Tsai HJ, Wilson JE. Functional Organization of Mammalian Hexokinases: Both N- and C-Terminal Halves of the Rat Type II Isozyme Possess Catalytic Sites. *Arch. Biochem. Biophys.* 1996;329(1):17–23.
60. Arora KK, Filburn CR, Pedersen PL. Glucose phosphorylation. Site-directed mutations which impair the catalytic function of hexokinase. *J. Biol. Chem.* 1991;266(9):5359–5362.
61. Aleshin AE, Zeng C, Bourenkov GP, Bartunik HD, Fromm HJ, Honzatko RB. The mechanism of regulation of hexokinase: new insights from the crystal structure of recombinant human brain hexokinase complexed with glucose and glucose-6-phosphate. *Structure* 1998;6(1):39–50.
62. Arora KK, Filburn CR, Pedersen PL. Structure/function relationships in hexokinase. Site-directed mutational analyses and characterization of overexpressed fragments implicate different functions for the N- and C-terminal halves of the enzyme. *J. Biol. Chem.* 1993;268(24):18259–18266.
63. White TK, Wilson JE. Isolation and characterization of the discrete N- and C-terminal halves of rat brain hexokinase: Retention of full catalytic activity in the isolated C-terminal half. *Arch. Biochem. Biophys.* 1989;274(2):375–393.
64. Aleshin AE, Kirby C, Liu X, Bourenkov GP, Bartunik HD, Fromm HJ, Honzatko RB. Crystal structures of mutant monomeric hexokinase I reveal multiple ADP binding sites and conformational changes relevant to allosteric regulation. *J. Mol. Biol.* 2000;296(4):1001–1015.

65. Rosano C, Sabini E, Rizzi M, Deriu D, Murshudov G, Bianchi M, Serafini G, Magnani M, Bolognesi M. Binding of non-catalytic ATP to human hexokinase I highlights the structural components for enzyme–membrane association control. *Structure* 1999;7(11):1427–1437.
66. Wyatt E, Wu R, Rabeh W, Park H-W, Ghanefar M, Ardehali H. Regulation and Cytoprotective Role of Hexokinase III. *PLoS ONE* 2010;5(11). doi:10.1371/journal.pone.0013823.
67. Ludvik AE, Pusec CM, Priyadarshini M, Angueira AR, Guo C, Lo A, Hershenhouse KS, Yang G-Y, Ding X, Reddy TE, Lowe WL, Layden BT. HKDC1 Is a Novel Hexokinase Involved in Whole-Body Glucose Use. *Endocrinology* 2016;157(9):3452–3461.
68. Quintens R, Hendrickx N, Lemaire K, Schuit F. Why expression of some genes is disallowed in β -cells. *Biochem. Soc. Trans.* 2008;36(3):300–305.
69. Massa ML, Gagliardino JJ, Francini F. Liver glucokinase: An overview on the regulatory mechanisms of its activity. *IUBMB Life* 2011;63(1):1–6.
70. Lenzen S, Panten U. Signal recognition by pancreatic B-cells. *Biochem. Pharmacol.* 1988;37(3):371–378.
71. Heimberg H, De Vos A, Moens K, Quartier E, Bouwens L, Pipeleers D, Van Schaftingen E, Madsen O, Schuit F. The glucose sensor protein glucokinase is expressed in glucagon-producing alpha-cells. *Proc. Natl. Acad. Sci. U. S. A.* 1996;93(14):7036–7041.
72. Katzen HM. The multiple forms of mammalian hexokinase and their significance to the action of insulin. *Adv. Enzyme Regul.* 1967;5:335–336.
73. Zelent D, Golson ML, Koeberlein B, Quintens R, van Lommel L, Buettger C, Weik-Collins H, Taub R, Grimsby J, Schuit F, Kaestner KH, Matschinsky FM. A glucose sensor role for glucokinase in anterior pituitary cells. *Diabetes* 2006;55(7):1923–1929.
74. Levin BE, Magnan C, Dunn-Meynell A, Le Foll C. Metabolic Sensing and the Brain: Who, What, Where, and How? *Endocrinology* 2011;152(7):2552–2557.
75. Oosterveer MH, Schoonjans K. Hepatic glucose sensing and integrative pathways in the liver. *Cell. Mol. Life Sci. CMLS* 2014;71(8):1453–1467.
76. Tiedge M, Lenzen S. Effects of glucose refeeding and glibenclamide treatment on glucokinase and GLUT2 gene expression in pancreatic B-cells and liver from rats. *Biochem. J.* 1995;308 (Pt 1):139–144.
77. Xu S, Catapang A, Braas D, Stiles L, Doh H, Lee J, Graeber T, Damoiseaux R, Shirihai O, Herschman H. A precision therapeutic strategy for hexokinase 1-null, hexokinase 2-positive cancers. *Cancer Metab.* 2018;6. doi:10.1186/s40170-018-0181-8.
78. Quintens R, Hendrickx N, Lemaire K, Schuit F. Why expression of some genes is disallowed in β -cells. *Biochem. Soc. Trans.* 2008;36(3):300–305.

79. Wu R, Smeele KM, Wyatt E, Ichikawa Y, Eerbeek O, Sun L, Chawla K, Hollmann MW, Nagpal V, Heikkinen S, Laakso M, Jujo K, Wasserstrom JA, Zuurbier CJ, Ardehali H. Reduction in Hexokinase II Levels Results in Decreased Cardiac Function and Altered Remodeling after Ischemia-Reperfusion Injury. *Circ. Res.* 2011;108(1):60–69.
80. Roberts DJ, Miyamoto S. Hexokinase II integrates energy metabolism and cellular protection: Acting on mitochondria and TORCing to autophagy. *Cell Death Differ.* 2015;22(2):248–257.
81. Anderson NL, Anderson NG. The human plasma proteome: history, character, and diagnostic prospects. *Mol. Cell. Proteomics MCP* 2002;1(11):845–867.
82. Federzoni EA, Valk PJM, Torbett BE, Haferlach T, Löwenberg B, Fey MF, Tschan MP. PU.1 is linking the glycolytic enzyme HK3 in neutrophil differentiation and survival of APL cells. *Blood* 2012;119(21):4963–4970.
83. Povey S, Corney G, Harris H. Genetically determined polymorphism of a form of hexokinase, HK III, found in human leucocytes. *Ann. Hum. Genet.* 1975;38(4):407–415.
84. Kaselonis GL, McCabe ERB, Gray SM. *HEXOKINASE 3 IS DEVELOPMENTALLY EXPRESSED IN RAT LUNG. † 1997.* Nature Publishing Group; 1996:335–335.
85. Parry DM, Pedersen PL. Intracellular localization and properties of particulate hexokinase in the Novikoff ascites tumor. Evidence for an outer mitochondrial membrane location. *J. Biol. Chem.* 1983;258(18):10904–10912.
86. Kropp ES, Wilson JE. Hexokinase binding sites on mitochondrial membranes. *Biochem. Biophys. Res. Commun.* 1970;38(1):74–79.
87. Nakashima RA, Mangan PS, Colombini M, Pedersen PL. Hexokinase receptor complex in hepatoma mitochondria: evidence from N,N'-dicyclohexylcarbodiimide-labeling studies for the involvement of the pore-forming protein VDAC. *Biochemistry* 1986;25(5):1015–1021.
88. Polakis PG, Wilson JE. An intact hydrophobic N-terminal sequence is critical for binding of rat brain hexokinase to mitochondria. *Arch. Biochem. Biophys.* 1985;236(1):328–337.
89. Rose IA, Warms JVB. Mitochondrial Hexokinase RELEASE, REBINDING, AND LOCATION. *J. Biol. Chem.* 1967;242(7):1635–1645.
90. Hashimoto M, Wilson JE. Kinetic and Regulatory Properties of HK I+, a Modified Form of the Type I Isozyme of Mammalian Hexokinase in Which Interactions between the N- and C-Terminal Halves Have Been Disrupted. *Arch. Biochem. Biophys.* 2002;399(1):109–115.
91. Bryan N, Raisch KP. Identification of a mitochondrial-binding site on the N-terminal end of hexokinase II. *Biosci. Rep.* 2015;35(3). doi:10.1042/BSR20150047.
92. Palma F, Agostini D, Mason P, Dachà M, Piccoli G, Biagiarelli B, Fiorani M, Stocchi V.

- Purification and characterization of the carboxyl-domain of human hexokinase type III expressed as fusion protein. *Mol. Cell. Biochem.* 1996;155(1):23–29.
93. Van Schaftingen E. A protein from rat liver confers to glucokinase the property of being antagonistically regulated by fructose 6-phosphate and fructose 1-phosphate. *Eur. J. Biochem.* 1989;179(1):179–184.
 94. Van Schaftingen E. Short-term regulation of glucokinase. *Diabetologia* 1994;37(2):S43–S47.
 95. Baltrusch S, Francini F, Lenzen S, Tiedge M. Interaction of Glucokinase With the Liver Regulatory Protein Is Conferred by Leucine-Asparagine Motifs of the Enzyme. *Diabetes* 2005;54(10):2829–2837.
 96. Sui D, Wilson JE. Structural Determinants for the Intracellular Localization of the Isozymes of Mammalian Hexokinase: Intracellular Localization of Fusion Constructs Incorporating Structural Elements from the Hexokinase Isozymes and the Green Fluorescent Protein. *Arch. Biochem. Biophys.* 1997;345(1):111–125.
 97. Roberts DJ, Miyamoto S. Hexokinase II integrates energy metabolism and cellular protection: Acting on mitochondria and TORCing to autophagy. *Cell Death Differ.* 2015;22(2):248–257.
 98. Xie GC, Wilson JE. Rat brain hexokinase: the hydrophobic N-terminus of the mitochondrially bound enzyme is inserted in the lipid bilayer. *Arch. Biochem. Biophys.* 1988;267(2):803–810.
 99. Mulichak AM, Wilson JE, Padmanabhan K, Garavito RM. The structure of mammalian hexokinase-1. *Nat. Struct. Mol. Biol.* 1998;5:555–560.
 100. Lemasters JJ, Holmuhamedov E. Voltage-dependent anion channel (VDAC) as mitochondrial governor—Thinking outside the box. *Biochim. Biophys. Acta BBA - Mol. Basis Dis.* 2006;1762(2):181–190.
 101. Colombini M. The VDAC channel: Molecular basis for selectivity. *Biochim. Biophys. Acta* 2016;1863(10):2498–2502.
 102. Zhang D, Yip YM, Li L. In silico construction of HK2-VDAC1 complex and investigating the HK2 binding-induced molecular gating mechanism of VDAC1. *Mitochondrion* 2016;30:222–228.
 103. Rosano C. Molecular model of hexokinase binding to the outer mitochondrial membrane porin (VDAC1): Implication for the design of new cancer therapies. *Mitochondrion* 2011;11(3):513–519.
 104. Pastorino JG, Hoek JB. Regulation of Hexokinase Binding to VDAC. *J. Bioenerg. Biomembr.* 2008;40(3):171–182.

105. Ardail D, Privat JP, Egret-Charlier M, Levrat C, Lerme F, Louisot P. Mitochondrial contact sites. Lipid composition and dynamics. *J. Biol. Chem.* 1990;265(31):18797–18802.
106. Skaff DA, Kim CS, Tsai HJ, Honzatko RB, Fromm HJ. Glucose 6-Phosphate Release of Wild-type and Mutant Human Brain Hexokinases from Mitochondria. *J. Biol. Chem.* 2005;280(46):38403–38409.
107. Quach CHT, Jung K-H, Lee JH, Park JW, Moon SH, Cho YS, Choe YS, Lee K-H. Mild Alkalinization Acutely Triggers the Warburg Effect by Enhancing Hexokinase Activity via Voltage-Dependent Anion Channel Binding. *PLoS ONE* 2016;11(8). doi:10.1371/journal.pone.0159529.
108. Nakashima RA. Hexokinase-binding properties of the mitochondrial VDAC protein: inhibition by DCCD and location of putative DCCD-binding sites. *J. Bioenerg. Biomembr.* 1989;21(4):461–470.
109. Kurokawa M, Yokoyama K, Ishibashi S. Polyamines stimulate the binding of hexokinase type II to mitochondria. *Biochim. Biophys. Acta BBA - Gen. Subj.* 1983;759(1):92–98.
110. Golshani-Hebroni S. Mg⁺⁺ requirement for MthK binding, and Mg⁺⁺ stabilization of mitochondrial membranes via activation of MthK & MtCK and promotion of mitochondrial permeability transition pore closure: A hypothesis on mechanisms underlying Mg⁺⁺'s antioxidant and cytoprotective effects. *Gene* 2016;581(1):1–13.
111. Bantug GR, Fischer M, Grählert J, Balmer ML, Unterstab G, Develioglu L, Steiner R, Zhang L, Costa ASH, Gubser PM, Burgener A-V, Sauder U, Löliger J, Belle R, Dimeloe S, Lötscher J, Jauch A, Recher M, Hönger G, Hall MN, Romero P, Frezza C, Hess C. Mitochondria-Endoplasmic Reticulum Contact Sites Function as Immunometabolic Hubs that Orchestrate the Rapid Recall Response of Memory CD8⁺ T Cells. *Immunity* 2018;48(3):542-555.e6.
112. Tanaka T, Saotome M, Katoh H, Satoh T, Hasan P, Ohtani H, Satoh H, Hayashi H, Maekawa Y. Glycogen synthase kinase-3 β opens mitochondrial permeability transition pore through mitochondrial hexokinase II dissociation. *J. Physiol. Sci.* 2018;68(6):865–871.
113. Zhang HH, Lipovsky AI, Dibble CC, Sahin M, Manning BD. S6K1 Regulates GSK3 under Conditions of mTOR-Dependent Feedback Inhibition of Akt. *Mol. Cell* 2006;24(2):185–197.
114. McManus EJ, Sakamoto K, Armit LJ, Ronaldson L, Shpiro N, Marquez R, Alessi DR. Role that phosphorylation of GSK3 plays in insulin and Wnt signalling defined by knockin analysis. *EMBO J.* 2005;24(8):1571–1583.
115. Henriksen EJ, Dokken BB. Role of glycogen synthase kinase-3 in insulin resistance and type 2 diabetes. *Curr. Drug Targets* 2006;7(11):1435–1441.
116. Golshani-Hebroni SG, Bessman SP. Hexokinase Binding to Mitochondria: A Basis for Proliferative Energy Metabolism. *J. Bioenerg. Biomembr.* 1997;29(4):331–338.

117. Shoshan-Barmatz V, Zakar M, Rosenthal K, Abu-Hamad S. Key regions of VDAC1 functioning in apoptosis induction and regulation by hexokinase. *Biochim. Biophys. Acta BBA - Bioenerg.* 2009;1787(5):421–430.
118. Pastorino JG, Shulga N, Hoek JB. Mitochondrial Binding of Hexokinase II Inhibits Bax-induced Cytochrome c Release and Apoptosis. *J. Biol. Chem.* 2002;277(9):7610–7618.
119. Schindler A, Foley E. Hexokinase 1 blocks apoptotic signals at the mitochondria. *Cell. Signal.* 2013;25(12):2685–2692.
120. Azoulay-Zohar H, Israelson A, Abu-Hamad S, Shoshan-Barmatz V. In self-defence: hexokinase promotes voltage-dependent anion channel closure and prevents mitochondria-mediated apoptotic cell death. *Biochem. J.* 2004;377(Pt 2):347–355.
121. Zecchin A, Stapor PC, Goveia J, Carmeliet P. Metabolic pathway compartmentalization: an underappreciated opportunity? *Curr. Opin. Biotechnol.* 2015;34:73–81.
122. Calmettes G, John SA, Weiss JN, Ribalet B. Hexokinase–mitochondrial interactions regulate glucose metabolism differentially in adult and neonatal cardiac myocytes. *J. Gen. Physiol.* 2013;142(4):425–436.
123. DeBerardinis RJ, Lum JJ, Hatzivassiliou G, Thompson CB. The Biology of Cancer: Metabolic Reprogramming Fuels Cell Growth and Proliferation. *Cell Metab.* 2008;7(1):11–20.
124. Otto AM. Warburg effect(s)—a biographical sketch of Otto Warburg and his impacts on tumor metabolism. *Cancer Metab.* 2016;4. doi:10.1186/s40170-016-0145-9.
125. On the origin of cancer cells. - PubMed - NCBI. Available at: <https://www.ncbi.nlm.nih.gov/pubmed/13298683>. Accessed November 12, 2019.
126. Bacci M, Lorito N, Ippolito L, Ramazzotti M, Luti S, Romagnoli S, Parri M, Bianchini F, Cappellesso F, Virga F, Gao Q, Simões BM, Marangoni E, Martin L-A, Comito G, Ferracin M, Giannoni E, Mazzone M, Chiarugi P, Morandi A. Reprogramming of Amino Acid Transporters to Support Aspartate and Glutamate Dependency Sustains Endocrine Resistance in Breast Cancer. *Cell Rep.* 2019;28(1):104-118.e8.
127. Cha YJ, Kim E-S, Koo JS. Amino Acid Transporters and Glutamine Metabolism in Breast Cancer. *Int. J. Mol. Sci.* 2018;19(3). doi:10.3390/ijms19030907.
128. Ancy P-B, Contat C, Meylan E. Glucose transporters in cancer - from tumor cells to the tumor microenvironment. *FEBS J.* 2018;285(16):2926–2943.
129. Heiden MG, Cantley LC, Thompson CB. Understanding the Warburg Effect: The Metabolic Requirements of Cell Proliferation. *Science* 2009;324(5930):1029–1033.
130. Lukey MJ, Katt WP, Cerione RA. Targeting amino acid metabolism for cancer therapy. *Drug Discov. Today* 2017;22(5):796–804.

131. Garcia-Bermudez J, Baudrier L, La K, Zhu XG, Fidelin J, Sviderskiy VO, Papagiannakopoulos T, Molina H, Snuderl M, Lewis CA, Possemato RL, Birsoy K. Aspartate is a limiting metabolite for cancer cell proliferation under hypoxia and in tumours. *Nat. Cell Biol.* 2018;20(7):775–781.
132. Meléndez-Rodríguez F, Urrutia AA, Lorendeau D, Rinaldi G, Roche O, Bögürücü-Seidel N, Ortega Muelas M, Mesa-Ciller C, Turiel G, Bouthelier A, Hernansanz-Agustín P, Elorza A, Escasany E, Li QOY, Torres-Capelli M, Tello D, Fuertes E, Fraga E, Martínez-Ruiz A, Pérez B, Giménez-Bachs JM, Salinas-Sánchez AS, Acker T, Sánchez Prieto R, Fendt S-M, De Bock K, Aragonés J. HIF1 α Suppresses Tumor Cell Proliferation through Inhibition of Aspartate Biosynthesis. *Cell Rep.* 2019;26(9):2257-2265.e4.
133. Sullivan LB, Luengo A, Danai LV, Bush LN, Diehl FF, Hosios AM, Lau AN, Elmiligy S, Malstrom S, Lewis CA, Vander Heiden MG. Aspartate is an endogenous metabolic limitation for tumour growth. *Nat. Cell Biol.* 2018;20(7):782–788.
134. Rodriguez AE, Ducker GS, Billingham LK, Martinez CA, Mainolfi N, Suri V, Friedman A, Manfredi MG, Weinberg SE, Rabinowitz JD, Chandel NS. Serine Metabolism Supports Macrophage IL-1 β Production. *Cell Metab.* 2019;29(4):1003-1011.e4.
135. Mashima T, Seimiya H, Tsuruo T. *De novo* fatty-acid synthesis and related pathways as molecular targets for cancer therapy. *Br. J. Cancer* 2009;100(9):1369–1372.
136. Zois CE, Harris AL. Glycogen metabolism has a key role in the cancer microenvironment and provides new targets for cancer therapy. *J. Mol. Med. Berl. Ger.* 2016;94:137–154.
137. Cho ES, Cha YH, Kim HS, Kim NH, Yook JI. The Pentose Phosphate Pathway as a Potential Target for Cancer Therapy. *Biomol. Ther.* 2018;26(1):29–38.
138. Jin L, Zhou Y. Crucial role of the pentose phosphate pathway in malignant tumors. *Oncol. Lett.* 2019;17(5):4213–4221.
139. Patra KC, Hay N. The pentose phosphate pathway and cancer. *Trends Biochem. Sci.* 2014;39(8):347–354.
140. Lis P, Dyląg M, Niedźwiecka K, Ko YH, Pedersen PL, Goffeau A, Ułaszewski S. The HK2 Dependent “Warburg Effect” and Mitochondrial Oxidative Phosphorylation in Cancer: Targets for Effective Therapy with 3-Bromopyruvate. *Molecules* 2016;21(12). doi:10.3390/molecules21121730.
141. Mathupala SP, Ko YH, Pedersen PL. Hexokinase II: Cancer’s double-edged sword acting as both facilitator and gatekeeper of malignancy when bound to mitochondria. *Oncogene* 2006;25(34):4777–4786.
142. Patra KC, Wang Q, Bhaskar PT, Miller L, Wang Z, Wheaton W, Chandel N, Laakso M, Muller WJ, Allen EL, Jha AK, Smolen GA, Clasquin MF, Robey B, Hay N. Hexokinase 2 is required for tumor initiation and maintenance and its systemic deletion is therapeutic in mouse models of cancer. *Cancer Cell* 2013;24(2):213–228.

143. Mathupala SP, Rempel A, Pedersen PL. Glucose catabolism in cancer cells. Isolation, sequence, and activity of the promoter for type II hexokinase. *J. Biol. Chem.* 1995;270(28):16918–16925.
144. Bustamante E, Morris HP, Pedersen PL. Energy metabolism of tumor cells. Requirement for a form of hexokinase with a propensity for mitochondrial binding. *J. Biol. Chem.* 1981;256(16):8699–8704.
145. Kaira K, Serizawa M, Koh Y, Takahashi T, Yamaguchi A, Hanaoka H, Oriuchi N, Endo M, Ohde Y, Nakajima T, Yamamoto N. Biological significance of 18F-FDG uptake on PET in patients with non-small-cell lung cancer. *Lung Cancer* 2014;83(2):197–204.
146. Tseng P-L, Chen C-W, Hu K-H, Cheng H-C, Lin Y-H, Tsai W-H, Cheng T-J, Wu W-H, Yeh C-W, Lin C-C, Tsai H-J, Chang H-C, Chuang J-H, Shan Y-S, Chang W-T. The decrease of glycolytic enzyme hexokinase 1 accelerates tumor malignancy via deregulating energy metabolism but sensitizes cancer cells to 2-deoxyglucose inhibition. *Oncotarget* 2018;9(27):18949–18969.
147. Xu S, Catapang A, Braas D, Stiles L, Doh HM, Lee JT, Graeber TG, Damoiseaux R, Shirihai O, Herschman HR. A precision therapeutic strategy for hexokinase 1-null, hexokinase 2-positive cancers. *Cancer Metab.* 2018;6(1):1–17.
148. Warrington R, Watson W, Kim HL, Antonetti FR. An introduction to immunology and immunopathology. *Allergy Asthma Clin. Immunol.* 2011;7(1):S1.
149. Kishton RJ, Sukumar M, Restifo NP. Metabolic Regulation of T Cell Longevity and Function in Tumor Immunotherapy. *Cell Metab.* 2017;26(1):94–109.
150. Parker DC. T cell-dependent B cell activation. *Annu. Rev. Immunol.* 1993;11:331–360.
151. Leopold Wager CM, Wormley Jr FL. Classical versus alternative macrophage activation: the Ying and the Yang in host defense against pulmonary fungal infections. *Mucosal Immunol.* 2014;7(5):1023–1035.
152. Ip WKE, Hoshi N, Shouval DS, Snapper S, Medzhitov R. Anti-inflammatory effect of IL-10 mediated by metabolic reprogramming of macrophages. *Science* 2017;356(6337):513–519.
153. Jha AK, Huang SC-C, Sergushichev A, Lampropoulou V, Ivanova Y, Loginicheva E, Chmielewski K, Stewart KM, Ashall J, Everts B, Pearce EJ, Driggers EM, Artyomov MN. Network Integration of Parallel Metabolic and Transcriptional Data Reveals Metabolic Modules that Regulate Macrophage Polarization. *Immunity* 2015;42(3):419–430.
154. Bouhrel MA, Derudas B, Rigamonti E, Dièvert R, Brozek J, Haulon S, Zawadzki C, Jude B, Torpier G, Marx N, Staels B, Chinetti-Gbaguidi G. PPARgamma activation primes human monocytes into alternative M2 macrophages with anti-inflammatory properties. *Cell Metab.* 2007;6(2):137–143.

155. Rodríguez-Prados J-C, Través PG, Cuenca J, Rico D, Aragonés J, Martín-Sanz P, Cascante M, Boscá L. Substrate Fate in Activated Macrophages: A Comparison between Innate, Classic, and Alternative Activation. *J. Immunol.* 2010;185(1):605–614.
156. Park BS, Lee J-O. Recognition of lipopolysaccharide pattern by TLR4 complexes. *Exp. Mol. Med.* 2013;45(12):e66.
157. Wolf AJ, Reyes CN, Liang W, Becker C, Shimada K, Wheeler ML, Cho HC, Popescu NI, Coggeshall KM, Arditi M, Underhill DM. Hexokinase Is an Innate Immune Receptor for the Detection of Bacterial Peptidoglycan. *Cell* 2016;166(3):624–636.
158. Zhang W, Wang G, Xu Z-G, Tu H, Hu F, Dai J, Chang Y, Chen Y, Lu Y, Zeng H, Cai Z, Han F, Xu C, Jin G, Sun L, Pan B-S, Lai S-W, Hsu C-C, Xu J, Chen Z-Z, Li H-Y, Seth P, Hu J, Zhang X, Li H, Lin H-K. Lactate Is a Natural Suppressor of RLR Signaling by Targeting MAVS. *Cell* 2019. doi:10.1016/j.cell.2019.05.003.
159. Cade BE, Chen H, Stilp AM, Louie T, Ancoli-Israel S, Arens R, Barfield R, Below JE, Cai J, Conomos MP, Evans DS, Frazier-Wood AC, Gharib SA, Gleason KJ, Gottlieb DJ, Hillman DR, Johnson WC, Lederer DJ, Lee J, Loredó JS, Mei H, Mukherjee S, Patel SR, Post WS, Purcell SM, Ramos AR, Reid KJ, Rice K, Shah NA, Sofer T, Taylor KD, Thornton TA, Wang H, Yaffe K, Zee PC, Hanis CL, Palmer LJ, Rotter JI, Stone KL, Tranah GJ, Wilson JG, Sunyaev SR, Laurie CC, Zhu X, Saxena R, Lin X, Redline S. Associations of variants in the hexokinase 1 and interleukin 18 receptor regions with oxyhemoglobin saturation during sleep. *PLoS Genet.* 2019;15(4). doi:10.1371/journal.pgen.1007739.
160. Lavie L. Oxidative stress in obstructive sleep apnea and intermittent hypoxia – Revisited – The bad ugly and good: Implications to the heart and brain. *Sleep Med. Rev.* 2015;20:27–45.
161. Wu J, Yan Z, Schwartz DE, Yu J, Malik AB, Hu G. Activation of NLRP3 Inflammasome in Alveolar Macrophages Contributes to Mechanical Stretch-Induced Lung Inflammation and Injury. *J. Immunol.* 2013;190(7):3590–3599.
162. Everson TM, Zhang H, Lockett GA, Kaushal A, Forthofer M, Ewart SL, Burrows K, Relton CL, Sharp GC, Henderson AJ, Patil VK, Rezwani FI, Arshad SH, Holloway JW, Karmaus W. Epigenome-wide association study of asthma and wheeze characterizes loci within HK1. *Allergy Asthma Clin. Immunol.* 2019;15(1):43.
163. Renner K, Singer K, Koehl GE, Geissler EK, Peter K, Siska PJ, Kreutz M. Metabolic Hallmarks of Tumor and Immune Cells in the Tumor Microenvironment. *Front. Immunol.* 2017;8. doi:10.3389/fimmu.2017.00248.
164. Bauerfeld CP, Rastogi R, Pirockinaite G, Lee I, Hüttemann M, Monks B, Birnbaum MJ, Franchi L, Nuñez G, Samavati L. TLR4-mediated AKT Activation is MyD88/TRIF-dependent and Critical for Induction of OxPhos and Mitochondrial Transcription Factor A in Murine Macrophages. *J. Immunol. Baltim. Md 1950* 2012;188(6):2847–2857.
165. Everts B, Amiel E, Huang SC-C, Smith AM, Chang C-H, Lam WY, Redmann V, Freitas

- TC, Blagih J, van der Windt GJW, Artyomov MN, Jones RG, Pearce EL, Pearce EJ. TLR-driven early glycolytic reprogramming via the kinases TBK1-IKK ϵ supports the anabolic demands of dendritic cell activation. *Nat. Immunol.* 2014;15(4):323–332.
166. Ham M, Lee J-W, Choi AH, Jang H, Choi G, Park J, Kozuka C, Sears DD, Masuzaki H, Kim JB. Macrophage Glucose-6-Phosphate Dehydrogenase Stimulates Proinflammatory Responses with Oxidative Stress. *Mol. Cell. Biol.* 2013;33(12):2425–2435.
167. Martinez FO, Gordon S, Locati M, Mantovani A. Transcriptional profiling of the human monocyte-to-macrophage differentiation and polarization: new molecules and patterns of gene expression. *J. Immunol. Baltim. Md 1950* 2006;177(10):7303–7311.
168. Nagy C, Haschemi A. Time and Demand are Two Critical Dimensions of Immunometabolism: The Process of Macrophage Activation and the Pentose Phosphate Pathway. *Front. Immunol.* 2015;6. doi:10.3389/fimmu.2015.00164.
169. Baardman J, Verberk SGS, Prange KHM, van Weeghel M, van der Velden S, Ryan DG, Wüst RCI, Neele AE, Speijer D, Denis SW, Witte ME, Houtkooper RH, O’neill LA, Knatko EV, Dinkova-Kostova AT, Lutgens E, de Winther MPJ, Van den Bossche J. A Defective Pentose Phosphate Pathway Reduces Inflammatory Macrophage Responses during Hypercholesterolemia. *Cell Rep.* 2018;25(8):2044-2052.e5.
170. Haschemi A, Kosma P, Gille L, Evans CR, Burant CF, Starkl P, Knapp B, Haas R, Schmid JA, Jandl C, Amir S, Lubec G, Park J, Esterbauer H, Bilban M, Brizuela L, Pospisilik JA, Otterbein LE, Wagner O. The Sedoheptulose Kinase CARKL Directs Macrophage Polarization through Control of Glucose Metabolism. *Cell Metab.* 2012;15(6):813–826.
171. Iles KE, Forman HJ. Macrophage Signaling and Respiratory Burst. *Immunol. Res.* 2002;26(1–3):095–106.
172. Koo S, Szczesny B, Wan X, Putluri N, Garg NJ. Pentose Phosphate Shunt Modulates Reactive Oxygen Species and Nitric Oxide Production Controlling *Trypanosoma cruzi* in Macrophages. *Front. Immunol.* 2018;9. doi:10.3389/fimmu.2018.00202.
173. Tyson RL, Perron J, Sutherland GR. 6-Aminonicotinamide inhibition of the pentose phosphate pathway in rat neocortex. *Neuroreport* 2000;11(9):1845–1848.
174. Wang J, Zhang X, Ma D, Lee W-NP, Xiao J, Zhao Y, Go VL, Wang Q, Yen Y, Recker R, Xiao GG. Inhibition of transketolase by oxythiamine altered dynamics of protein signals in pancreatic cancer cells. *Exp. Hematol. Oncol.* 2013;2(1). doi:10.1186/2162-3619-2-18.
175. Huang J-B, Kindzelskii AL, Petty HR. Hexokinase translocation during neutrophil activation, chemotaxis, and phagocytosis: disruption by cytochalasin D, dexamethasone, and indomethacin. *Cell. Immunol.* 2002;218(1):95–106.
176. Shoshan-Barmatz V, De Pinto V, Zweckstetter M, Raviv Z, Keinan N, Arbel N. VDAC, a multi-functional mitochondrial protein regulating cell life and death. *Mol. Aspects Med.* 2010;31(3):227–285.

177. Sen S, Kaminiski R, Deshmane S, Langford D, Khalili K, Amini S, Datta PK. Role of hexokinase-1 in the survival of HIV-1-infected macrophages. *Cell Cycle Georget. Tex* 2015;14(7):980–989.
178. Mi H, Muruganujan A, Ebert D, Huang X, Thomas PD. PANTHER version 14: more genomes, a new PANTHER GO-slim and improvements in enrichment analysis tools. *Nucleic Acids Res.* 2019;47(D1):D419–D426.
179. Wang S, Song R, Wang Z, Jing Z, Wang S, Ma J. S100A8/A9 in Inflammation. *Front. Immunol.* 2018;9. doi:10.3389/fimmu.2018.01298.
180. Jia J, Arif A, Terenzi F, Willard B, Plow EF, Hazen SL, Fox PL. Target-selective Protein S-Nitrosylation by Sequence Motif Recognition. *Cell* 2014;159(3):623–634.
181. Thomsen LL, Scott JMJ, Topley P, Knowles RG, Keerie A-J, Frend AJ. Selective Inhibition of Inducible Nitric Oxide Synthase Inhibits Tumor Growth in Vivo: Studies with 1400W, a Novel Inhibitor. *Cancer Res.* 1997;57(15):3300–3304.
182. Sun L, Shukair S, Naik TJ, Moazed F, Ardehali H. Glucose Phosphorylation and Mitochondrial Binding Are Required for the Protective Effects of Hexokinases I and II. *Mol. Cell. Biol.* 2008;28(3):1007–1017.
183. BeltrandelRio H, Wilson JE. Interaction of mitochondrially bound rat brain hexokinase with intramitochondrial compartments of ATP generated by oxidative phosphorylation and creatine kinase. *Arch. Biochem. Biophys.* 1992;299(1):116–124.
184. Golshani-Hebroni SG, Bessman SP. Hexokinase binding to mitochondria: a basis for proliferative energy metabolism. *J. Bioenerg. Biomembr.* 1997;29(4):331–338.
185. Zeng C, Aleshin AE, Hardie JB, Harrison RW, Fromm HJ. ATP-Binding Site of Human Brain Hexokinase As Studied by Molecular Modeling and Site-Directed Mutagenesis †. *Biochemistry* 1996;35(40):13157–13164.
186. Padgett CM, Whorton AR. S-nitrosoglutathione reversibly inhibits GAPDH by S-nitrosylation. *Am. J. Physiol.-Cell Physiol.* 1995;269(3):C739–C749.
187. Sanman LE, Qian Y, Eisele NA, Ng TM, van der Linden WA, Monack DM, Weerapana E, Bogyo M. Disruption of glycolytic flux is a signal for inflammasome signaling and pyroptotic cell death. Cravatt BF, ed. *eLife* 2016;5:e13663.
188. John S, Weiss JN, Ribalet B. Subcellular Localization of Hexokinases I and II Directs the Metabolic Fate of Glucose. *PLOS ONE* 2011;6(3):e17674.
189. Hauser DN, Mamais A, Conti MM, Primiani CT, Kumaran R, Dillman AA, Langston RG, Beilina A, Garcia JH, Diaz-Ruiz A, Bernier M, Fiesel FC, Hou X, Springer W, Li Y, de Cabo R, Cookson MR. Hexokinases link DJ-1 to the PINK1/parkin pathway. *Mol. Neurodegener.* 2017;12. doi:10.1186/s13024-017-0212-x.

190. Gardiner NJ, Wang Z, Luke C, Gott A, Price SA, Fernyhough P. Expression of hexokinase isoforms in the dorsal root ganglion of the adult rat and effect of experimental diabetes. *Brain Res.* 2007;1175:143–154.
191. Saraiva LM, Silva GSS da, Galina A, da-Silva WS, Klein WL, Ferreira ST, Felice FGD. Amyloid- β Triggers the Release of Neuronal Hexokinase 1 from Mitochondria. *PLOS ONE* 2010;5(12):e15230.
192. Fouquerel E, Goellner EM, Yu Z, Gagné J-P, Barbi de Moura M, Feinstein T, Wheeler D, Redpath P, Li J, Romero G, Migaud M, Van Houten B, Poirier GG, Sobol RW. ARTD1/PARP1 Negatively Regulates Glycolysis by Inhibiting Hexokinase 1 Independent of NAD⁺ Depletion. *Cell Rep.* 2014;8(6):1819–1831.
193. Magri A, Belfiore R, Leggio L, Guarino F, Messina A. A Synthetic Peptide from the N-Terminal of Hexokinase I Prevents the Interaction Between VDAC1 and SOD1 G93A Mutant Recovering the Viability of an ALS Cell Model. *Biophys. J.* 2017;112(3):349a.
194. Ray A, Dittel BN. Isolation of Mouse Peritoneal Cavity Cells. *J. Vis. Exp.* 2010;(35). doi:10.3791/1488.
195. Schägger H. Tricine–SDS-PAGE. *Nat. Protoc.* 2006;1(1):16–22.
196. Schindelin J, Arganda-Carreras I, Frise E, Kaynig V, Longair M, Pietzsch T, Preibisch S, Rueden C, Saalfeld S, Schmid B, Tinevez J-Y, White DJ, Hartenstein V, Eliceiri K, Tomancak P, Cardona A. Fiji: an open-source platform for biological-image analysis. *Nat. Methods* 2012;9(7):676–682.
197. Alonso-Castro AJ, Salazar-Olivo LA. The anti-diabetic properties of *Guazuma ulmifolia* Lam are mediated by the stimulation of glucose uptake in normal and diabetic adipocytes without inducing adipogenesis. *J. Ethnopharmacol.* 2008;118(2):252–256.
198. Shrum B, Anantha RV, Xu SX, Donnelly M, Haeryfar SM, McCormick JK, Mele T. A robust scoring system to evaluate sepsis severity in an animal model. *BMC Res. Notes* 2014;7(1):233.
199. Majewski N, Nogueira V, Robey RB, Hay N. Akt Inhibits Apoptosis Downstream of BID Cleavage via a Glucose-Dependent Mechanism Involving Mitochondrial Hexokinases. *Mol. Cell. Biol.* 2004;24(2):730–740.
200. Chong J, Wishart DS, Xia J. Using MetaboAnalyst 4.0 for Comprehensive and Integrative Metabolomics Data Analysis. *Curr. Protoc. Bioinforma.* 2019;68(1):e86.